THE ROLE OF HISTORICAL LAND-COVER CHANGES AS A MECHANISM FOR GLOBAL AND REGIONAL CLIMATE CHANGE

Thomas N. Chase

NPS Contracts No. CA 1268-2-9004 COLR-R92-0204
USGS Contract No. 99CRAG0005 SA 9005CS0014,
and NASA Grant No. NAG8-1511
Roger A. Pielke Sr., P.I. and Adviser

Colorado State University

DEPARTMENT OF ATMOSPHERIC SCIENCE

PAPER NO. 685

THE ROLE OF HISTORICAL LAND-COVER CHANGES AS A MECHANISM FOR GLOBAL AND REGIONAL CLIMATE CHANGE

Thomas N. Chase

Graduate Degree Program in Ecology
Colorado State University
Fort Collins, Colorado
Spring 1999

Atmospheric Science Paper No. 685

ABSTRACT

THE ROLE OF HISTORICAL LAND-COVER CHANGES AS A MECHANISM FOR GLOBAL AND REGIONAL CLIMATE CHANGE

This paper describes the results from several modeling studies and an observational analysis as to the effect of historical land-cover change on regional and global climates. We discuss methods for determining historical vegetation change and present results from model simulations at the global and regional scale which compare climates generated using currently observed vegetation versus natural vegetation as a boundary condition. We also compare these modeling studies with recent observational data and with simulations of climate change resulting from increased greenhouse gases.

We conclude from this research that vegetation change, as it has already occurred, globally and regionally, can have significant effects on both global and regional climates. These effects are not limited to the regions of direct land-cover change forcing. For example, as a result of tropical deforestation, the position and intensity of the ITCZ is affected by the change in land surface characteristics resulting in global-scale effects which are similar in nature to the climatic effects associated with El Niño Southern Oscillation (ENSO). These include changes in high-latitude circulations, the generation of low frequency waves which appear to propagate to the extratropics in well-defined teleconnection patterns, and reduced low-level easterlies over most of the tropical Pacific basin under current vegetation. This implies an interaction mechanism between tropical deforestation and ENSO.

The model simulations of climate change due to landcover change compare favorably in spatial pattern and amplitude with recently observed temperature trends. Additionally, a comparison between simulations of climate changes due to landcover disturbance and

changes due to rising atmospheric CO_2 concentration show that global land-cover changes, as they have already occurred, are responsible for shifts in climate which are of similar amplitude and occur in the same regions as simulated climate changes resulting from increased CO_2.

A comparison of three independent observational datasets shows strong disagreement not only in the sign of recent globally-averaged temperature trends but also disagree as to regions where significant climate shifts are occurring. Unlike model simulations of greenhouse gas warming, warm anomalies do not occur preferentially over land during this period and do not increase with height in the tropics.

Thomas N. Chase
Graduate Degree Program in Ecology
Colorado State University
Fort Collins, Colorado 80523
Spring 1999

ACKNOWLEDGEMENTS

Funding for this study was provided by NPS Contract No. CA 1268-2-9004 COLR-R92-0204, NPS Contract No. CA 1268-2-9004 CEGR-R92-0193, USGS Contract No. 99CR-AG0005 SA 9005CS0014, and NASA Grant No. NAG8-1511. I would like to acknowledge the National Center for Atmospheric Research (NCAR) for use of computing resources and models. NCAR is sponsored by the National Science Foundation.

Thanks to my adviser, Roger Pielke Sr., for his good ideas and for helping me through bumps in the road. Thanks to members of my committee, Jorge Ramirez, Mike Coughenour, and Dennis Ojima. My thanks to the co-authors of the papers coming out of this dissertation: Tim Kittel, Jill Baron, Tom Stohlgren, Rama Nemani, and Steve Running. Thanks to Dallas McDonald and Tara Pielke for help in preparation of the dissertation. Thanks to all the students and project members I have worked with over the years. I appreciate your help and input.

TABLE OF CONTENTS

LIST OF FIGURES

LIST OF TABLES

Chapter 1

INTRODUCTION

1.1 A General Overview of Vegetation Effects on Soils and Climate

That the biological systems of Earth are affected by the physical systems surrounding them is not a controversial statement. Climate, the soil substrate, and other physical factors in some sense define the vegetation which can be supported. In some cases, climate observations alone are used as a proxy for vegetation cover because they are often so highly correlated (Holdridge 1947). The extent to which the biological systems of Earth affect their surroundings is, however, a matter of considerable debate. Clear evidence exists that vegetation can alter the chemistry and texture of soils, the chemical composition of the atmosphere and regulate the Earth's surface energy balance though the exact mechanisms and interactions between these influences are complex and generally unknown.

In the case of soils, for example, Berendse (1994) showed both observational and numerical model evidence that the direction of natural selection can be altered as a result of the effects of a dominant vegetation species on the underlying soil. In a more general study, van Breenan (1993) reviewed several observational studies and found that most vegetated soils have more nutrients, more moisture, and more air than unvegetated soils thereby favoring increased Net Primary Production (NPP) in a positive feedback cycle. He concluded that in most cases vegetation is not only beneficial but necessary in order to produce sufficient nutrient concentration to maintain a stable biota.

It has also been hypothesized that the chemical composition of the Earth's atmosphere and therefore the Earth's climate are strongly regulated by the Earth's vegetation. The relative constancy of global temperature over the history of life on Earth despite a large (approximately 40%) increase in solar luminosity is the major observation behind

this contention. While even the extent of this climatic stability is contested (e.g., Resnick 1992), it seems fair to say that terrestrial surface temperatures have remained in a range allowing the existence of liquid water. Fossil evidence, however, indicates quite a bit less temperature variability than this (Kasting 1989). Paleo-climate model simulations reviewed in Crowley (1983) indicated that a 5–10% reduction in solar luminosity would result in an ice covered planet, if no biological feedback mechanisms were invoked. Lovelock (1979) provided one explanation for the persistence of global temperature by invoking an evolutionary biogeochemical phenomenon whereby the biotic and abiotic worked together to maintain life by regulating atmospheric chemistry and the relative strength of the greenhouse effect. An alternative, non-biological, climate control in the form of a negative feedback in the carbonate – silicate geochemical cycle, was proposed by Kasting (1989). Warmer temperatures allowed more weathering of silicates and greater deposition of carbonates thereby removing carbon from the atmosphere which in turn would regulate global temperatures. That this mechanism exists seems unquestionable. However, rates of weathering without the aid of biological activity might be insufficient for observed temperature regulation. Schwartzman and Volk (1989) examined the biotic influence on weathering and cooling and estimated that Earth's biota accelerates silicate weathering by one to three orders of magnitude above the abiotic rate. They calculate that without the 10, 100, or 1000-fold increase of weathering due to biotic influence there would be a 15, 30, or 45 degree planetary temperature decrease, respectively, undermining the idea of a purely abiotic weathering control.

Beyond composition and chemistry, it is also clear that vegetation has an effect on the atmosphere as an active modulator of energy flow through soils and from the planetary surface and, more passively, through variable physical properties such as reflectivity and frictional effects. This has been demonstrated particularly in modeling studies which usually examine the effects on a modeled climate of changes in some or all vegetation properties. Observational evidence of the effects of changing vegetation is also mounting. These aspects of vegetational influence on climate are the main focus of the present paper and are discussed in detail below as are limitations to the approach.

Several reviews of numerical experiments (e.g., Mintz 1984; Garratt 1992; Rowntree 1988; Betts et al. 1996) show that the surface designation in a numerical model can have quite large and significant impacts on modeled climate. Many of these experiments, particularly the earliest examples, have estimated the impacts of vegetation change simply as a change in surface albedo (e.g., Charney et al. 1977; Sagan et al. 1979; Potter et al. 1981; Henderson-Sellers and Gornitz 1984; Meehl 1994; Dirmeyer and Shukla 1994) assuming that the largest impact found in vegetation would be its effect on reflectivity. All the above experiments found that the designation of surface albedo had a significant effect on the simulated climate, though to differing degrees, and were highly dependent on the magnitude of estimated albedo changes. The increased surface albedo generally associated with removal of vegetation generally decreased surface temperatures when no moisture feedback was accounted for because more solar energy was reflected back into space. However, decreased precipitation associated with decreased net surface radiation resulted in a dryer surface and less evaporation/transpiration which often overcame the albedo effect and warmed the surface.

Similar experiments have been performed in an effort to ascertain the role of momentum absorption due to vegetation. This is usually described as a change change in roughness length. Changes in surface roughness consistent with removal of vegetation is often found to have an impact on low-level water vapor convergence and therefore precipitation distribution in model simulations (e.g., Sud and Smith 1984; Sud et al. 1988; Henderson-Sellers 1993; Collins and Avissar 1994).

Changes in canopy resistance to moisture loss or in Leaf Area Index (LAI), a vegetation property which regulates canopy resistance as well as reflectivity also have been shown to have an effect on climate simulations. Li and Avissar (1993), found that LAI was the most important variable contributing to errors due to neglecting subgrid-scale land-surface variability. Zhang (1994) found that a dense vegetation cover effectively made surface heat fluxes independent of ground surface conditions, particularly soil moisture. Chase et al. (1996) found that historical changes in LAI, particularly in the tropics, had large effects on global circulations.

Combining several physical vegetation properties into the simulations, the regional and global effects of tropical deforestation have been actively studied. Garratt (1992), in a review of some of these experiments, shows that the common elements among those experiments with a land-surface scheme includes a reduced hydrological cycle and an increased near-surface air temperature in the region of the change. Globally, there were few averaged effects and it has been noted that realistic vegetation changes may not be able to force climate on a global scale but might be capable of altering regional-scale climate (Henderson-Sellers 1984). Some recent studies have examined the effects of extratropical landcover change on regional climate (e.g., Bonan et al. 1992, Copeland 1995) and have found both local and remote climatic effects. Most recent efforts have been understandably concentrated more on regional effects of tropical deforestation and regional desertification, however, because of the vulnerability of these ecosystems and their importance to human populations (e.g., Xue and Shukla 1993; Xue 1997; Claussen 1998).

1.2 Observations of the Climatic Effects of Landuse Change

While model simulations are the simplest way to explore vegetative influences on climate, the observational evidence for the effects of landuse change on climate is growing. Meher-Homji (1991), found that surface temperature fluctuates more and precipitation decreases in non-forested regions as opposed to forested areas. Hulme (1996) showed observational evidence that all the world's drylands have significant warming trends and that in 8 of 14 cases these trends were steeper than seen in the globally-averaged surface observational record. Hulme (1996) suggests that this increased warming may be due to human pressures on marginal areas which increases surface albedo and then serves as a positive feedback through increased desertification leading to yet higher albedos (a mechanism first proposed by Charney 1975). Balling (1997) also found that increased desertification was having an impact on the global temperature record. O'Brien (1997) documented regional climate changes in Mexico as a result of tropical deforestation. Stohlgren et al. (1997) found evidence that a regional cooling in the Colorado Front Range might be related to changes in land cover.

1.3 Vegetation Feedbacks to Climate Change

In all the above numerical experiments many processes are not being allowed to develop independently or are being left out of simulations entirely and this remains a major limitation. Models of the climate system are just beginning to include representations of all the complex physical, chemical and biological interactions which are evident in nature. Field et al. (1995) discussed the vastly complex and interwoven feedback systems associated with interacting biological and abiological systems. The full system of feedbacks is poorly understood and is never accounted for in numerical model studies. Additionally, the problem of scale enters when assessing the sign of impacts. For example, plant stomatal resistance increases in most cases when elevated atmospheric CO_2 exists. But carbon fertilization allows total leaf area to increase which leads to decreased canopy resistance. While this compensatory mechanism does not generally fully overcome the effects of increased stomatal resistance it greatly diminishes the effect and at times can be of larger magnitude. Jacobs and Debruin (1992) found that because of the non-linearity of the climate-vegetation problem, feedbacks from atmosphere can have a larger effect on the final model solution than the initial perturbation. In this case it was shown that for a 'deforestation' experiment, estimates of transpiration could be off by a factor of two or three if feedbacks from the planetary boundary layer are ignored.

Henderson-Sellers et al. (1995) performed global model calculations of the reaction of climate both to the radiative effect of doubled CO_2 and to doubled stomatal resistance (a presumed first order feedback effect of vegetation to increased atmospheric CO_2). They found a small positive feedback due to increased stomatal resistance. Lashof (1989) also performed global modeling studies and attempted to estimate the gain from each of several postulated feedback processes associated with global warming. These feedbacks included changes in ice albedo, water vapor and clouds (geophysical feedbacks) as well as added CO_2 due to increased microbial activity, decreased atmospheric CO_2 due to carbon fertilization, and a DMS feedback (biophysical feedbacks). He found some weak negative feedbacks and only in the case of carbon fertilization removing carbon from the atmosphere was the feedback a significant portion of the original signal.

While ostensibly not directly related to vegetation influences, Mitchell et al. (1997) found that feasible changes in the shape and/or size of cirrus cloud ice crystals could increase Earth's shortwave reflectance by 9.3 W/m2 which is larger in magnitude but opposite in sign to the first-order effects of doubled CO_2 on climate simulations. Changes in vegetation type or density can chemically and mechanically affect the kinds of aerosols which serve as ice nuclei and therefore may have some role in the regulation of ice crystal habit.

The above examples are fairly static model representations of feedback mechanisms and as such are problematic. More realistic, dynamic feedback models have also been put into production. King and Nielson (1992) suggest that dynamic vegetation change resulting from a warming climate will generally result in increased carbon storage above ground (by 4–17% in their calculations) providing a negative feedback. They do note that a climate change which occurs too quickly might result in a dieback of vegetation and an initial positive feedback in CO_2. This would probably reverse sign, however, as new vegetation grew up. Therefore, the sign of the feedback may depend on the rate of climate change and whether the biota has the opportunity to react.

Henderson-Sellers and McGuffie (1995) also performed doubled CO_2 model experiments and included a simple interactive biosphere in the calculations. Relative to the cases with constant vegetation they found that cases with interactive vegetation responded to doubled CO_2 by decreased planetary albedos and cloud amounts. Though final increases in temperature were almost non-existent in these models due to dynamic vegetation, the albedo effects represent positive vegetative feedbacks to the initial perturbation. It must be pointed out that many processes such as carbon fertilization effects on vegetation were not included in these experiments. The importance of these omissions are unclear. Davis (1989) looked at fossil pollens for vegetative response to past climate changes and found that the understory can react fast (tens of years) to climate change while the canopy may take centuries. The vegetation may therefore not be able to track climate change and this may lead to dieback, extinction and a temporarily increased carbon flux. Clearly more sophisticated accounts of the interaction between all components of the climate system are necessary if we are to have confidence in model results.

Given the complications, uncertainties and limitations outlined in the preceding sections, the goal of the research presented here is to realistically estimate the extent of human impact on land cover both globally and in a regional-scale case study in the Front Range of Colorado in order to evaluate the hypothesis that these changes are already of sufficient magnitude to have affected regional and global climates. We then use recent observational data and an independent simulation of climate change due to increased CO_2 concentration to evaluate the relative magnitude of present-day climate changes due to both vegetative and CO_2 forcing and assess the applicability of those changes to observed climate trends.

Chapter 2

GLOBAL CLIMATE SIMULATIONS OF HISTORICAL LANDCOVER CHANGE

2.1 Introduction

While some of the earliest studies of the effects of landuse change were of global scope (e.g., Sagan et al. 1979 and others reviewed in Mintz 1984), and some recent studies have examined the effects of extratropical landcover change on regional climate (e.g., Bonan et al. 1992, Copeland 1995, Stohlgren et al. 1998), most recent efforts have been understandably concentrated more on regional effects of tropical deforestation and regional desertification because of the vulnerability of these ecosystems and their importance to human populations (e.g., Xue and Shukla 1993; Xue 1997; Claussen 1998). Little acceptance has been given to the idea, however, that anthropogenic landcover changes of the type already observed can significantly influence global climate. Of the few studies which have commented on this subject, McGuffie et al. (1995) noted weak, remote, high latitude effects in a complete tropical deforestation simulation (i.e., all tropical rainforests converted to grasslands), while Chase et al. (1996) hypothesized that large, winter hemisphere climate anomalies in a simulation of the effects of realistic global green leaf area change were due to tropical deforestation affecting low latitude convection and therefore global-scale circulations in the winter hemisphere. Zhang et al. (1997) further explored simulated mid-latitude teleconnections due to complete tropical deforestation with a linear wave model and found that appropriate conditions existed for the propagation of tropical waves into the extratropics in that case. Others have since noted isolated extratropical effects due to simulated tropical vegetation physical or physiological changes (Sud et al. 1996, a complete deforestation scenario; Sellers et al. 1996, a study of the effect of increased atmospheric CO_2 on radiation and plant physiology).

It should be expected that changes in tropical landcover affects higher latitudes, particularly in the winter hemisphere. The three major tropical convective heating centers are associated with tropical land surfaces of Africa, Amazonia, and the maritime continent of Indonesia, Malaysia, New Guinea and surrounding regions (e.g., Kreuger and Winston 1973; Chen et al. 1988; Berbery and Nogués-Paegle 1993). While the existence of the rainforest and other moist vegetation types has often been considered to be solely a function of local precipitation fed by advected moisture from adjacent oceans, significant precipitation recycling does occur due to the presence of transpiring vegetation (e.g., Lettau et al. 1979; Burde and Zangvil 1996). Removal of that vegetation has major impacts on the momentum and radiant energy absorbed at the surface and its partitioning into latent and sensible forms which affect boundary layer energetics and structure and generally culminate in a reduction of precipitation though this seems to be a function of season and region (e.g., Dickinson and Kennedy 1992, Pielke et al. 1997; Zhang et al. 1997; Nobre et al. 1991; Eltahir 1996; Polcher and Laval 1994; Zheng and Eltahir 1997; Eltahir 1998). As a result of removal of tropical vegetation, regional convection might be expected to be reduced in magnitude on average, and shifted in space as a result of compensating circulations and other localized forcings. Small changes in the magnitude and spatial pattern of tropical convection may then alter the magnitude and pattern of high-level tropical outflow which feeds the higher latitude zonal jet (e.g., Bjerknes 1969; Krishnamurti 1961; Chen et al. 1988; Oort and Yienger 1996). Additionally, these changes may also force anomalous Rossby waves which can propagate to high latitudes in a westerly background flow when not trapped by a critical line (e.g., Wallace and Gutzler 1981; Tiedtke 1984; James 1994; Tribbia 1991; Berbery and Nogués-Paegle 1993) and which tend to organize into a few recognizable teleconnection patterns regardless of the spatial nature of convective anomalies (e.g., Geisler et al. 1985, Hoerling and Ting 1994). These forcings may affect weather and climate regimes at high latitudes and are analogous to the remote effects due to anomalous tropical sea surface temperatures during the opposing phases of the El Niño-Southern Oscillation (ENSO).

Our purpose here, then, is to realistically estimate the extent of human impact on global landcover in order to evaluate the hypothesis that these changes, particularly in

the tropics, are already of sufficient magnitude to have affected the global climate state through the mechanisms discussed above. Building on the work of Chase et al. (1996), we used an updated estimate of global landcover change in a global numerical model along with comparisons with reported observational data.

2.2 Model Description

We used the standard version of the NCAR CCM3 (Kiehl et al. 1996) coupled with the land-surface model (LSM) (Bonan 1996). This version of the CCM3 had prescribed SSTs. The CCM3 is a spectral model with triangular truncation at wavenumber 42 and 18 vertical levels reaching 3mb. The model grew out of an earlier version (CCM2) and modifications were made to correct several deficiencies in the climate simulation including a large warm bias in northern hemisphere summer land surfaces, an excessive hydrological cycle, as well as substantial phase and amplitude errors in stationary wave climatology (Kiehl et. al. 1998). While the dynamical portions of the model remained constant, radiation, cloud, convective, boundary layer and land-surface parameterizations were all modified from the earlier model version.

The model accounts now for the radiative effects of trace gases (CFC's, CH4, N2O) as well as a background aerosol content. Optical properties of clouds now include ice clouds and differing effective radius prescriptions for marine and terrestrial clouds. These modifications appear to have corrected, for the most part, biases in annually-averaged absorbed solar and outgoing longwave radiation at the top of the atmosphere. Adjustments to boundary layer physics appears to have improved the simulation of PBL depth. Because of their importance to the present simulations, a more thorough discussion of the land-surface and convective parameterizations is warranted.

The LSM is a GCM-scale parameterization of atmospheric land-surface exchanges and accounts for vegetation properties as functions of one of 24 basic vegetation types. The LSM includes a single-level canopy, a lake model, and calculates averaged surface fluxes due to subgrid-scale vegetation types and hydrology. Two phonological properties, leaf and stem area index (LAI and SAI), are interpolated between prescribed monthly values.

Albedos are calculated as a function of LAI and SAI among other factors. All other vegetation properties are seasonally constant. Implementation of the model had little impact on upper-level wind or temperature climatology relative to the standard CCM land-surface parameterization though some effects on surface temperatures and humidity are ascribed to implementation of the LSM (Bonan 1998).

The land-surface climatology for summer and winter seasons for the coupled CCM3/LSM (from Bonan 1998) differenced from observed surface climatology (Legates and Willmott 1990) are shown in Fig. 2.1. There are biases of both sign in both seasons which exceed 2.5 C over most of the global land surfaces. A cold bias is evident over most land surfaces in summer which has been attributed to a still overactive hydrological cycle which allows for excessive soil moisture. In northern winter, warm biases of between 2.5 and 10.0 C are evident over much of the high latitude northern hemisphere, while cold biases dominate in the tropics and southern hemisphere in the winter season.

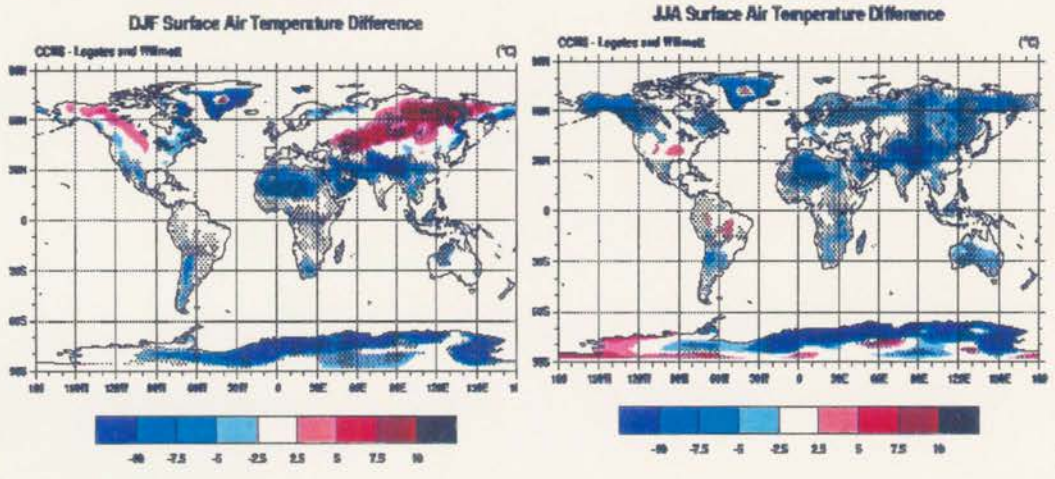

(a) (b)

Figure 2.1: CCM3/LSM near-surface land temperature climatology differenced from observations for (a) the winter season (December-January-February), and (b) the summer season (June-July-August) (from Bonan 1998).

Because of the importance tropical convection is expected to have in these simulations and because of the sensitivity of the global climate to its details, the convective model used here is examined in some detail. Convective precipitation is represented using the schemes

of Zhang and McFarlane (1995) for deep convection and that of Hack (1994) for shallow convection. The combined use of these schemes was, in part, responsible for a reduction of the overactive hydrological cycle seen in an earlier version of the model (CCM2) and a more reasonable depiction of the northern hemisphere standing wave climatology (Hack et al. 1998).

If the atmosphere is moist adiabatically unstable then the temperature and moisture fields are adjusted using the Zhang and McFarlane (1995; referred to as ZH95 subsequently) convective parameterization while the shallow and mid-level effects of convective adjustment are represented using the scheme of Hack (1994). The deep convective component of ZH95 is based on an ensemble of convective updrafts and downdrafts which may exist at any point which is conditionally unstable. The scheme is similar to that of Arakawa and Schubert (1974) though with several simplifications. Only those plumes which are buoyant enough to penetrate the stable layer are included in the ensemble. All ensemble updrafts have an identical mass flux at cloud base and convection only occurs where convective available potential energy (CAPE) exists. As a closure condition it is assumed that CAPE is destroyed at an exponential rate by parcel ascent in the updraft according to a specified time scale.

The ZH95 scheme defines budget equations for cloud and sub-cloud layers which are identified below. For the cloud layer the temperature and moisture convective fluxes are written:

$$c_p \left(\frac{\partial T}{\partial t}\right)_{cl} = -\frac{1}{\rho}\frac{\partial \left(M_u S_u + M_d S_d - M_c S\right)}{\partial z} + L(C - E) \tag{2.1}$$

$$\left(\frac{\partial q}{\partial t}\right)_{cl} = -\frac{1}{\rho}\frac{\partial \left(M_u q_u + M_d q_d - M_c q\right)}{\partial z} + E - C \tag{2.2}$$

The effect on the subcloud layer is written:

$$c_p \rho \left(\frac{\partial T}{\partial t}\right)_{sub} = -\frac{1}{\triangle Z_m}\left(M_b \left[S\left(z_m\right) - S_u\left(z_m\right)\right] + M_d \left[S\left(z_m\right) - S_d\left(z_m\right)\right]\right) \tag{2.3}$$

$$\rho\left(\frac{\partial q}{\partial t}\right)_{sub} = -\frac{1}{\triangle z_m}\left(M_b\left[q\left(Z_m\right) - q_u\left(z_m\right)\right] + M_d\left[q\left(z_m\right) - q_d\left(z_m\right)\right]\right) \tag{2.4}$$

In the above equations M_c is the net vertical mass flux which is composed of both upward (M_u) and downward (M_d) components. M_b is the cloud base mass flux and is the same for all plumes. C is the large-scale condensation while E is the large-scale evaporation rate. S, S_u, S_d, q, q_u, q_d are the corresponding components of the dry static energy and the specific humidity. $\triangle z_m$ is the height of the subcloud layer.

Adjustment due to both updrafts and downdrafts are included in this scheme. The updrafts are an ensemble of entraining plumes each with a fractional entrainment rate. Mass detrainment occurs in a thin layer at the top of the plume and has the same thermal properties as the environmental air. All plumes are constrained to be deep enough to detrain in the conditionally stable portion of the upper atmosphere.

Zhang and McFarlane (1995) describe the effects of the implementation of this convective scheme on the Canadian Climate Center (CCC) GCM relative to a simple moist convective adjustment scheme used previously. They found that the new scheme warmed the troposphere, generated more high clouds and increased planetary albedo in the zonal average at every latitude. They also concluded that not only were the specifics of the convective adjustment scheme important to the climate simulation of the GCM but also that other parameterizations which interact with the convective scheme (the radiation scheme in particular) are crucial to the ultimate effect of the convective adjustment on the climate simulation. The effect of the implementation of ZH95 on the CCM3 have not been reported in isolation. Because of the limited generality of the effects of ZH95 on the climates of differing GCMs, extrapolation of the results from the CCC GCM are not particularly useful.

The CCM3/LSM coupled model was integrated for 12 annual cycles using a representation of current, observed vegetation cover versus a simulation which had a representation of natural, potential vegetation in equilibrium with current climate (an estimate of vegetation undisturbed by human activity) as the bottom boundary condition. The derivation of these datasets is discussed in Section 2.3. Results from this experiment are given in

terms of 10 averaged Januaries, the month when the maximum communication between the tropics and the northern hemisphere is expected. These followed more than two years of model spin-up.

2.3 Vegetation Datasets

Maps of the current vegetation distribution in regions of anthropogenic disturbance and the natural vegetation distribution are shown in Fig. 2.2. These datasets were derived with guidance from global maps of maximum LAI which was retrieved for current vegetation from maximum normalized difference vegetation index (NDVI) satellite products (Nemani et al. 1996) at 1 degree pixel size. Assuming that vegetation is nearly in equilibrium with climate and soils, using long-term precipitation and temperature data, soils data and employing the close empirical relationships between transpiration and LAI (e.g., Nemani and Running 1989), a distribution of maximum LAI for natural, potential vegetation necessary to close the average water budget at each 1×1 degree grid point on the globe was produced (Nemani et al. 1996).

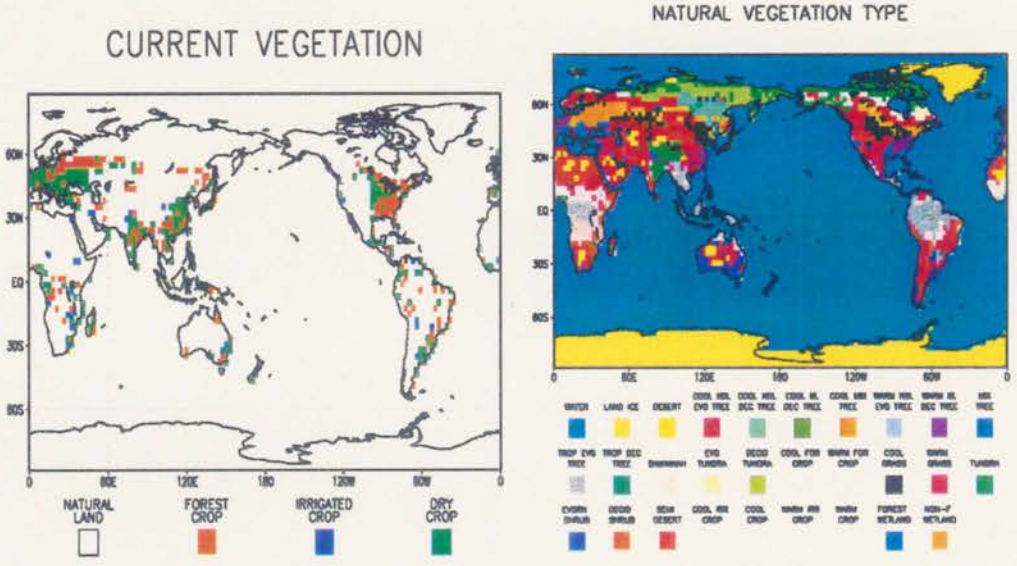

Figure 2.2: Vegetation classifications. (a) Current vegetation types for regions where current and natural vegetation differ (i.e., anthropogenically disturbed regions), and (b) natural vegetation types.

For use in the CCM3, an updated current vegetation dataset was produced simply by declaring regions where the difference between the current and natural maps of maximum

LAI was greater than 1 and which were not already agricultural land in the standard CCM dataset (Matthews 1983, Olson et al. 1983) to be anthropogenically disturbed. These anthropogenically disturbed points were assigned one of 3 kinds of agricultural land in keeping with the standard LSM vegetation categories (irrigated in regions where LAI increased under current vegetation, dryland crop, and mixed crop-forest where LAI decreased) depending on the magnitude of maximum LAI difference, latitude and vegetation type in the standard CCM dataset (Matthews 1983 and Olson et al. 1983). That observed vegetation types, such as mixed crop grasslands or mixed crop and tropical forest are not among the LSM vegetation categories is a source of inaccuracy in the present simulations, but it was determined important to stay within the confines of the standard parameterization for these initial simulations.

Despite considering only relatively highly affected regions (Δ LAI > 1) this current vegetation dataset includes larger estimated areas of agricultural land than the standard CCM landcover data particularly in the southeast Asian peninsula, Indonesia, Malaysia, and surrounding regions. Even though larger areas of landcover change were included than in the standard CCM data, our representation of the extent of human landcover disturbance (approximately 15%) remains conservative. A recent estimate (Vitousek et al. 1997) claims over 40% of the Earth's land surface is currently affected by anthropogenic landcover change.

The natural vegetation cover was created by taking the standard CCM dataset and filling in agricultural areas with an appropriate vegetation type. We did this using our estimated potential maximum LAI with values for specific vegetation types roughly following Neilson and Marks (1994), the latitude, and adjacent vegetation for guidance. Differences in vegetation categories between the two simulations resulted in changes in the fraction of the grid cell covered by vegetation, changes in soil moisture in irrigated regions, and differences in vegetation physical and physiological properties in the vegetated fraction.

2.4 First Day Response

Climate processes are so intricately interwoven that separating direct chains of cause and effect is often impossible. In this section, we briefly examine simulated weather

differences due to changes in landcover after the first 24 hours of model integration. These first day differences are expected to be primary in the sense that the the full climate system has not fully adjusted to them. The subsequent development and equilibrium response of the model climate can be associated with these initial perturbations.

Sensible and latent heat flux differences (Fig. 2.3a,b) after 24 hours of simulation (date of model initialization is September first) show small differences between the two simulations which are confined almost exclusively to areas where changes in vegetation occur. These differences are particularly evident in regions of moist tropical vegetation with the largest differences already occurring in southeast Asia and land areas of the Maritime continent, Amazonia and the southeastern coasts of South America and Africa. At higher latitudes, Western Europe and the central United States are also affected after a single day of simulation. Differences in near surface air temperature (Fig. 2.3c) are evident over a large portion of western Europe and other, smaller differences appear only in regions where direct landcover change forcing is present.

These initial, small changes in surface fluxes and temperature occurred only in regions directly affected by landcover change. After lengthy integration, these anomalies move upscale and develop into differences in the 10-year average general circulation which are of larger magnitude and larger spatial extent than the initial perturbations. These are discussed in subsequent sections. The largest anomalies no longer occur in regions of direct landuse change forcing in the 10-year average indicating a complex atmospheric adjustment process to landcover changes. Because we expect the largest communication between changes in tropics and the mid-latitudes in northern winter we now concentrate on 10-year January averages in the presentation of subsequent results.

2.5 Global Averages

Table 2.1 shows selected January global averages for several climate variables. Changes in global averages were quite small in most instances, though larger differences were generally found over land than over oceans or sea ice. There was a small global warming which approached 0.2 C over land. Little change in globally-averaged precipitation occurred. Low-level winds (850 mb), however, were substantially affected in the

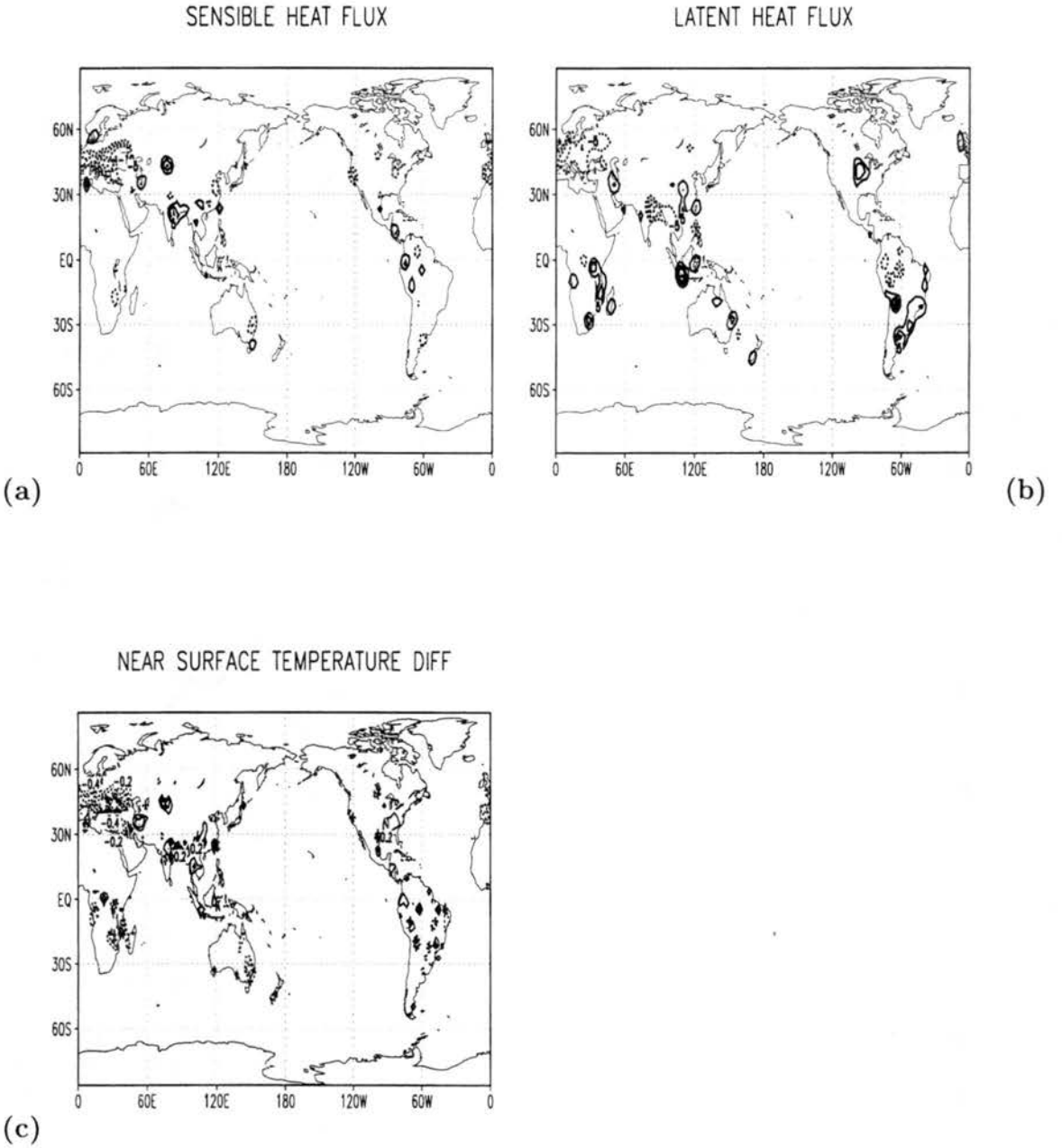

Figure 2.3: Difference fields (current–natural) after 24 hrs of simulation for (a) sensible heat flux, (b) latent heat flux, and (c) near surface temperature.

global average increasing over land and decreasing over oceans in the current vegetation case. High-level winds (200 mb) decreased over all surfaces.

Table 2.1: January globally-averaged values and differences for selected fields.

	CURRENT	NATURAL	CURR-NAT
REF TEMP (K)			
GLOBAL:	284.73	284.68	.05
LAND:	275.95	275.79	.16
SEA:	288.19	288.19	.00
CONV PRECIP (mm/day)			
GLOBAL AVG:	2.57	2.57	.00
LAND AVG:	1.97	1.94	.03
SEA AVG:	2.81	2.81	.00
LARGE-SCALE PRECIP (mm/day)			
GLOBAL AVG:	.49	.49	.00
LAND AVG:	.41	.40	.01
SEA AVG:	.52	.52	.00
850 mb U ($m\ s^{-1}$)			
GLOBAL AVG:	.91	.96	-.05
LAND AVG:	.71	.55	.16
SEA AVG:	.97	1.09	-.11
200 mb U ($m\ s^{-1}$)			
GLOBAL AVG:	18.13	18.51	-.38
LAND AVG:	18.34	18.55	-.21
SEA AVG:	18.05	18.50	-.45

2.6 Effects on Tropical Climate

With the exception of area averages, we present results in this section as differences in 10 averaged Januaries between the current vegetation case and the natural vegetation

case (current–natural) overlayed on a map of Student's t test statistic shaded at the 90 and 95%, 1 tailed, significance levels following Chervin and Schneider (1976).

Because we are focusing here on the global effects of historic landuse change, we do not perform a detailed analysis of the mechanism for changes in tropical convection except to note that statistically significant changes in the distribution of surface heat fluxes (sensible and latent; Fig. 2.4a,b) resulting from changes in surface properties in the tropics are associated with shifts in tropical convection. Some surface heat flux anomalies are associated with direct surface forcing from altered landcover though the largest heating anomalies result from large-scale circulation changes and occur in regions remote from direct forcings. For example, latent heat flux anomalies of nearly +40 W m^{-2} cover large portions of the tropical central and eastern Pacific. These are of similar magnitude to latent heat flux differences between observed warm and cold ENSO events (e.g., Wu and Newell 1998). Decreased latent heat fluxes averaged over tropical land surfaces (30N – 30S) were positively correlated in space ($r=0.45$; $p<0.001$, Spearman's rank correlation coefficients) with decreased convective precipitation over tropical land surfaces (approximately 25% of convective precipitation in the latitude range 30N - 30S occurred directly over land) and negatively correlated with increases in sensible heat fluxes ($r=-0.48$; $p<0.001$) compatible with the assertion that tropical boundary-layer equivalent potential temperature and therefore convection are strongly determined by boundary-layer humidity (e.g., Brown and Bretherton 1998). Correlations with net radiation changes were insignificant ($p > 0.1$).

For reference, Figure 2.5 shows the global distribution of highest simulated January convective precipitation in the current vegetation case. This tropical precipitation band represents the intertropical convergence zone (ITCZ). Of importance to the present discussion are three regional maxima in convective precipitation which are associated with the tropical land masses of Amazonia, Southern Africa and the maritime continent. The maximum over the land masses of the maritime continent also blends with a maximum over the western Pacific warm pool maximum. That the maxima in convective precipitation are all associated with land surfaces is an indication that the changes in surface energy

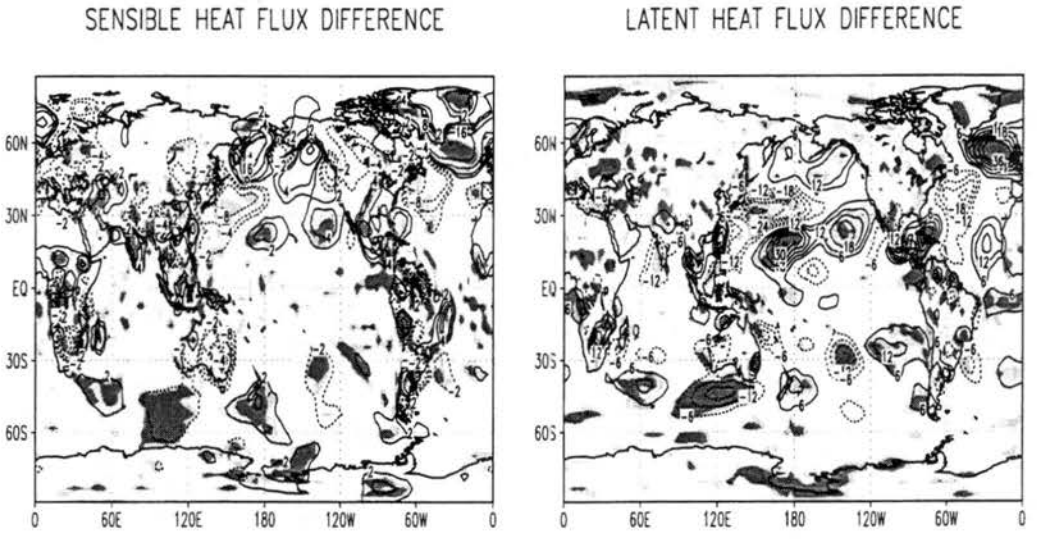

Figure 2.4: Surface heat flux differences (current–natural) using a 9-point spatial filter for easier visibility. (a) Sensible heat flux (contour by 2, 4, 8, 16, 32 W m^{-2}), and (b) latent heat flux (contour by 6 W m^{-2}). Light shading represents the 90% significance level for a 1-sided t-test. Dark shading represents the 95% significance level.

relations associated with landcover change might be an important mechanism for disrupting the spatial patterns and intensity of tropical convective precipitation and therefore, upper-level heating patterns which drive the major global-scale circulations.

Figure 2.6a shows the distribution of the differences in convective precipitation and the associated t statistic map which indicate significant changes in precipitation of both sign over all 3 tropical convective centers. Figure 2.6b is a zonally-averaged plot of convective precipitation from 45S-45N which shows that the effect of these changes was to diminish and move the intertropical convergence zone northward in the current vegetation case. The secondary maximum near 38N was also diminished. The difference in 20N-20S averaged convective precipitation (Fig. 2.6c) shows regional shifts in convection and, of particular interest, a reduction in convective activity in the western Pacific and over the maritime continent while an increase in convective precipitation occurs in the central and eastern Pacific under current vegetation.

Tropical zonal circulations were also affected as seen in the differences in low-level (850 mb) east-west winds (Fig. 2.7) which shows diminished easterlies over most of the central and eastern tropical Pacific (seen as positive wind anomalies because of the easterly

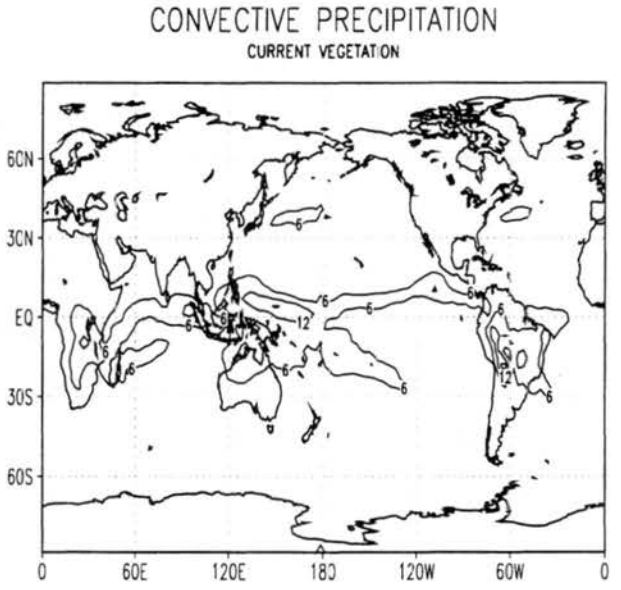

Figure 2.5: January convective precipitation in the current vegetation case. Contour by 6 mm/d.

flow). Though these changes are not statistically significant over the entire region, this reduction in easterlies is consistent with reduced convection over the western Pacific and Indonesia which acted to diminish the tropical zonal circulation. Because warm Southern Oscillation episodes are also characterized by decreased easterlies in these regions which are of similar magnitude to those simulated here (e.g., Philander 1990), our results indicate that circulation changes resulting from tropical landuse change may act, to first order, to enhance the magnitude, frequency and duration of warm Southern Oscillation episodes and to diminish cold episodes.

2.7 Effects on Higher Latitudes

The tropical-extratropical response to the landcover changes simulated in this experiment may be better understood if we break up the circulation into rotational and divergent components using Helmholz's theorem. We then have

$$\mathbf{V}_\psi = \hat{k} \times \nabla\psi; \mathbf{V}_\chi = \nabla\chi \tag{2.5}$$

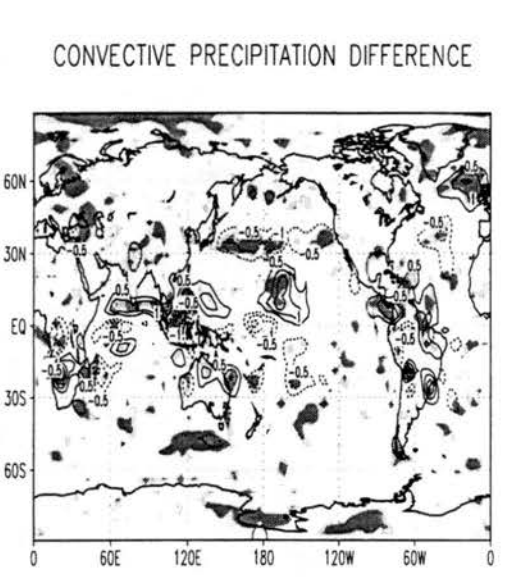

(a)

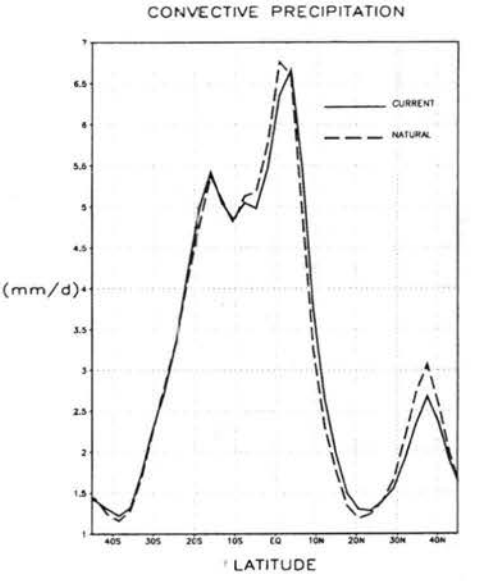

(b)

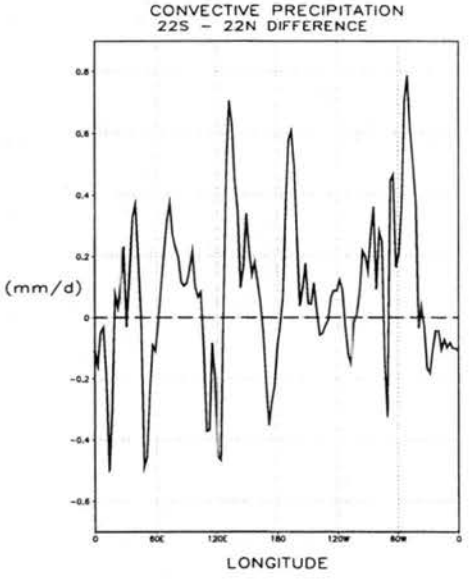

(c)

Figure 2.6: (a) Convective precipitation differences (current–natural, contour by 0.5 mm/day) using a 9-point spatial filter for easier visibility. Shaded regions as in Figure 2.4. (b) Comparison of the 45N–45S zonally-averaged convective precipitation for the 2 cases. (c) Difference in 20N–20S meridional average (current–natural) for the 2 cases.

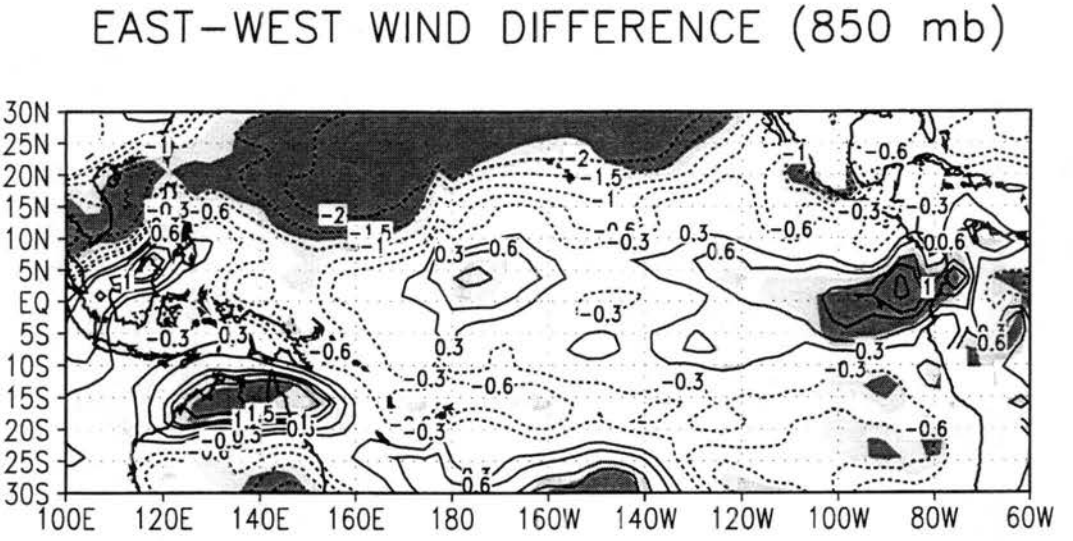

Figure 2.7: Tropical Pacific east-west wind component difference at 850 mb (contour by 0.3, 0.6, 1.0, 1.5, 2.0 m s^{-1}. Shading as in Fig. 2.4. Note: easterly winds are of negative sign so that decreased tropical easterlies are represented by positive wind anomalies.

where χ is the velocity potential representing the divergent component of the flow and ψ is the streamfunction representing the purely rotational portion of the flow. The total wind is then the sum of the two components.

$$\mathbf{V} = \mathbf{V}_\psi + \mathbf{V}_\chi \tag{2.6}$$

Figure 2.8a shows the divergent wind and isotachs at 200mb in the current vegetation case. Three upper-level divergent regions associated with the tropical convective precipitation maxima shown in Fig. 2.5 are evident in this figure. These represent Hadley cell outflow regions and are areas where maximum communication between the deep tropics and sub-tropics occurs. Figure 2.8b shows the rotational wind and isotachs at 200 mb in the current vegetation case. The three regional maxima of the mid-latitude jet, composed almost entirely of rotational flow, are evident in this figure as is the fact that the three regional jets are associated with the three divergent outflow regions shown in Fig. 2.8a which are in turn associated with tropical precipitation maxima. Krishnamurti et al. (1973) first suggested an association between these observed phenomena and more recent work (Chen et al. 1988, Vincent et al. 1997) has established a connection between tropical heating

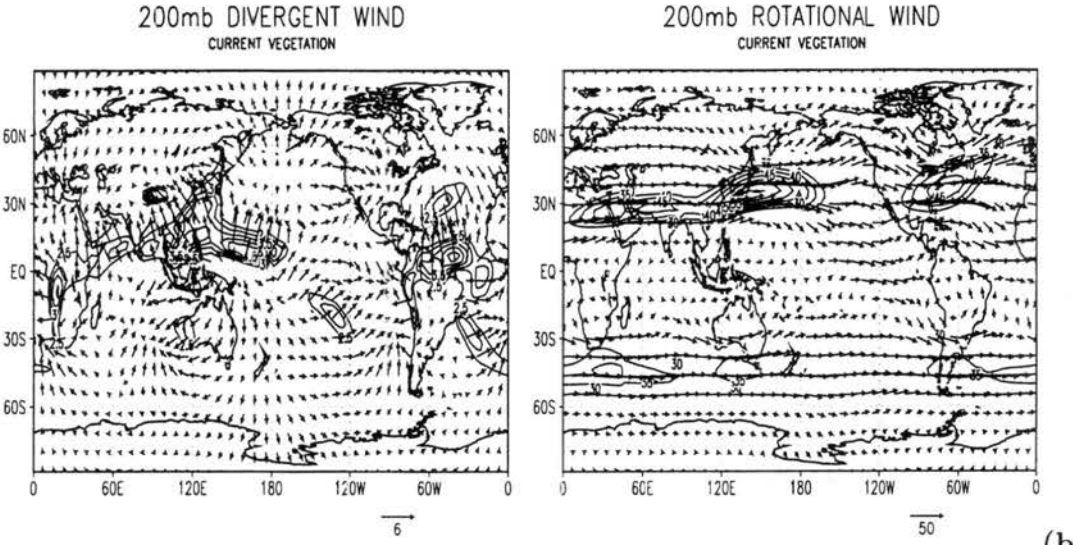

Figure 2.8: 200 mb wind vectors in the current vegetation case. (a) Rotational component in vectors with velocity contoured by 5 m s^{-1} for values above 30 m s^{-1}. (b) Divergent component with velocity contoured by 0.5 m s^{-1} for values above 2.5 m s^{-1}.

maxima, divergent outflow and regional jet maxima which suggests that tropical landuse change, should it alter tropical convection, would be effective at altering the properties of the higher latitude jet.

We now turn attention to the details of how historical changes in tropical vegetation cover may have affected higher latitude weather and climate. The total kinetic energy (KE) of the atmospheric flow may be decomposed in a manner similar to the decomposition of the winds in Eq. 2.6. We define a rotational and divergent KE which are composed solely of the rotational or divergent part of the wind respectively.

$$KE_\psi = \frac{\mathbf{V}_\psi \cdot \mathbf{V}_\psi}{2} \tag{2.7}$$

$$KE_\chi = \frac{\mathbf{V}_\chi \cdot \mathbf{V}_\chi}{2} \tag{2.8}$$

and the total kinetic energy is the sum of the two components.

$$KE = KE_\psi + KE_\chi \tag{2.9}$$

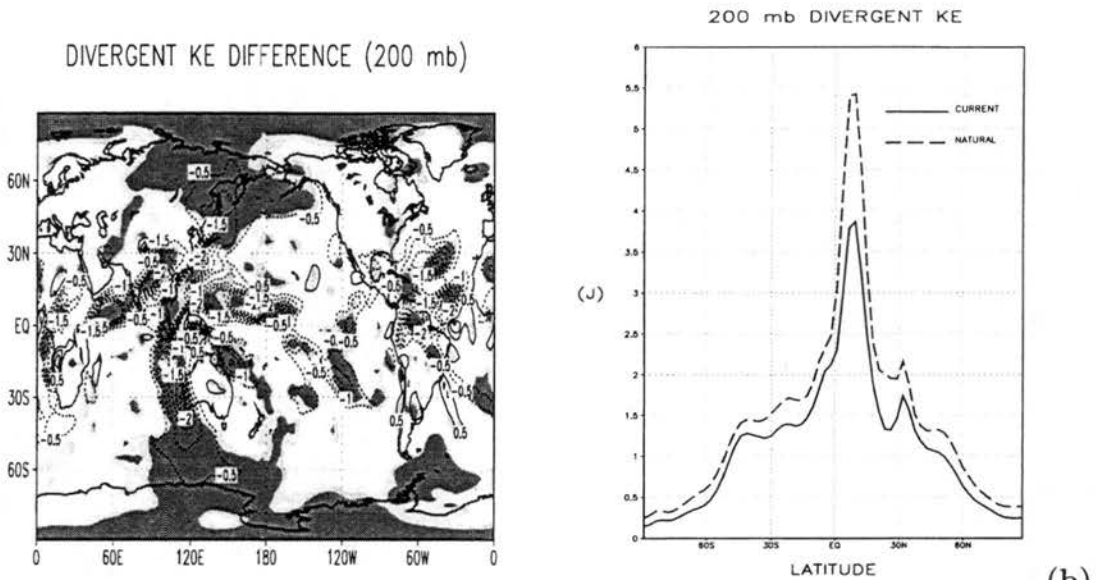

(a) (b)

Figure 2.9: (a) Divergent wind kinetic energy (KE) differences at 200 mb. (Contour = 0.5 J). Shaded regions as in Fig. 2.4. (b) Comparison of zonally-averaged 200 mb KE for the 2 cases.

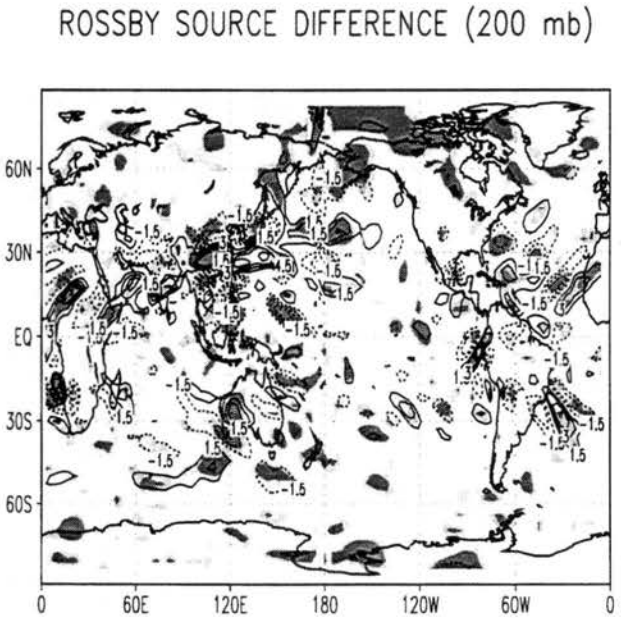

Figure 2.10: Rossby source term differences (current–natural) $\times 10^{10}$ (Contours by 1.5 s^{-2}). Shaded regions as in Fig. 2.4.

The kinetic energy per unit mass associated with the divergent components (U_χ and V_χ) of the wind, where $KE_\chi = (U_\chi^2 + V_\chi^2)/2$ can be used as a measure of tropical high-level outflow and its influence on the extratropical circulation. The difference in this quantity at 200 mb (Fig. 2.9a) shows a significant decrease in divergent high-level tropical outflow in all three major tropical heating centers in the current vegetation case. By far the largest effect is in southeast Asia/Indonesia and the western Pacific. In the zonal average (Fig. 2.9b), 200 mb divergent kinetic energy is reduced everywhere but particularly in the tropical maximum which is a reflection of both a diminished global meridional circulation and diminished tropical zonal circulations in the current vegetation case. Because divergent KE is quickly converted to the rotational KE associated with the mid-latitude jet (Wiin-Nielsen and Chen 1993), there is considerably less energy available to directly feed the jet in the current vegetation case.

Starting with the definitions in Eqs. 2.7, and 2.8. the full KE budget equations may be derived for each wind component (e.g., Wiin-Nielson and Chang 1993). However, here the approximate form of these equations after Chen et al. (1978) are used. These take the form

$$\frac{\partial K_\chi}{\partial t} \sim -\nabla \cdot (\mathbf{V}_\chi KE) - (f + \zeta)(u_\chi v_\psi - u_\psi v_\chi) - \mathbf{V}_\chi \cdot \nabla \phi \tag{2.10}$$

for the divergent KE budget and

$$\frac{\partial K_\psi}{\partial t} \sim \nabla \cdot (\mathbf{V}_\psi KE) + (f + \zeta)(u_\chi v_\psi - u_\psi v_\chi) - \mathbf{V}_\psi \cdot \nabla \phi \tag{2.11}$$

for the rotational KE budget. The first forcing terms on the right hand side of Eqs. 2.4 and 2.5 represent local generation of KE by KE flux convergence. The second term is the same in each equation but of opposite sign and represents the conversion between rotational and divergent components of the total KE. The full KE budget equations have several conversion terms between divergent and rotational KE including conversions resulting from vertical interactions (e.g., Vincent et al. 1997, Chen et al. 1988). These terms are small relative to the conversion term included here and so are ignored in the present discussion. The third forcing term in each equation represents generation of KE

through the conversion of the potential energy of the horizontal height gradient to the kinetic energy of flow down that gradient.

Several studies (Vincent et al. 1997, Wiin-Nielson and Chen 1993) have shown that the conversion from available potential energy (APE) to KE is done first by converting APE to divergent KE which is then quickly and nearly completely converted to rotational KE through the conversion term in Eqs. 2.10 and 2.11. We have shown substantial changes in the amplitude and spatial distribution of divergent KE as a result of changing landcover. These changes would then be expected to have some impact on the rotational flow of the mid-latitude jet because of this quick and complete conversion. Figure 2.11 shows this conversion between divergent and rotational KE for the two cases and the difference between them. These figures show positive values (conversion from divergent to rotational flow in the present sign convention) equatorward of the jet in most regions and negative values poleward of the jet in a pattern similar to that found in Wiin-Nielson and Chen (1993). In the northern hemisphere, two regions of maximum conversion occur. A positive maximum centered on Japan and a negative maximum centered off the eastern United States. Both these regions become reduced in area and amplitude in the current vegetation case relative to natural vegetation. Additionally, most other secondary regions of conversion are also reduced in the current vegetation case. This can be seen most easily in a comparison of the zonally-averaged conversion term (Fig. 2.11d) where the generation of rotational KE from divergent KE in the tropical regions is reduced under current vegetation while the opposite transformation (rotational energy converted to divergent) is reduced under current vegetation at mid-latitudes until about 62N. Poleward of 62N, conversion from divergent to rotational KE is again reduced under the current vegetation scenario.

Changes in tropical convection not only reduced the intensity of the upper-level divergent tropical outflow under current vegetation and altered the patterns of conversion of divergent to rotational KE, anomalous vorticity forcings were also generated which appear to affect high northern hemisphere latitudes. Starting with the barotropic vorticity (ζ) equation

$$\frac{\partial \zeta}{\partial t} + \mathbf{V} \cdot \nabla \zeta = -\zeta(\nabla \cdot \mathbf{V}) \tag{2.12}$$

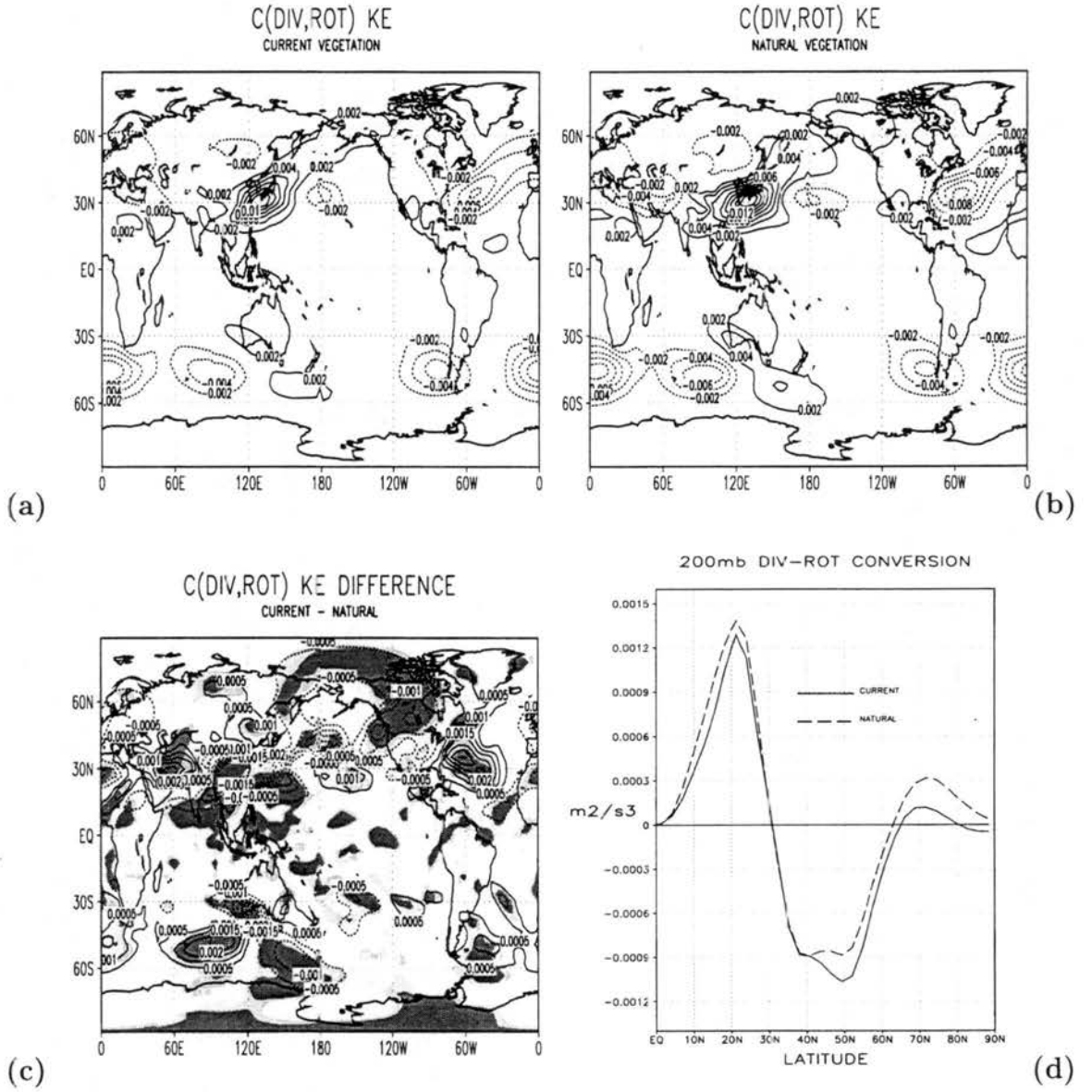

Figure 2.11: 200 mb conversion between divergent KE and rotational KE in m2/s3 for (a) current vegetation, (b) natural vegetation, (c) difference (current–natural), and (d) zonal average.

and again defining a divergent ($\mathbf{V}_\chi$) and rotational ($\mathbf{V}_\psi$) component of the wind, a vorticity equation can be written in the form (Sardeshmukh and Hoskins 1988, James 1994):

$$\frac{\partial \zeta}{\partial t} + \mathbf{V}_\psi \cdot \nabla \zeta = -\zeta(\nabla \cdot \mathbf{V}) - \mathbf{V}_\chi \cdot \nabla \zeta = -\nabla \cdot (\mathbf{V}_\chi \zeta). \tag{2.13}$$

The forcing term on the far righthand side of 2.13 is a function solely of the divergent component of the wind (refer to the divergent KE in Figs. 2.9a,b) and differences in this forcing term (known as the Rossby source term) between the current and natural vegetation scenarios at 200 mb are presented in Fig. 2.10. Significant anomalies of both sign are generated in all three tropical heating centers though the strongest and most widespread effect occurs in southeast Asia and to its south and east. The strongest Rossby source anomalies in the region of southeast Asia and the central Pacific occur in locations of westerlies which allows for the possibility of propagation to higher latitudes, thereby potentially affecting mid-latitude weather and climate regimes as discussed in the introduction.

The possible connection between anomalous Rossby wave forcing in the western and central Pacific and the higher northern latitudes can be clarified with a correlation analysis of height data. A correlation in the January average 500 mb height difference fields between the natural and current vegetation simulations with the differences at the base point 21N-158W (Fig. 2.12) (a center of action for tropical Pacific convection differences and a region of westerlies at all tropical latitudes) reveals a teleconnection pattern which affects the entire northern hemisphere and is similar in spatial structure to the tropical northern hemisphere (TNH) pattern described in studies examining extratropical connections to El Niño (e.g., Livezey and Mo 1987). These correlations are significant at the 5% level at most of the amplitude extrema throughout the hemisphere.

Significant changes in large-scale, high-latitude northern hemisphere flow were generated as a result of the historic changes in landcover and are attributable to changes in tropical convection discussed above. The differences in east-west winds at 200 mb (Fig. 2.13a) shows a prominent northward shift in the mid-latitude jet stream over most of the globe under the current vegetation scenario. This shift is most apparent in the

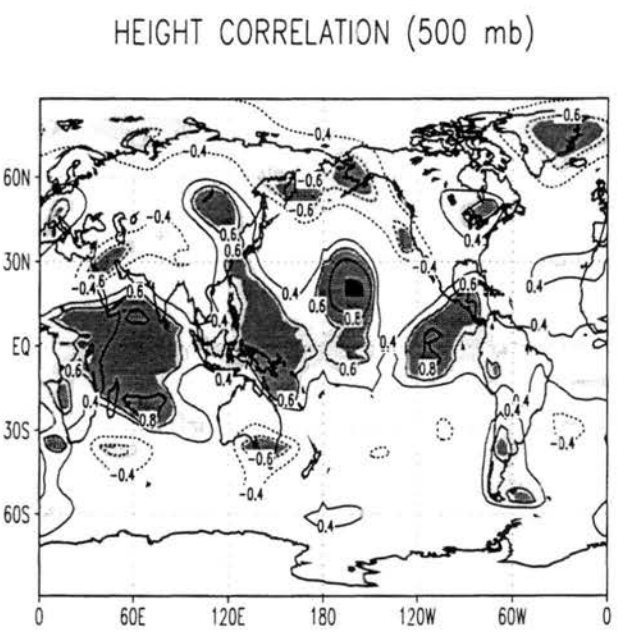

Figure 2.12: Correlation of differences in 500 mb height field with difference at 21N and 158W. Contour is 0.4, 0.6, 0.8. Blackened region in central Pacific represent the region of near perfect correlation. Shading as in Fig. 2.4 but for significance of correlation.

northern Pacific. Zonal averages of the 200 mb east-west wind (not shown) display this northerly shift and a decrease in the maximum magnitude of the jet core in the current case by approximately 5 m s^{-1}; a decrease of more than 10%. The northern shift and decreased magnitude of the mid-latitude jet (a feature noted in the global landcover change experiment of Chase et al. 1996 and the desertification experiment of Dirmeyer and Shukla 1996) are consistent with the decreased upper-level tropical outflow in the current vegetation case which can provide less direct energy to the jet (Fig. 2.9), and with a decreased and more northerly temperature gradient maximum in the current case. This change in gradient can be seen in the zonally-averaged north-south gradient in 200 mb heights in the northern hemisphere (a measure of the vertically-averaged horizontal temperature gradient, Fig. 2.13b) which shows a northerly shift and weakening in the zone of maximum baroclinicity in the current vegetation case. It should be noted that changes in the mean flow such as those described above will also affect the propagation characteristics of, and interact with, waves superimposed on that flow (e.g., Rasmussen and Wallace 1983; Kang

1990, Ting et al. 1996) which introduces yet another source of variability between current and natural vegetation scenarios. Finally, under current vegetation, zonally-averaged temporal variability, measured here as the monthly-averaged standard deviation of daily 500 mb heights (Fig. 2.14) in jet stream regions, was reduced as would be expected from diminished baroclinicity.

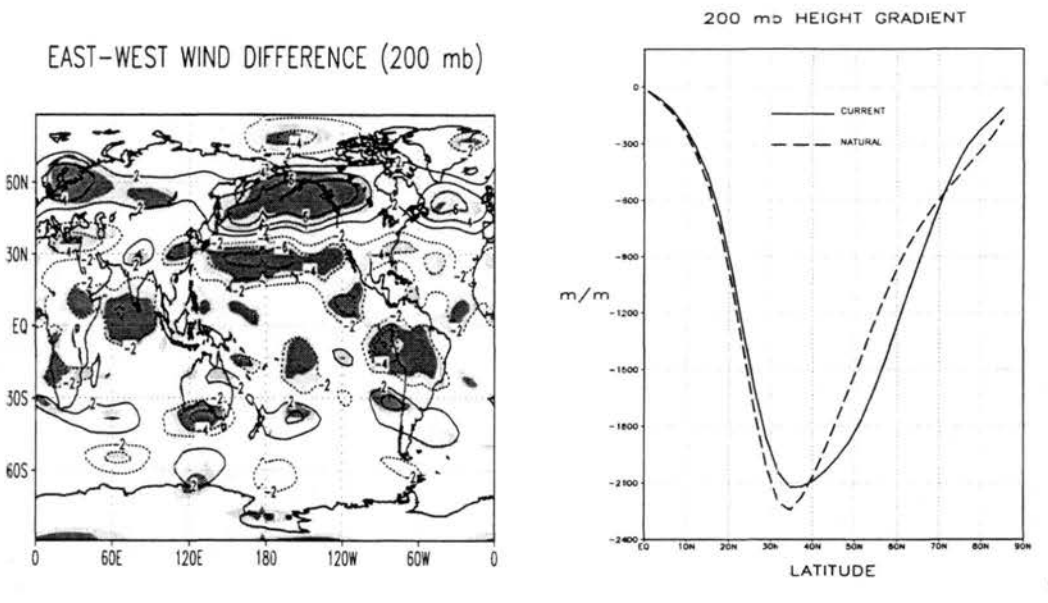

Figure 2.13: (a) Difference in 200 mb east-west wind (current–natural). Contour by 2 m s^{-1}. Shaded regions as in Fig. 2.4. (b) Comparison of north-south derivative of zonally-averaged 200 mb heights (d(Z200)/dy) in the northern hemisphere.

Figure 2.15 shows near-surface air temperature difference between current and natural vegetation. Significant changes in temperature are associated with all tropical land masses and many higher latitude regions. In the northern hemisphere, a wave number 3 pattern of warming and cooling centers is apparent. Warming occurs on most land surfaces under current vegetation and is centered in temperate and eastern Boreal North America, southern Asia, and central Europe. Cooling centers include the western Arctic (including the North Pacific and Alaska), Greenland, and the North Atlantic and central Asia. Average temperature changes from 30N – 90N are +0.3 C over land and –0.1 over ocean and sea ice which are of the same magnitude as observed in the surface record in recent decades (e.g., Pielke et al. 1998a,b). Globally, temperatures warmed by 0.05 degrees in the current case. It should be noted that the atmospheric temperatures over ocean and

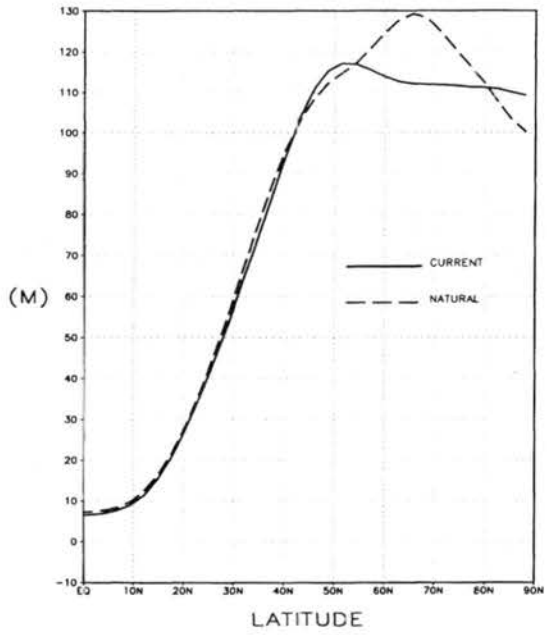

Figure 2.14: Comparison of northern hemisphere zonally- and monthly-averaged daily standard deviation in 500 mb heights.

sea ice are limited by the imposed surface temperatures in those regions. This warming of northern hemisphere land surfaces is associated with weakened equatorward, low-level, winter monsoon flow which allowed the ITCZ to occupy its more northerly position in the current vegetation case (Fig. 2.6b). These temperature differences, which are a result of large-scale circulation changes and which are statistically significant at 5 of the 6 cooling/warming centers, are interesting given observed northern hemisphere winter climate trends which are discussed below.

2.8 Horizontal Fluxes

Further information on the complexity of the global atmospheric adjustment resulting from the imposed change in landcover can be gained from an examination of the differences in the northward fluxes and flux divergence of eddy momentum in the northern hemisphere.

Figure 2.16 compares the upper-level (300-100 mb average) northward momentum fluxes and flux divergences resulting from high frequency transients (1 day) and from stationary waves.

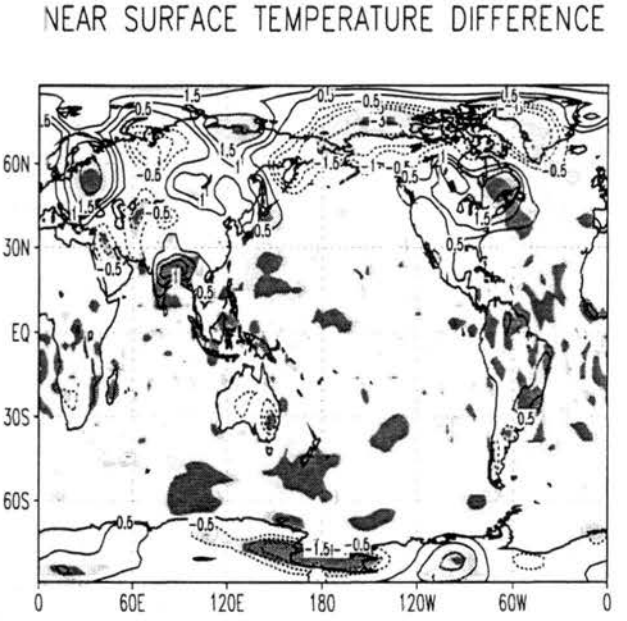

Figure 2.15: Difference in near surface air temperature (current–natural) using a 9-point spatial filter for easier visibility. Contour by 0.5, 1.0, 1.5, and 3.0°C. Shaded regions as in Fig. 2.4.

The transient momentum flux, Fig. 2.16a, shows a decreased overall magnitude of high-frequency transient eddy activity and a slight shift northward on its peak at approximately 32N in the current vegetation case. The total flux of momentum is larger, however, in the current vegetation case for stationary waves Fig. 2.16b. This is an indication that the atmospheric adjustment to the changes in vegetation cover is complex, with differing responses in transient and stationary eddy activity.

The corresponding transient eddy flux divergences is shown in Fig. 2.16c and indicates that the peak convergence of transient eddy momentum flux between 40 and 50N is reduced and shifted northward in the current vegetation case consistent with the simulated position and magnitude of the zonally averaged jet in that case. While much smaller in overall magnitude than the transient eddy flux divergence, the stationary eddy flux divergence Fig. 2.16d also shows a slight northward shift of the convergent maximum at 50N in the current vegetation case. The larger amplitude of the stationary wave convergent maximum in the current vegetation case is consistent with the increased stationary wave activity

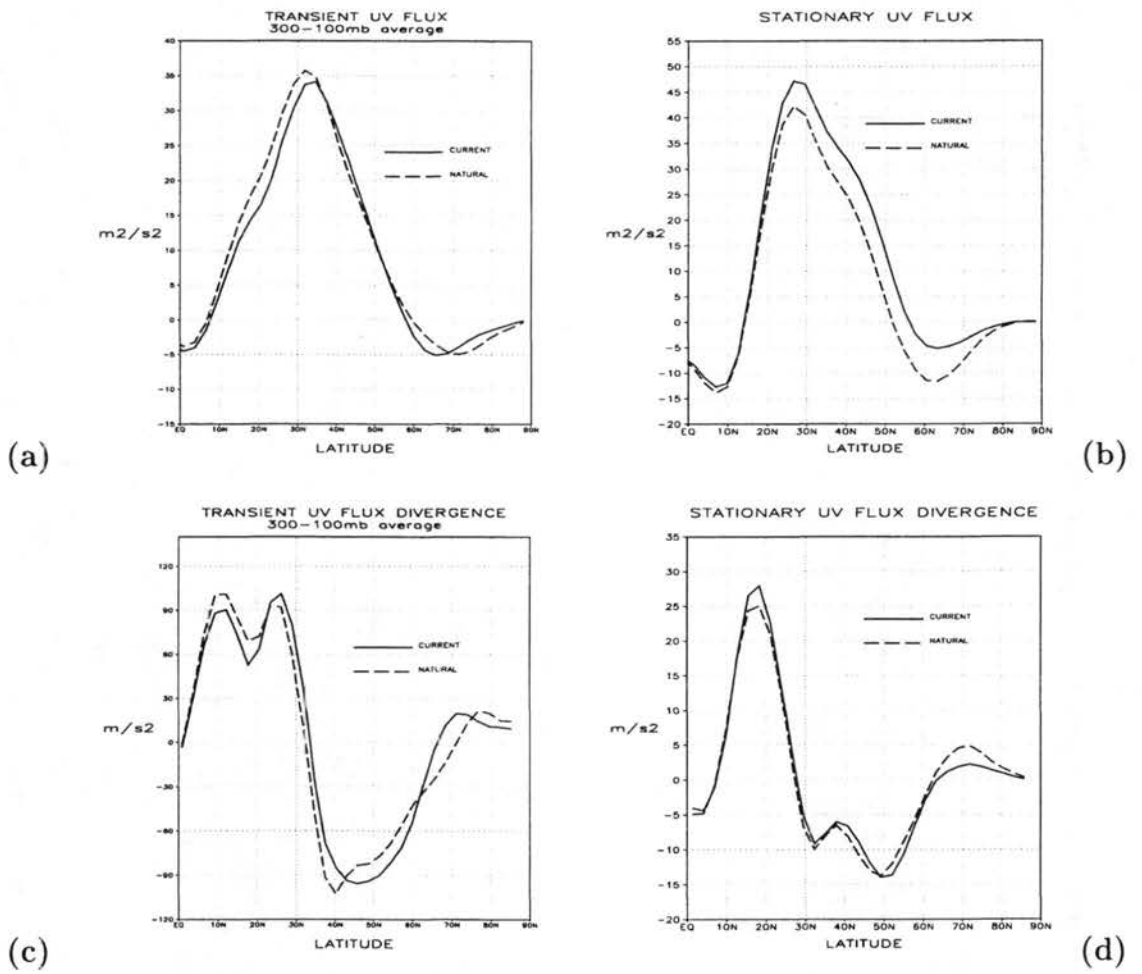

Figure 2.16: 300-100 mb zonally-averaged northern momentum flux and flux divergence for (a) transient wave flux, (b) stationary wave flux, (c) transient wave flux divergence, and (d) stationary wave flux divergence.

noted above under current vegetation. However, the transient flux convergence is quite a bit larger and overpowers the stationary wave effect.

2.9 Comparison with Recently Observed Global Circulation Changes

Because a fully dynamic coupling between all atmospheric, oceanic, and land-surface processes is not achieved in these simulations, it is necessary to interpret our results as sensitivities within a simplified system. Only if land-surface changes were dominant or the couplings with other components of the climate system were weak or on longer time scales, would we expect to see an immediately obvious correspondence between observational evidence of the effects of landuse change and model results. In this section, we look for possible signals corresponding to the model simulations in reported observations recognizing the above limitations.

The January warming in the current vegetation case simulated over much of the land area in the northern hemisphere including most of North America, Europe, and parts of Siberia as well as the cooling over ocean areas is, in some ways, consistent with observational evidence which notes recently increased surface air temperatures over land in northern hemisphere winter, while oceans appear to be cooling (e.g., Wallace et al. 1996; Hurrell 1996; Palecki and Leathers 1993). These authors relate these temperature trends to anomalous circulations associated primarily with the Pacific North America pattern (PNA) and the north Atlantic oscillation (NAO) though other recognized modes of variability such as the tropical northern hemisphere (TNH) pattern (discussed in Section 2.5) are also implicated.

Anomalous circulations in the northern Pacific have been associated with changes in sea surface temperature forcing of tropical convection and seem to be related to recent increases in the duration and magnitude of El Niño events (Trenberth and Hurrell 1994), an effect we have no representation of in the present simulations due to prescribed, annually cycling SSTs. The observed effects of this increase in El Niño events include a heightened tropical hydrological cycle, an amplification and southerly movement of the mid-latitude northern hemisphere storm tracks and an eastward movement and deepening

of the Aleutian low. An index of these observed changes (the NP index= area-averaged surface pressure from 30-65N and from 160E-140W; Trenberth and Hurrell 1994) shows a recent increase in the magnitude of this index of 2.2 mb from the long-term average.

Our simulated circulation changes in the extratropical northern Pacific as measured by the NP index is a decrease of nearly 1.5 mb and shows decreased tropical outflow and a northerly movement of the jet. These effects are opposite in sign to those observed and are consistent with a less active tropical hydrologic cycle in the current vegetation case. This is not surprising because our simulations include no representation of the observed, more frequent, warm eastern and central tropical Pacific ocean temperatures associated with increased El Niño events which appear to have a strong relationship with observed atmospheric circulation changes in the Northern Pacific (Ponte and Rosen 1994, Kumar et al. 1994; Yulaeva and Wallace 1994). However, our simulations indicate decreased easterlies over much of the tropical Pacific Basin under current vegetation which, to first order, might act to amplify the magnitude and frequency of El Niño events (e.g., Trenberth and Hoar 1996).

As a result of the current phase of the NAO the North Atlantic has also experienced large-scale circulation changes during northern winter which have resulted in strong surface warming over land in western Europe and Siberia. These very strong regional warming trends make up a significant portion of the observed area averaged northern hemisphere and global warming trends. An index of the phase of NAO which compares surface pressure between Lisbon, Portugal and Stykkisholmur, Iceland shows the NAO in a positive phase since 1980 with values of the index between +1 to +3 mb (Hurrell 1996). A calculation of the same index in our simulation between the two vegetation cases gives a +3 mb value when going from natural to current vegetation. No strong connection between tropical SST and large-scale circulation changes in the Atlantic (e.g., Kumar et al. 1994) exists. Our results suggest the possibility of an interaction between circulations driven by landcover change and Atlantic climate anomalies.

2.10 Discussion and Conclusions

Landuse changes, particularly in the tropics, should be expected to have global effects. Unlike the fluctuations associated with opposing phases of ENSO, the direct surface heating anomalies and subsequent changes in circulation associated with landuse change are essentially permanent. To investigate the hypothesis that observed landuse change can have effects at global scales, we examined 10 years of modeled equilibrium January climate differences between simulations which were forced at the surface by: a) a spatially realistic depiction of the current land surface, and b) an estimate of natural potential vegetation in equilibrium with current climate.

Wu and Newell (1998) concluded that SST variations in the tropical eastern Pacific have three unique properties that allow the tropical ocean to influence the atmosphere effectively: large magnitude, long persistence, and spatial coherence. Both direct landuse changes and resulting circulation changes in the tropics have similar properties which, in our simulations, resulted in climate anomalies at higher latitudes. The largest climatic changes were not limited to the region of direct landuse change indicating that feedbacks within the tropics and teleconnections from the tropics to higher latitudes were more important than the direct forcing in this case.

Differences between the current and natural vegetation scenarios included a zonally-averaged northward shift and decreased magnitude of tropical convection as well as east-west shifts in tropical convective precipitation particularly in the Pacific basin and the maritime continent. The changes in tropical convection resulted in reduced high-level outflow from the tropics, less direct conversion of divergent kinetic energy to the rotational kinetic energy of the mid-latitude jet which contributed to a northerly shift and a reduction in peak magnitude of the zonally-averaged jet. This is consistent with a reduction in the associated meridional temperature gradient. The shift in pattern and strength of tropical convection also generated anomalous vorticity sources under the current vegetation scenario which appear to have affected climate at high latitudes throughout the northern hemisphere. Shifts in tropical convection also produced reduced easterlies over

much of the tropical Pacific basin and a central Pacific positive convective anomaly suggesting further high latitude effects could arise through a positive interaction with the warm phase of ENSO. These effects are of greatest magnitude in the regions of southeast Asia and the maritime continent which suggests that landuse change in these areas is of considerable importance to the study of global climate. That our vegetation distribution reflects more deforestation in this region than most others may explain, in part, why our extra-tropical results are more clearly evident relative to other GCM landcover change experiments.

A previous simulation (Chase et al. 1996) using a GCM with the same dynamical framework though with differing physical parameterizations from the present work produced similar effects (including a northern shift of the ITCZ and a northward movement and weakening of the zonally-averaged mid-latitude jet) by simply realistically altering the amount of green leaf area in regions affected by human activity. This indicates that vegetative effects on tropical convection may be as controlled by physiological processes as much as by biophysical factors such as albedo and roughness length. This view is given support by Kleidon and Heimann (1998) who found that rooting depth, a biological control on transpiration and soil moisture availability, was a significant factor in the production of latent heat and temperature in tropical regions and therefore affected tropical convection.

These results also suggest that teleconnection patterns due to anthropogenic landcover changes which have already occurred are capable of affecting the temperature and precipitation distributions worldwide and may have already done so. Such effects are traditionally unaccounted for in global climate trend analyses (e.g., North and Stevens 1998) but growing evidence indicates that these effects may have to be accounted for in climate change monitoring efforts (e.g., Pielke et al. 1998a,b and references therein) necessitating further examination of their scope and significance.

Finally, while we do not consider this, or any, climate simulation model to be comprehensive enough to provide reliable climate predictions (e.g., because of the lack of a dynamical ocean component in the present case [Campbell et al. 1995] but also because of imprecise depictions of vegetation properties and the nonlinear feedbacks between these

processes), some observed trends in tropical and northern hemisphere winter circulations are, in part, suggestive of a global response due to landuse change. While the spatial pattern of northern hemisphere warming is not identical in our simulations to that observed, the large-scale circulation changes responsible for it are sufficiently similar to those thought responsible for the observed warming to suggest an interaction. Additionally, the observed pattern of more intense and longer warm ENSO events at the expense of cold ENSO events which is implicated in much of the observed higher latitude winter warming is implicitly simulated by decreased easterlies in the tropical Pacific and a positive convective anomaly in the central Pacific which appears to affect high latitudes as a result of changed landcover. This result highlights a further avenue for investigation. These patterns of recently warming surface temperatures over northern hemisphere land areas resulting solely from dynamical atmospheric shifts have been difficult to associate convincingly with global CO_2 warming (e.g., Plantico et al. 1990; Jones 1988; Hurrell 1996) and our results suggest that global landcover change may already have had an important and measurable effect on the observed global climate state.

Chapter 3

COMPARISON WITH OBSERVED AND CO_2-FORCED CLIMATE CHANGES

3.1 Comparisons of Zonally-Averaged Changes in Thermal and Dynamical Structure

While the results from our global simulations discussed in Chapter 2 bear some resemblance to recently reported changes in long-term climate variability, direct comparisons of model experimental results with more recent observational data (National Center for Environmental Prediction (NCEP) reanalysis; Kalnay et al. 1996) are also very interesting. Figure 3.1a compares changes in the observed, zonally-averaged 200 mb height gradient in the northern hemisphere between the first 10 years (1958-1967) of the current NCEP reanalysis and the last 10 years (1988-1997). This field is interesting for climate change studies because it quickly summarizes the depth-averaged thermal state of the atmosphere and also, by the thermal wind relation, can be used to infer the dynamical state of the atmosphere including the position and intensity of the mid-latitude jet. Figure 3.1a shows a decreased minimum in height gradient at approximately 33N which represents a decrease in maximum baroclinicity in the last decade relative to the first decade of the observations. There has also been a slight shift northward of the southern edge of the minimum and a northerly broadening of the minimum on its northern side in the last decade. Near 70N, differences between the two curves change sign.

Figure 3.1c shows the northern hemisphere 200 mb height gradient field as simulated in the current and natural vegetation cases. A comparison with Fig. 3.1a show substantial agreement between the observed changes in gross structure of the atmosphere between the beginning and end of the NCEP reanalysis time series and the differences simulated due to historical landcover change. The similarities between observed changes in the most recent

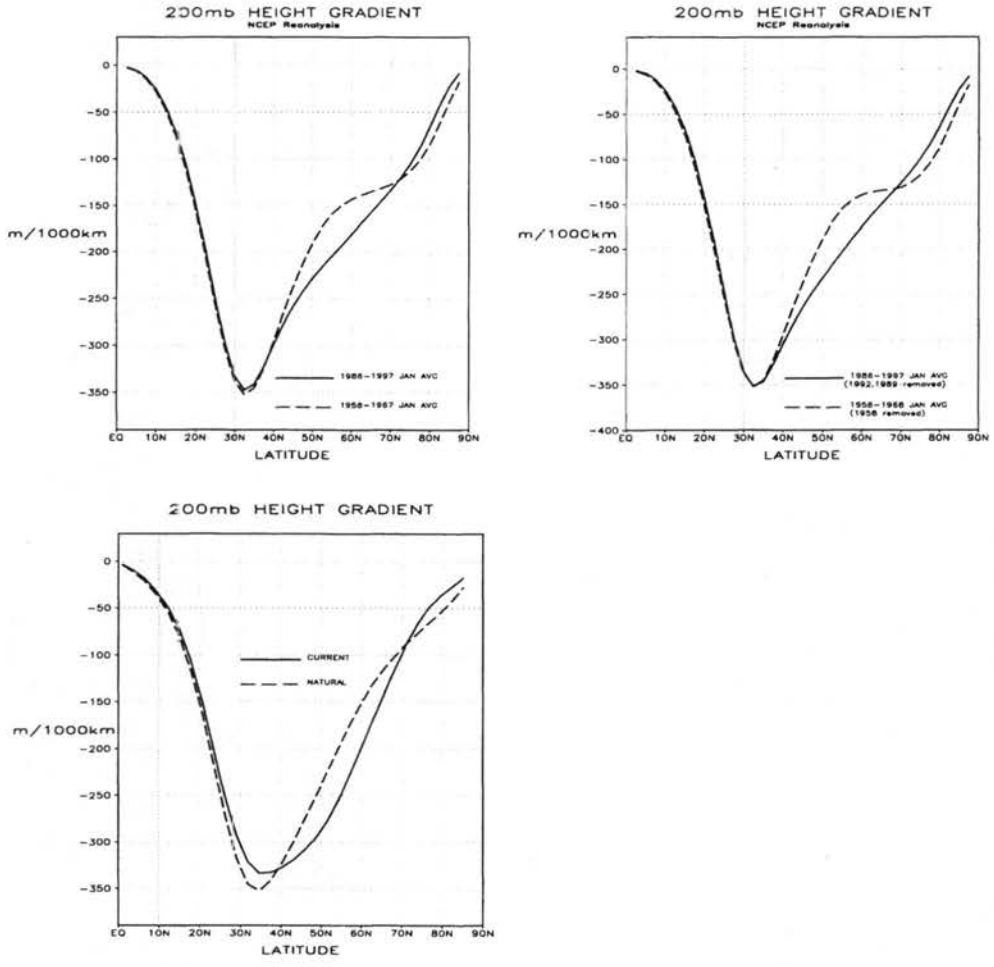

Figure 3.1: Observed NCEP January 200 mb gradient in geopotential height zonally averaged in the northern hemisphere for (a) comparison of the 1958-1967 average with 1988-1997 average, (b) comparison of the 1958-1968 average with the 1986-1997 average with the years 1958, 1989, and 1992 removed in order to isolate years without strong ENSO fluctuations (discussed in text), and (c) Current and Natural vegetation simulation (same as Fig. 2.13b)

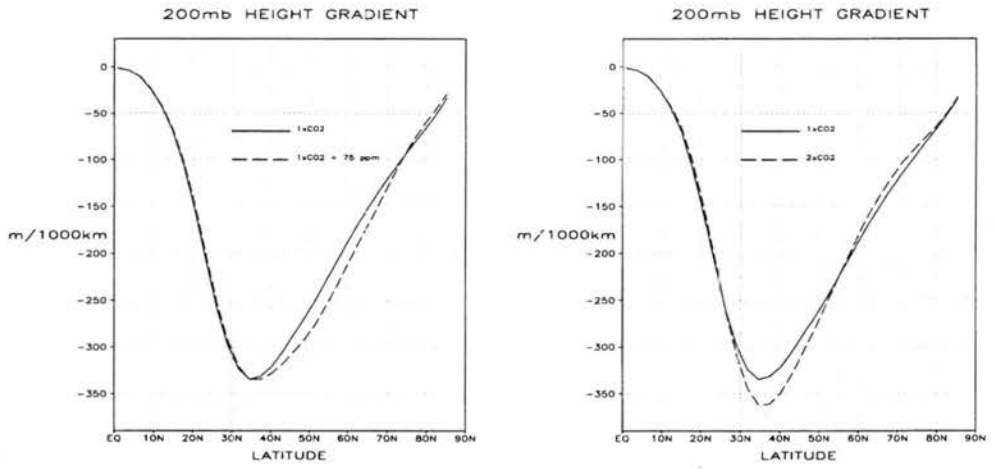

(a) (b)

Figure 3.2: 200 mb height gradient as simulated in a transient increasing CO_2 simulation for (a) $1\times$ CO_2 vs. $1 \times CO_2 + 75$ ppm, and (b) $1 \times CO_2$ vs. $2 \times CO_2$.

decade and under current vegetation include a reduced minimum, a northerly broadening, a shift north, and a change in sign of the differences in height gradient between the two curves at about 70N.

The differences in atmospheric structure between the beginning and end of the reanalysis time series are also likely to be affected by changes in ENSO during the period. In order to examine the effects of ENSO on these fields Fig. 3.1b compares the gradient in 200 mb heights but has years with the strongest ENSO fluctuations (defined here as years when nino3 > 1.5 which included 1958, 1989, 1992) removed from the averages. These were replaced with 1968, 1986 and 1985 respectively to maintain a ten-year average. In this case the amplitude of the minimum is hardly changed between the beginning and end of the time series unlike the landcover change response seen in Fig. 3.1c. The broadening to the north of the minimum is more apparent when strong ENSO years are removed which is more like the simulated response to altered landcover.

For comparison, we used data from a transient CO_2 experiment performed by a collaboration between the Japanese Electric Power Institute and the National Center for Atmospheric Research (NCAR; files available through the NCAR CSM homepage as experiment B06). These simulations were performed using the CCM3/LSM coupled model but also included a full dynamical ocean and sea-ice model. This is not strictly a one-to-one

comparison because of differences in model configuration, but does highlight important features in simulations of potential climate changes. The same gradient in 200 mb heights for an experiment where CO_2 was increased at 1% per year is shown in Fig. 3.2. $1 \times CO_2$ + 75 ppm represents the current level of CO_2 loading above pre-industrial and in this case, changes in the structure of this field are of similar magnitude both to observed changes and to changes as a result of observed changes in vegetation. In this case, the minimum appears to have decreased slightly and the gradient has moved somewhat northerly and also broadened to the north in a similar manner as under vegetation change. By the time CO_2 has doubled, however (Fig. 3.2b), the maximum baroclinicity has clearly increased beyond that of the control and the northerly shift and broadening is no longer apparent. This is an opposite response to that seen in observations in the last 19 years as well as to that seen in the vegetation change scenario.

3.2 Comparisons of Changes in 1000-850 mb Depth-Averaged Temperatures

As a way to examine the spatial structure of observed climate changes, Fig. 3.3 compares depth-averaged temperature trends from 1000-850 mb as observed in the NCEP reanalysis satellite data from 1979-1997 with differences in this field between current and natural vegetation cases and with a representation of the effect of current CO_2 loading. Data before 1979 is suspect in the NCEP reanalysis due to a large jump presumably resulting from the inclusion of satellite data in the late 1970's (e.g., Santer et al. 1998, Pielke et al. 1998) which to some degree limits our ability to make longer term comparisons. It should be noted here that there is some question as to the validity of this observational dataset. (e.g., Santer et al. 1998). There is however, a close spatial correspondence between the NCEP data and the Microwave Sounding Unit (MSU) data, particularly at high northern latitudes and over land (Chase et al. 1999 and discussed further in chapter 4). A comparison of the reliability of regional trends in observational data including the NCEP reanalysis, the microwave sounding unit (MSU) and the surface data network is given in Chapter 4.

Simulated January temperature differences resulting from vegetation change (Fig. 3.3c) have similar magnitude regional changes occurring in the same places as in

the reanalysis. Additionally, remarkably similar spatial patterns in the northern hemisphere occur as a result of vegetation change as in the observed trends in Fig. 3.3a. Both show a warming over the continental United States and Southern Canada, a cooling over Northern Canada, Greenland, Alaska and the eastern tip of Siberia; a warming over most of eastern Asia, a cooling in central Asia and eastern Europe, and a warming in western Europe. Strong observed cooling trends in Antarctica are not reproduced by the model though cooling at the southern tips of South America and Africa and Australia are generated in the model in agreement with observations.

The July temperature differences resulting from vegetation change again show differences in the same regions and of the same amplitude as those observed though with little of the similarity in spatial pattern seen in the January averages, The largest differences are in the winter hemisphere in both cases as would be expected if changes in the position and amplitude of the winter hemisphere jet were most affected.

As a final comparison, Fig. 3.3e shows the difference in January temperatures due to an increase in CO_2 of 75 ppm (approximately the present level of CO_2 loading above ambient). Temperature differences are of slightly higher amplitude in this case when compared with differences due to vegetation and are therefore more similar in amplitude with observed changes in the past 2 decades. The spatial pattern, however, is less similar than that due to changes in vegetation. Again, the largest changes occur in the same regions in all plots. In July, the observed trends are larger than those due to either simulated forcing (CO_2 or vegetation). The CO_2 forced simulation shows mostly warming trends except in Antarctica which is not borne out by observations. In the CO_2-forced case in July (Fig. 3.3f), the largest differences are still in the northern hemisphere in opposition to both observations and to the vegetation-forced case. This is an indication that the hypothesis of tropical landuse dominated climate change as suggested in Chase et al. (1996, 1999) may be more supportable than that of greenhouse gas induced global warming, at least over the past two decades.

Comparisons between observed changes in the last 19 years with simulations with present levels of CO_2 change and vegetation change indicate that changes in vegetation,

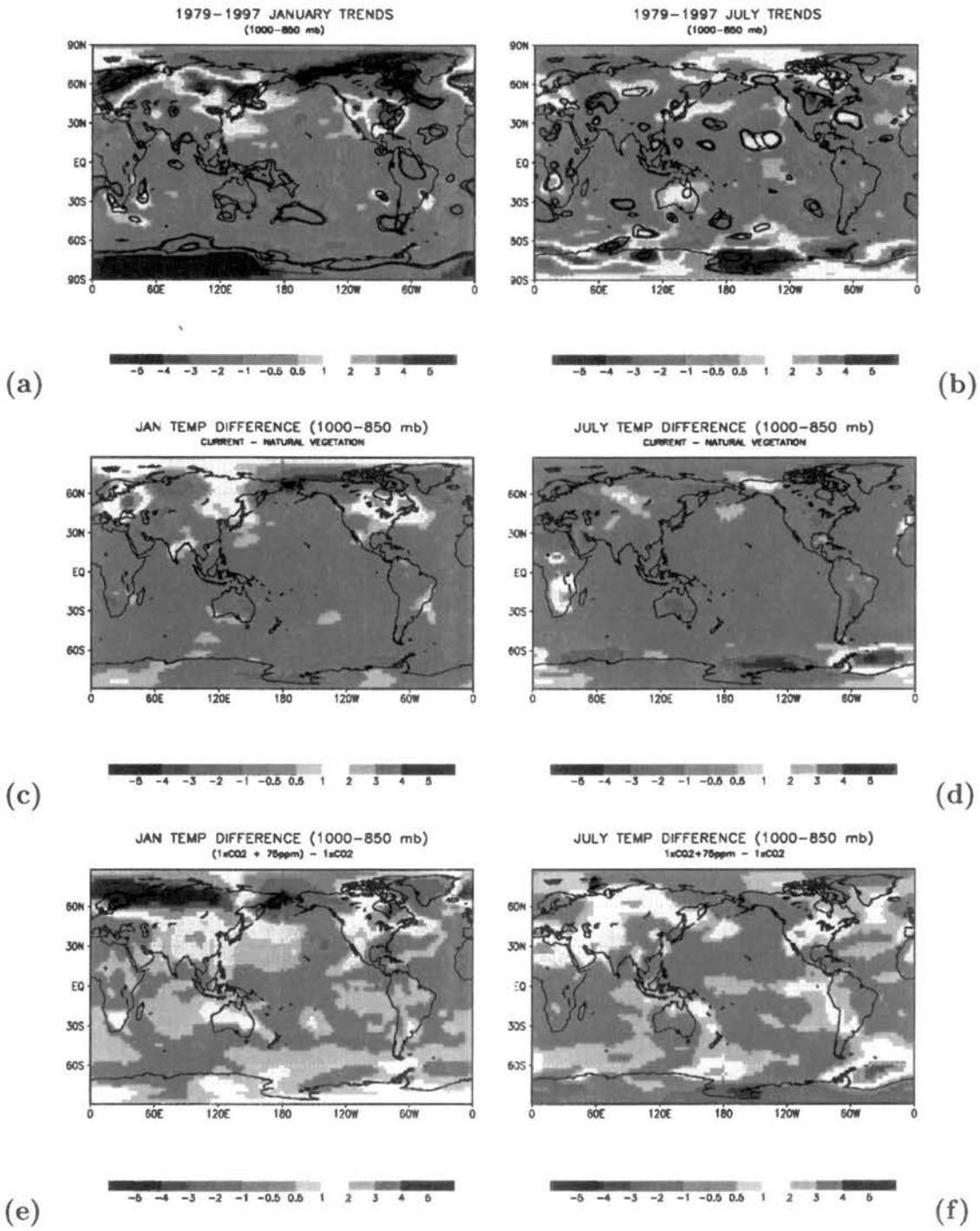

Figure 3.3: (a) Observed January 1000-850 mb depth-averaged temperature change from 1979-1997 (C/19 years). (b) Observed July 1000-850 mb depth-averaged temperature change from 1979-1997 (C). (c) 1000-850 mb January temperature difference due to vegetation change (current–natural) (C). (d) 1000-850 mb July temperature difference due to vegetation change (current–natural) (C). e) 1000-850 mb January temperature difference due to present CO_2 loading ($1\times$ CO_2 + 75 ppm – 1 × CO_2) (C). (f) 1000-850 mb July temperature difference due to present CO_2 loading (1 × CO_2 + 75 ppm – 1 × CO_2).

of the magnitude already observed, appear to be a climate forcing of substantially equal magnitude that due to present levels of atmospheric CO_2 loading. Despite this, claims have been made that the detection of a climate signal resulting from increased CO_2 have been made on numerous occasions (IPCC 1996). The present research suggests that the detection of such a signal may be convoluted with other factors such as landuse change which have not been sufficiently accounted for. There is also some evidence that the climatic signal resulting from landcover change may be responsible for a signal which is more similar to observed changes in climate than that of rising CO_2. An full ensemble mean of several CO_2 and landcover climate change experiments would be necessary, however, to fully explore the representativeness of these patterns.

Chapter 4

A REGIONAL COMPARISON OF TRENDS IN OBSERVATIONAL DATASETS

4.1 Introduction

Significant controversy exists over the accuracy of all long-term global temperature datasets. The surface network as a whole is hampered by inadequate spatial sampling, missing data, as well as by discontinuities which affect each station differently including changes in sensor type, sensor interpretation, positioning, microclimate, local land use change and the possibility that a particular station is unrepresentative of the broad region around it (e.g., Karl and Jones 1989, Balling 1991). These effects have not been fully quantified (Jones 1995; Karl et al. 1995). The rawinsonde network shares many of the uncertainties of the surface network with documented problems due to inadequate spatial sampling as well as spurious trends due to systematic equipment changes (e.g., WMO 1986, Jenne and McKee 1985, Gaffen et al. 1991, Parker et al. 1997, Gaffen 1994). df The two primary datasets used in this study, the Microwave Sounding Unit (MSU) 2r Version C satellite data (Spencer and Christy 1990) and the National Center for Environmental Prediction (NCEP) reanalysis (Kalnay et al. 1996) are attractive to those concerned with regional climate changes both because of their uniform global coverage and the relative uniformity of methodology and sensors and therefore a corresponding ease in documenting biases. However, spurious trends have been identified in both the MSU data and NCEP reanalysis (Hurrell and Trenberth 1998, Stendel et al. 1998, Santer et al. 1998, Pielke et al. 1998c) to the extent that some (e.g., Hurrell and Trenberth 1998; Summary from Proceedings of the First WCRP Conference on Reanalyses 1998) have argued that both datasets are unsuitable for trend analysis.

In this paper, we examine the regional trends in depth-averaged tropospheric temperatures as represented in the NCEP reanalysis data and in the MSU data for the period 1979-1997. This period is interesting not only because of the availability of independent data sources but also because it has been suggested by some observational and modeling studies that the greenhouse warming fingerprint should become most evident at about this time (e.g., Bengtsson 1997, Yu-Hong and Shao-Wu 1992). Despite the fact that the surface network observations must be used cautiously at regional scales (Jones 1995), we also compare the MSU and NCEP data to the surface data in order to assess regional consistency. We attempt to circumvent the issue of spurious trends by focusing solely on regional temperature trends that are of statistical significance and have larger magnitudes than any documented bias. These are regions that are most likely to be experiencing real climatic shifts, particularly when they are mirrored in several datasets. Regional trends are also a more basic quantity than zonal or global averages and are therefore more important to monitor for trend and bias detection, for comparisons with climate model simulations and for use by the impact assessment community (Beniston 1998).

4.2 Documented Biases

The MSU satellite data has received significant scrutiny for discontinuities and biases because globally-averaged linear trends in these data contradict those of the surface observing network (e.g., Stendel et al. 1998, Santer et al. 1998, Jones et al. 1997, Hurrell and Trenberth 1997). Discontinuities in 1981 and 1991 resulting from changes in satellite (Hurrell and Trenberth 1997) have apparently been adjusted for in the MSU data used here (Version C; Stendel et al. 1998, Christy 1998). Additional biases due to orbital decay (Wenzt and Schabel 1998) and instrument heating have not, as yet, been compensated for, but preliminary estimates of their combined impact on the MSU data is slightly less than 0.1 °C/19 years in the global average (Christy 1998, Stendel et al. 1998). These errors in trend estimates have been discussed in terms of global averages and any possible regional biases due to these adjustments are undocumented. Potential errors in MSU retrievals due to systematic regional changes in atmospheric hydrometeor content have also been

identified (Prabhakara et al. 1996) though strong trends in these quantities have not, as yet, been shown over this time period nor is there consensus on the magnitude of the error (Spencer et al. 1996). All regional trends significant at the 90% level in a 2-tailed t-test in the MSU data also exceeded 0.1 °C/19 years in this analysis and so can be considered reliable in the sense that they exceed an average documented bias and are statistically different from zero.

Though more difficult to quantify than in the MSU data because of the use of various data sources in different regions, several biases in the NCEP reanalysis data have also been documented. The first is a large upward jump in temperatures in the late 1970's possibly as a result of the inclusion of satellite data at this time (Pielke et al. 1998c, Santer et al. 1998). Since we use only data after 1979 in the present study, this shift will not affect our results. Other, smaller discontinuities in the NCEP data have also been recorded though their magnitude is insufficiently quantified (Basist and Chelliah 1997, Hurrell and Trenberth 1997). Additionally, biases carried over from inclusion of rawinsonde and satellite data may introduce regional errors in this dataset. The largest documented systematic difference in rawinsonde and satellite data which are assimilated into the reanalysis appear to also be on the order of 0.1 °C/19 years, though individual stations may have larger biases (Gaffen 1994). Shifts due to changing algorithms in the reanalysis also appear to be of this order. We therefore again use this threshold to determine a reliable, base level, regional trend in the NCEP reanalysis. However, because regional biases are not well quantified for either dataset, we compare the sensitivity of our results when the minimum trend considered is increased by up to a factor of five. We also examine spatial consistency between the two datasets and with the surface observational network as a step toward both identifying local biases and confirming real trends.

4.3 MSU 2r Regional Trends

Figure 4.1 shows the 1979-1997 trends from the MSU channel 2r. We ignore all regions which are not significant at the 90% level in a 2-tailed t test and which also are not larger in magnitude than documented systematic biases (see discussion in Section 2).

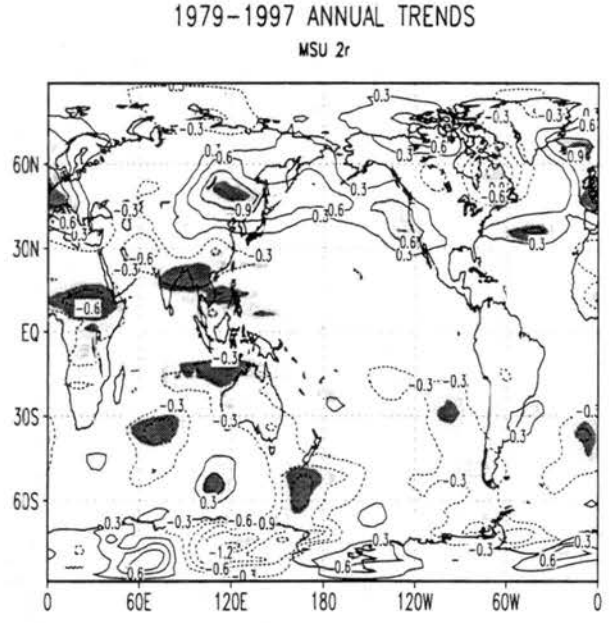

(a)

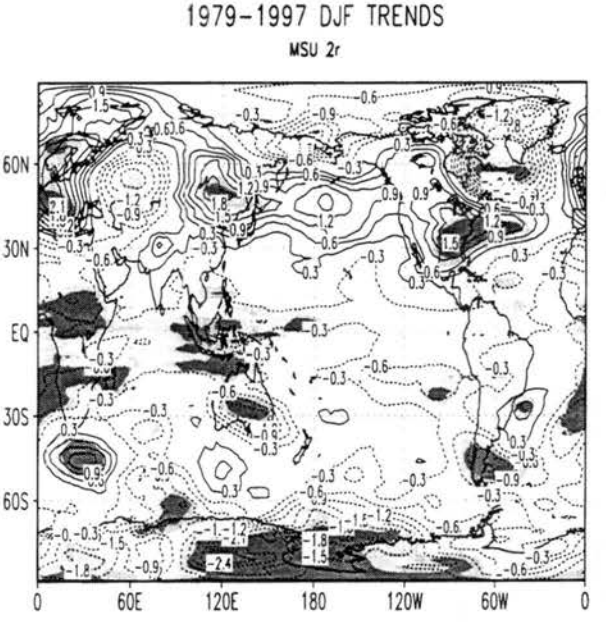

(b)

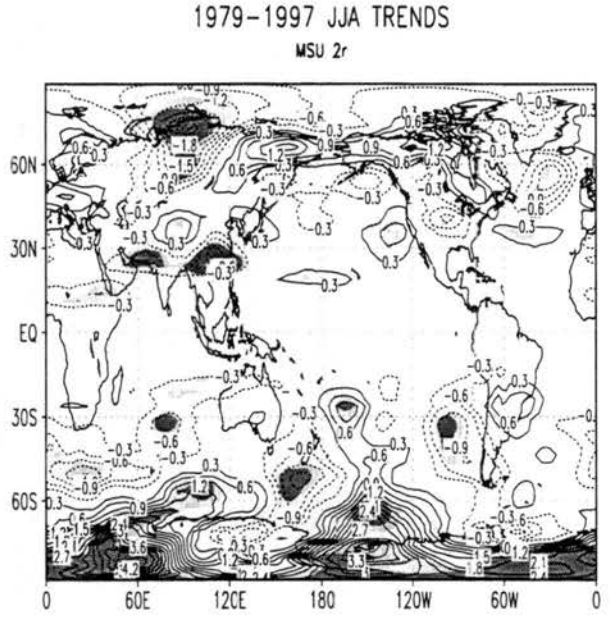

(c)

Figure 4.1: MSU 2r temperature trends in C/19 years for (a) annual averages, (b) winter (DJF) averages, and (c) summer (JJA) averages.

In the annual average (Fig. 4.1a) several regions show strong trends of both warming and cooling in the MSU data. Regions of significant warming include central east Asia, the western coast of the United States, the central North Atlantic, the northern North Atlantic, western Europe and one region in the southern hemisphere ocean. Regions of significant cooling include tropical Africa, southern Asia, eastern Canada, the northwest coast of Australia and adjacent ocean as well as several other regions in the southern hemisphere oceans. An area weighted average over the significant regions only (Table 4.1) gives a trend of –0.1555 °C/19 years. When weighted over the entire globe, the average significant trend is –0.0185 °C/19 years. Because MSU trends in regions of high terrain such as Antarctica are suspect (Christy 1998, Stendel et al. 1998), we also provide averages which exclude regions south of 60S (Table 4.2). In the annual average the average trend for the globe north of 60S is –0.1403 °C/19 years weighted over regions with significant trends and –0.0176 °C/19 years when the significant trends are weighted over the area north of 60S. Tables 4.1 and 4.2 also provide the global average of all trends for comparison.

In the winter averages (December, January, February; for the purposes of this paper, seasons are defined with respect to the northern hemisphere) strong, significant trends of both signs are also evident (Fig. 4.1b). Note that for 1979, only January and February are included in the winter average. Warming occurs in western Europe, east central Asia, the North Pacific, the central North Atlantic, the eastern United States and off the southern coast of Africa. Cooling occurs in eastern Canada, tropical and southern Africa, southeast Asia and the maritime continent, the equatorial Pacific, Australia, the southern tip of south America and off the eastern coast of South America. The global average of these trends for the winter season weighted over regions of significance is –0.3912 °C/19 years (Table 4.1) and –0.2345 °C/19 years (Table 4.2) excluding regions south of 60S.

In the summer averages (June, July, August; Fig. 4.1c), trends of both sign are again apparent. Small regions of warming occur in western Alaska, the central North Pacific, off the west coast of the continental United States, the central North Atlantic, the central South Pacific and two regions off the coast of Antarctica centered at approximately 90E and 150W. Regions of cooling include northwestern Asia, southern and southeastern Asia,

Table 4.1: 1979-1997 globally-averaged trends in °°C/19 years. Significant trends weighted over areas of significance. Significant trends weighted over area of globe where zero trends were assumed if the regional trends were statistically insignificant; global average trends where no level of minimum bias or significance is assumed.

MSU 2r	Sig. Trends	Global Average Sig. Trends	Global Average Trends
ANNUAL	-0.1555	-0.0185	-0.0846
DJF	-0.3912	-0.0708	-0.1671
JJA	0.1610	0.0115	0.0014
NCEP 1000-500 mb			
ANNUAL	-0.3199	-0.0514	-0.1053
DJF	-0.4989	-0.0743	-0.1927
JJA	0.0779	0.0085	0.0029

Table 4.2: As in Table 1 but averaged from 60S-90N.

MSU 2r	Sig. Trends	Global Average Sig. Trends	Global Average Trends
ANNUAL	-0.1403	-0.0176	-0.0807
DJF	-0.2345	-0.0405	-0.1113
JJA	-0.5511	-0.0320	-0.0706
NCEP 1000-500 mb			
ANNUAL	-0.2379	-0.0380	-0.1017
DJF	-0.1572	-0.0213	-0.1269
JJA	-0.3944	-0.0382	-0.0786

tropical Africa, and 4 centers in the southern hemisphere oceans. The average of these regions for the summer season weighted over areas of significance is 0.1610°C/19 years (Table 4.1) and –0.5511 °C/19 years (Table 4.2) excluding regions south of 60S.

4.4 NCEP Regional Trends

Figure 4.2 shows the corresponding NCEP 1000-500 mb depth-averaged temperature trends. This layer includes most of the atmosphere sampled by the MSU 2r sensor which has a weighting function peaking near 740 mb (Christy 1995). For the annual trends, (Fig. 4.2a) a warming occurs in central east Asia, the western coast of the United States, the central North Atlantic, western Europe and a center in south central Africa. Cooling regions include northern and southern Africa, west central Asia, the central North Pacific, the maritime continent, northern South America, and four centers in the southern hemisphere oceans. The global averages of these trends for the regions of significance are –0.3199 °C/19 years (Table 4.1) and –0.2379 °C/19 years (Table 4.2) for regions north of 60S. Significant trends weighted over the area of the globe are –0.0514 °C/19years and –0.0380 °C/19 years for the area north of 60S.

For the winter season (Fig. 4.2b), warming occurs in central and western Europe, east central Asia, the Arabian sea, the southeastern United States and off the southern tip of Africa. Cooling occurs in west central Asia, northern and southern Africa, eastern Canada, and southern South America. The area averages of these trends weighted over regions of significance are –0.4989°C/19 years (Table 4.1) and –0.1572°C/19 years (Table 4.2) excluding regions south of 60S.

The summer season (Fig. 4.2c) also shows trends of both sign in the NCEP data with warming centers in southwestern Asia, southern Africa, Alaska, and the central North Atlantic. Large areas of warming also occur off the coast of Antarctica in three different areas. Cooling is centered on northwestern Asia, south central Asia, the Arabian Sea, the maritime continent, Amazonia and three centers in the southern hemisphere oceans. The global trend for the regions of significance are 0.0779 °C/19 years (Table 4.1) and –0.3944°C/19 years (Table 4.2) excluding regions south of 60S.

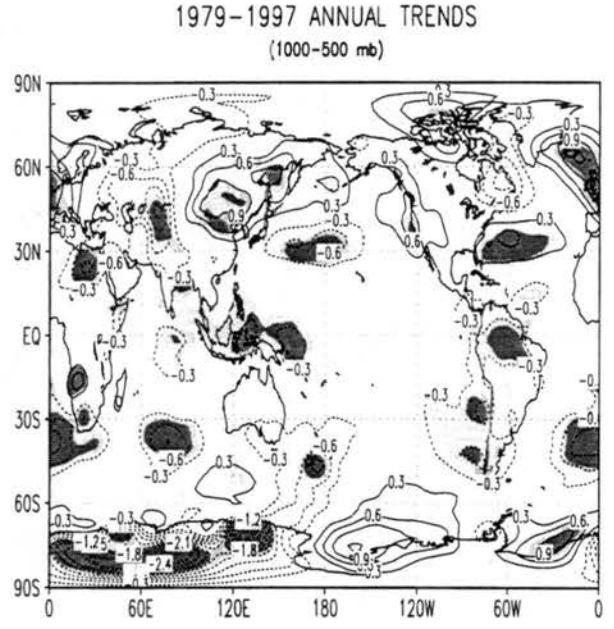

(a)

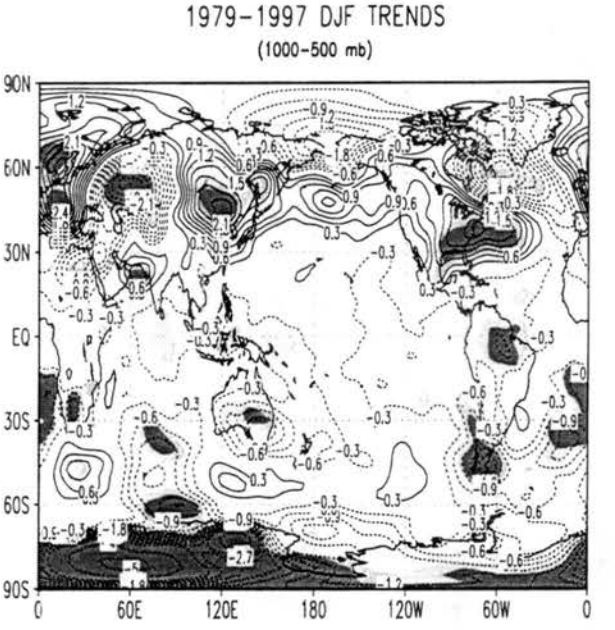

(b)

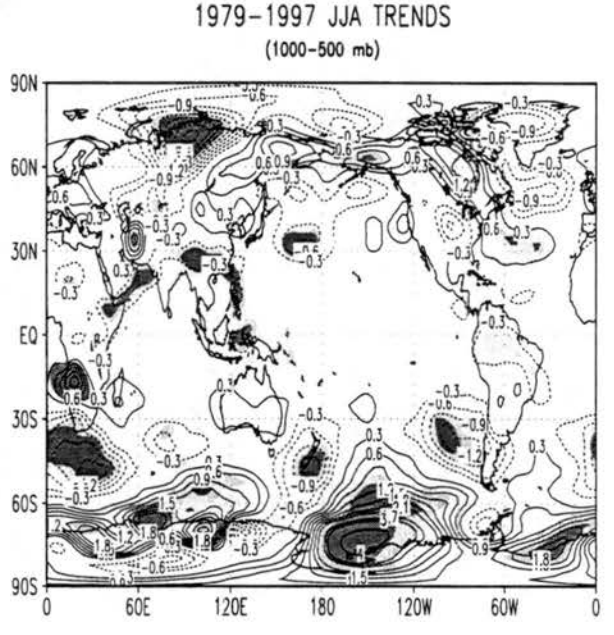

(c)

Figure 4.2: NCEP 1000-500 mb depth-averaged temperature trends in C/19 years for (a) annual averages, (b) winter (DJF) averages, and (c) summer (JJA) averages.

What is clear from these regional trends is that warming is not dominant in either area or magnitude among the most reliable trends in both datasets. Both in winter and in the annual average, summing over regions of significant trends in the last 19 years, the areally weighted trend is cooling. In the summer season there is a warming of lesser magnitude than the winter cooling though this appears to occur mostly in Antarctica since cooling dominates regions to the north of 60S in the winter, summer and annual averages. We next examine the coherence of the two datasets with respect to the regional trends.

4.5 Regional Comparison between MSU and NCEP trends

While these datasets are not exactly comparable in terms of vertical weighting, our purpose here is not a strict intercomparison but rather to highlight the similarities and differences between the regional trends found in MSU data and those found using the depth-averaging technique based on height data discussed by Pielke et al. (1998a, b) for the NCEP data. It is well known that the MSU data and NCEP reanalysis data are highly correlated temporally (e.g., Hurrell and Trenberth 1998, Santer et al. 1998); we now examine the spatial consistency of trends in these data since 1979.

We first compare all trends in both datasets. Spatial correlations between the MSU and NCEP 1000-500mb annual, winter and summer trends are given in Table 4.3 and an overlay of the two datasets is presented in Fig. 4.3. Figure 4.3 shows high correspondence between the two datasets at high latitudes (particularly over land) in both the northern and southern hemispheres which is reflected, for the most part, in the strong correlation coefficients for these latitude belts in Table 4.3. This adds confidence to these high latitude regional trends. The spatial correspondence between the two datasets decreases markedly for tropical regions, particularly for 0-30S in the annual average. Correlations between the two datasets are generally highest in the northern hemisphere and in the winter averages. Correlations in the annual average can be quite a bit smaller than both the winter and summer correlations indicating stronger anti-correlation in the spring and fall for those latitude belts. While both datasets show overall tropical cooling, the disagreement makes all annual, summer and winter regional trends in these regions suspect until other, independent confirmation occurs.

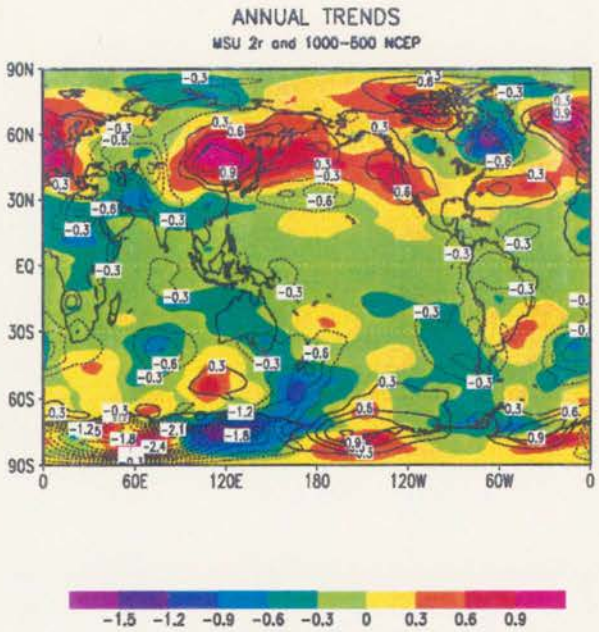

(a)

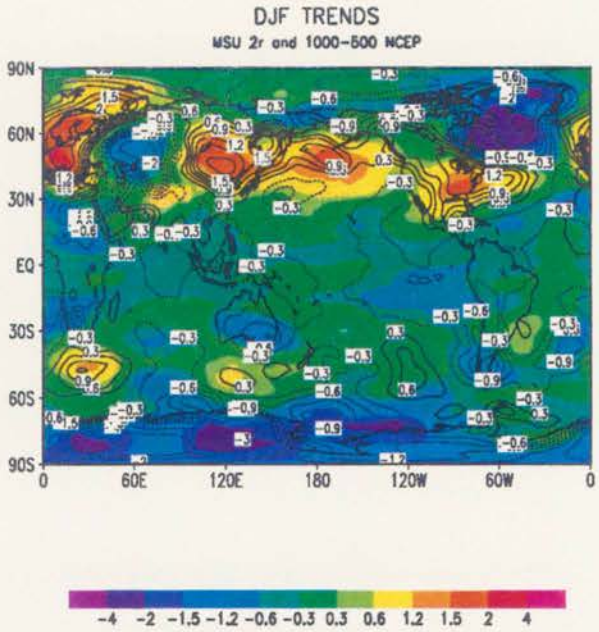

(b)

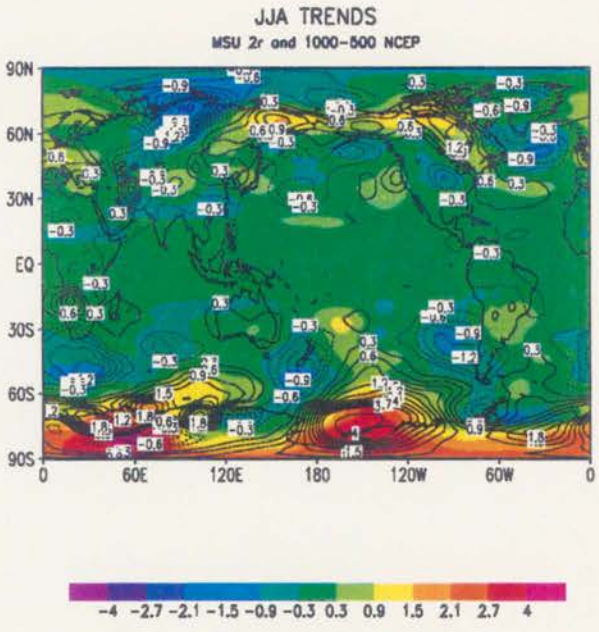

(c)

Figure 4.3: MSU (shaded) and NCEP 1000-500 mb depth-averaged (contoured) temperature trends in °C/19 years for (a) annual averages, (b) winter (DJF) averages, and (c) summer (JJA) averages.

Table 4.3: As in Table 4.1 but a comparison of MSU and NCEP 1000-500 mb annual trends at increasing minimum trend level.

MSU 2r	Sig. Trends	Global Average Sig. Trends	Global Average Trends
0.1°C/19yr	-0.1555	-0.0185	-0.0846
0.3°C/19yr	-0.1381	-0.0137	-0.0846
0.5°C/19yr	-0.0033	-0.0002	-0.0846
NCEP 1000-500 mb			
0.1°C/19yr	-0.3199	-0.0514	-0.1053
0.3°C/19yr	-0.3297	-0.0451	-0.1053
0.5°C/19yr	-0.3456	-0.0306	-0.1053

We next focus only on regions of significant trends in the annual, winter and summer averages. These regions are often offset slightly in space and can cover different total areas in the two data sets. However, there exists substantial qualitative agreement on the position and strength of significant annual trends (Figs. 4.1a and 4.2a) in mid-latitudes of both hemispheres. Agreement again decreases significantly in the tropics though both datasets show a general annual cooling among significant trends in this region. Significant warming trends over east central Asia, the western coast of the United States, western Europe and the central North Atlantic appear in both datasets. Cooling centers in eastern Canada (statistically insignificant in the NCEP data) and in the southern hemisphere oceans also show substantial positional agreement. Regions of large disagreement between the two datasets include significant cooling centers in central Asia, the central North Pacific, tropical Africa, and Amazonia which appear in the NCEP data but not in the MSU data.

In the winter season (Figs. 4.1b and 4.2b), warming trends in east central Asia, the eastern United States and western Europe appear in both datasets. The cooling center in west central Asia appears in both datasets in this season but is insignificant in the MSU data. A cooling center in eastern Canada is significant in the winter season in both datasets. In the southern hemisphere, warming off the southern coast of Africa and cooling off the southern coast of South America also appears in both datasets. Australian cooling

is significant in the MSU data, but not in the NCEP data. Most tropical regions show cooling in both data sets though the MSU data has a larger region of the tropics cooling significantly.

For the summer season (Figs. 4.1c and 4.2c), a large, strong cooling center in north central Asia appears in both datasets as does cooling in south central and southeastern Asia. Four cooling centers in the southern hemisphere oceans also appear in both datasets. A warming in the central North Atlantic and in western Alaska also shows up in both datasets. Regions of significant disagreement in the summer season include a strong warm trend in southern Africa in the NCEP data which is not indicated in the MSU data and a cooling in Amazonia in the MSU data is not shared by the NCEP data.

4.6 Higher Amplitude Trends

Because our selection of a bias cutoff for strong, reliable trends is somewhat arbitrary (particularly in the case of the NCEP reanalysis), and uses spatially-averaged values for the most part, we compare significant regional trends at higher amplitude cutoff values than the 0.1°C/19 years discussed in Sections 3 and 4 and shown in Tables 4.1 and 4.2. For comparison, Table 4.4 shows annual average results when only trends greater than 0.3°C/19 years and 0.5°C/19 years are included in the analysis. For comparison, the difference in global trends between the MSU data and the surface record during this time period is nearly 0.4°C/19 years (Table 4.1 and Table 4.6).

Table 4.4: Correlation between MSU and NCEP 1000-500 layer-averaged trends by latitude belt.

	Globe	60S-90N	90S-60S	60S-30S	30S-0	0-30N	30-60N	60-90N
ANN	0.4964	0.7393	0.1732	0.6131	0.0974	0.4889	0.8031	0.7818
DJF	0.7934	0.8665	0.5861	0.7286	0.4763	0.6652	0.8878	0.9248
JJA	0.7053	0.7922	0.3149	0.8398	0.3103	0.3124	0.7443	0.8842

For the annual MSU trends, all trends of higher amplitude still show average cooling although the magnitude of the trends become less negative as the cutoff value increases. For the 1000-500 mb NCEP trends, a similar pattern of consistently negative

trends emerges. These, however, become more negative as the amplitude of the cutoff increases.

4.7 Comparisons with Shallower NCEP Layers

Because depth averaging may remove real differences in atmospheric vertical structure, we examine shallow layer annual averages in the NCEP data and compare them to the 1000-500 mb layer shown in Fig. 4.1a. Figure 4.4 shows the NCEP reanalysis annual averages for the 1000-850 mb layer (Fig. 4.4a) and for the 1000-925 mb layer (Fig. 4.4b). Both figures show a similar distribution of significant regional trends as the 1000-500 mb layer.

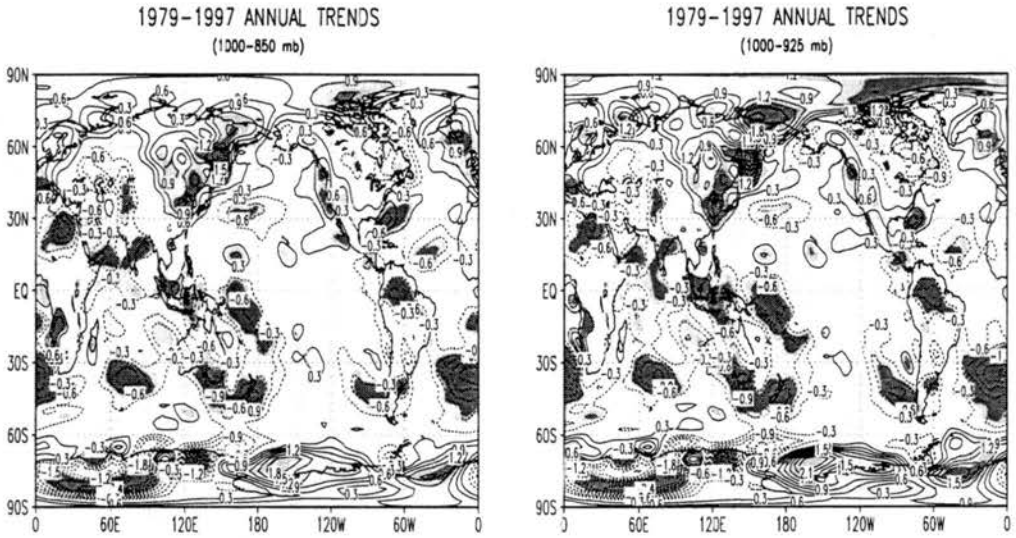

Figure 4.4: NCEP depth averaged annual temperature trends for (a) 1000-850 mb, and (b) 1000-925 mb.

The strength, statistical significance and area affected by significant trends generally increases, however, as the depth of the layer decreases. For instance, the warm anomaly in east central Asia in Fig. 4.2a covers a smaller area than the corresponding anomaly in the 1000-850 mb (Fig. 4.4a) and 100-925 mb (Fig. 4.4b) layers. It has a maximum magnitude of approximately 0.9°C/19 years in the deepest layer, while in the 1000-850 layer it reaches a magnitude of more than 1.5°C/19 years and in the 1000-925 layer it exceeds 2.0°C/19 years. Warming in northern Canada increases with decreasing layer depth as does the

cooling in the 4 cooling centers in the southern Hemisphere oceans and the cooling center over, and to the west of the maritime continent. All anomalies over Antarctica increase with decreasing layer depth.

However, warming centers in western Europe and off the east coast of the United States and a cooling center in the central North Atlantic diminish with decreasing layer depth. The warming center off the west coast of the United States increases in area and magnitude from the 1000-500 layer to the 1000-850 layer but decreases in area in the shallowest layer.

Table 4.5 compares average annual value for each layer discussed in this section and shows cooling dominates in all layers to varying degrees with the 1000-850 mb being intermediate in amplitude to the 1000-500 mb layer and the 1000-925 mb layer, with the shallowest layer showing the strongest cooling.

Table 4.5: As in Table 4.1 but a comparison of NCEP regional, annual trends in various layers.

	Sig. Trends	Global Average Sig. Trends	Global Average Trends
1000-500 mb	-0.3199	-0.0514	-0.1053
1000-850 mb	-0.2930	-0.0580	-0.0682
1000-925 mb	-0.3263	-0.0699	-0.0772

4.8 Comparison with the Surface Temperature Record

For comparison purposes we include a similar analysis performed on the surface temperature record described in Parker et al. (1994) over the same time period. While caution needs to be exercised when applying this data to point and regional scales (Jones 1995) due to missing values and uncorrected discontinuities, we attempt to identify where regionally significant trends show agreement between these and the tropospheric atmosphere data presented in previous sections.

Figure 4.5 shows the annual, winter and summer season trends in the surface data network. In the annual trends (Fig. 4.5a), the surface network shows the broad area of

warming in eastern Asia evident in both the MSU and NCEP data. Trends in this region are stronger than in the other two datasets and significant over a much larger area which extends across the North Atlantic and far into southeast Asia. Both the MSU and NCEP datasets show cooling in southeast Asia and over much of the maritime continent. A warming trend in the western United States is also shared between all three datasets, though again in the case of the surface data the area covered is larger and the amplitude of the trends are usually larger. The region of significant warming spreads out far into the tropical Pacific and far south into Mexico which is not shown in the other two datasets. A warming in western Europe also shows up in all three datasets as does a warming in the North Atlantic off the eastern coast of the United States. In the case of the surface data, these two significant regions of warming are connected. However, in western Europe, warming tends to be of lesser magnitude than in the other two datasets.

The region of cooling in central Asia shown in both the MSU 2r and NCEP datasets, while perhaps hinted at in the surface data, is insignificant. Common to all datasets are small areas of significant cooling at the southern tip of Africa and South America. Small areas of significant cooling are also shared by all datasets in the southern oceans at about 10W and about 60E though these trends tend to be weaker in the surface data than in the other two datasets. The surface data shows large areas of the southern oceans covered by significant warming. A region south of Australia shows as warming in all datasets though is statistically significant only in the surface data and the NCEP data. All other warming trends in the surface record are not confirmed in the tropospheric datasets.

In the annual average, the surface network shows a general tropical warming among significant regional trends which is directly at odds with the tropospheric datasets both of which show a general tropical cooling. This is interesting because based on atmospheric general circulation model (AGCM) simulations of increased greenhouse gas forcing, tropical warming trends are expected to increase with height as a result of the lapse-rate feedback effect (Manabe et al. 1991; Boer et al. 1992). This does not occur for any of the regionally significant surface trends in either of the two tropospheric datasets.

In the winter season (Fig. 4.5b), regionally significant trends are still evident in the surface observations in eastern Asia and across the North Atlantic. This warming shows

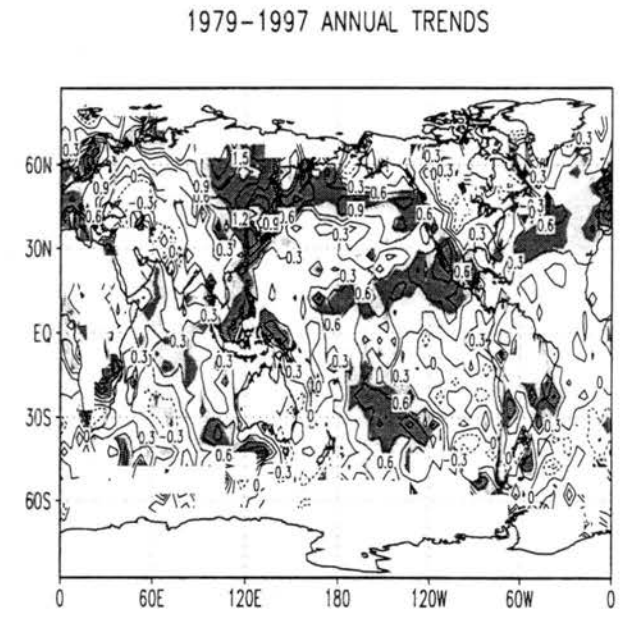

(a)

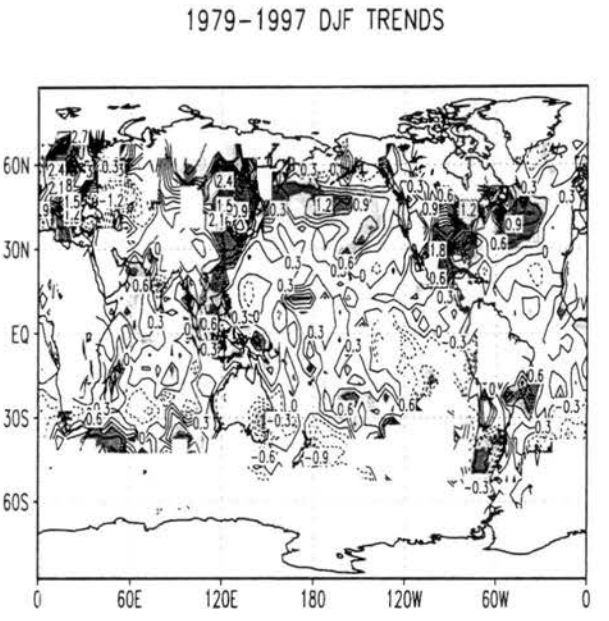

(b)

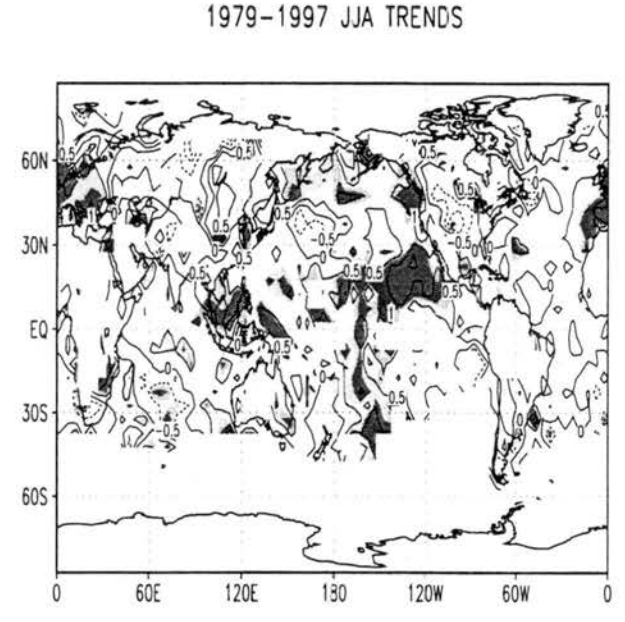

(c)

Figure 4.5: Surface network temperature trends in C/19 years for (a) annual averages, (b) winter (DJF) averages, and (c) summer (JJA) averages.

up in all three datasets and tends to be stronger in eastern Asia in both upper-air datasets while the warming across the northern Atlantic is stronger in the MSU data than both the surface and NCEP data. The surface data shows warming all the way down to southeast Asia which is not corroborated by the other two datasets. A central and eastern United States warming trend shows up in all datasets as does a cooling in eastern Canada (there is little data in the surface record in this region and so the northern extent of the cooling in these data cannot be confirmed). A warming off the eastern coast of the United States appears in all datasets though in the case of the surface data it extends much farther north than in the other two datasets. Warming is also evident in western Europe in the surface data and this again shows up in both the other datasets.

In the southern hemisphere, cooling is shared in all three datasets in the southern tip of Africa, the southern tip of South America and southeast Australia (though this trend is insignificant in the NCEP data). A warming region off the southern coast of Africa also appears in all datasets though its magnitude is difficult to ascertain in the surface record because of missing data to the south.

Summer season trends (Fig. 4.5c) show the largest discrepancies between the surface record and the tropospheric datasets. A warming across the North Atlantic is not shown in either of the tropospheric datasets. A warming in the tropical North Pacific west of Baja California which extends all the way into the southern hemisphere extratropics does not appear in the MSU data though there is a hint of the northern hemisphere warming in the NCEP data in two small, weakly significant centers. A strong western Europe warming in the surface record does not show up in either upper-air dataset in this season nor does a large region of warming over the maritime continent.

Table 4.6 gives the area-averaged trends of greater magnitude than 0.1°C/19 years for the surface network. All area-averaged trends are positive in the surface observations, though globally-averaged trends which include all the data are approximately halved in winter, summer and annual averages when only regionally significant trends are considered.

Comparison between the NCEP and MSU data and the surface observational network show significant disagreement as to regions where significant trends occur and their amplitude. This has been shown previously in the Jones et al. (1997) comparison of the MSU

Table 4.6: As in Table 4.1 but surface observational network trends.

	Sig. Trends	Global Average Sig. Trends	Global Average Trends
ANNUAL	0.6549	0.1665	0.2965
DJF	0.8311	0.1198	0.2788
JJA	0.7837	0.1288	0.3307

2r data with the surface record for the period 1979-1996. Significant regional trends cover very small portions of the globe and in almost no instance in that study do significant trends in the two datasets occur in the same place (refer to Fig. 1a,b in Jones et al. 1997). Therefore, global, hemispheric and zonal averages calculated in that study are not only composed overwhelmingly of areas of the planet where trends are indistinguishable from zero but, where a trend is identifiable, it is not agreed upon in the two datasets. The agreement between the surface and MSU is somewhat better with the addition of another year of data in the present study. However, many of the significant trends in the surface data appear over oceans in very poorly sampled regions and are not mirrored in either the MSU 2r and NCEP datasets.

4.9 Discussion and Conclusions

All observational datasets are likely to have biases, some documented, some unknown. We do not argue that one dataset is intrinsically better because we have no objective standard with which to make that judgment. We assume all datasets have difficulties, especially when attempting to identify small trends in noisy data. In an effort to circumvent the issue of spurious trends we have examined here only those trends which are significantly larger than documented linear biases in the respective datasets. Because global trends are a construct of regional changes, regional trends are a more appropriate diagnostic for climate change assessment and comparison with model simulations. This is particularly important given the contradictory results among major observational datasets as to recent tropospheric temperature trends (e.g., Santer et al. 1998). Because regional

trends can also be quite large in amplitude, we can gain confidence in their reality despite known biases in the observational platform.

We have shown regional trends in both the MSU and the 1000-500 mb NCEP reanalysis which are much larger in magnitude than the documented, average systematic biases of the datasets. These trends are of both sign and are clearly not favoring an increase in temperature as would be expected should CO_2-induced warming be a dominant forcing on this timescale. On average, there is a cooling in both the winter season and in the annual average among the most reliable trends in both datasets. A weaker summer season warming is also present in both datasets which becomes an average cooling if regions south of 60S are excluded from the average. Assuming an average bias of up to 0.5°C/19 years still results in an average cooling in these data.

In the case of the surface data, regionally significant trends show warming though to a lesser magnitude than when all regions are considered. However, many of these regions of significant trends occur in regions of limited observations over oceans and are not confirmed by other datasets. Tropical regions where significant warming occurs in the annual surface data are in no instance mirrored by larger magnitude warming in either of the two tropospheric datasets. AGCM simulations of the effects of elevated CO_2 suggest an enhanced warming with altitude in the tropics which is the opposite response to that seen here.

We have also shown that the regional trends of both sign in the NCEP data tend to become stronger as the layer becomes shallower though this is not universally the case. This observation and the fact that the 1000-925 mb layer also has the largest average negative trend indicates that warming does not generally increase with height in the troposphere. That individual trends of both sign have a varied response in shallower layers also indicates that the disagreement between the MSU/NCEP datasets and the surface record is not necessarily a global-scale difference in atmospheric response at different atmospheric levels (i.e., a large-scale change in static stability) but instead indicates a highly regional response. This view is further strengthened when regional trend discrepancies between the surface data and the tropospheric data which show no systematic differences

(e.g., consistently stronger or weaker in one dataset in regions where they agree). It appears unlikely that a small number of systematic biases in the satellite record could be responsible for the differences between the surface and tropospheric datasets.

Additionally, cooling trends in the MSU and NCEP data decrease in all the annual, winter, and summer seasons when only regional data is considered while in the case of the surface data, strong warming trends in annual, summer, and winter averages decrease substantially. Therefore, the discrepancy between the globally-averaged surface trends and those of the MSU and NCEP reanalysis are diminished when only regionally significant trends are considered, relative to globally-averaged trends.

While the majority of the globe is unsampled in this analysis because of insignificant trends, it is possible that real and coherent but statistically insignificant trend could overwhelm those regions of significance. This does not appear to be the case as the globe as a whole is also cooling in both tropospheric datasets. Additionally, regionally specific biases, particularly in the NCEP data, are a likelihood. A systematic bias could then be dominating the signal. This is less likely where the MSU and NCEP data agree and are most independent. Regional disagreement in the tropics as to strength (but not sign) of trends is also problematic. This is the region responsible for much of the global cooling signal in the tropospheric data and it is possible that errors here could change the sign of the globally-averaged trends in these datasets. The existence of these regional trends in the tropics will have to be confirmed by comparisons with other data including a careful assessment of local observational bias.

Finally, this study highlights the point that regional trends result from regional-scale forcing both real and spurious. Global trends, on the other hand, are the sum of these regional trends. In order to understand changes in global climate and the reliability of observational data we first must understand processes responsible for changes in regional climate.

Chapter 5

REGIONAL CASE STUDY FOR ROCKY MOUNTAIN NATIONAL PARK

5.1 Introduction

While large-scale deforestation, especially in the tropics, has been identified as a potential source of local and global climate impacts both in the present study and in other work (e.g., Zhang et al. 1996; Bonan et al. 1992; Chase et al. 1996) the effects on regional weather and climate due to localized changes in landuse in the mid-latitudes is relatively undocumented (e.g., see Cotton and Pielke 1995 for a survey as of 1992). Significant disruptions in the natural state of the land surface at mid-latitudes can be seen to perhaps no greater extent than on the Great Plains in northeastern Colorado. In the last century, large portions of the shortgrass steppe which once almost exclusively covered the region have been replaced with areas of irrigated and non-irrigated crop and managed grazing lands (Gutman et al. 1997). While many of these changes were made before mid-century, the process is ongoing. A 50% increase in the number of irrigated acres in this region occurred between 1974-1980 (Colorado Department of Agriculture data derived from the Federal Census of Agriculture, U.S. Commerce Department. Data available at http://www.ag.state.co.us/Resource/stat.list.htm.) while recent population growth is generating more urban and semi-urban landcover.

The direct effects of landcover change in the plains are dramatic increases in soil moisture in warm seasons due to irrigation, as well as changes in albedo, aerodynamic roughness, and other surface properties. These direct influences on surface characteristics may initiate indirect effects on local weather and climate in two differing ways. First, the large-scale change of averaged properties of a region can affect climate at all scales by altering surface radiation balances and surface flux partitioning over the entire region (e.g., Garratt 1993; Sud et al. 1988).

Secondly, discontinuities in surface properties within a region can generate mesoscale circulations, both in models and in observations (Segal et al. 1989, Vidale 1998), which would not exist otherwise. These circulations can be similar in magnitude to the typical sea breeze and may interfere constructively or destructively with other ambient atmospheric circulations (e.g., Ookouchi et al. 1984; Segal et al. 1988, 1989; Lee 1992; Seth and Giorgi 1996; Mahfouf et al. 1987; Avissar 1995). These circulations may also provide a region favored for low-level convergence and convective activity (Pielke et al. 1993).

There is some confirmation of effects on weather due to the presence of agricultural vegetation in the observational record. In northern Texas, Barnston and Schickedanz (1984) discovered an increase in precipitation in regions with heavy irrigation. A general cooling of surface temperatures of 1-2°C was also reported in irrigated regions though the net effect was a slight increase in convective instability (a decrease in lifted index) due to increased moisture. Beebe (1974) found irrigation to enhance severe storms in Texas by increasing available energy. Rabin and Martin (1996) found in a 2-year observational study of shallow cumulus cloud development in the midwestern United States that the average characteristics of soil and vegetation cover may exert as strong a forcing on the development of cumulus clouds as does the sloping terrain which characterizes the region. On the other hand, Fowler and Helvey (1974) found little effect from widespread irrigation in Washington State.

We are trying to answer three questions. What has been the effect on weather, and potentially, climate, of changing landuse on the Great Plains? What interactions between the plains and mountains allow those effects to be transmitted to higher elevations? Finally, if they are transmitted, how do they affect weather and climate in the higher altitudes of the Rocky Mountains? In an attempt to answer these questions we present a regional temperature trend analysis in Section 4.2. We then present results from high resolution, numerical model simulations of the atmosphere coupled with a land-surface biophysics model. We applied this model in a case study covering the three days from July 30-August 2, 1992. These days were chosen to represent climatological conditions in the region and were characterized by weak synoptic forcing. Cloudiness and precipitation

were therefore diurnally forced by the regional circulation rather than by broader-scale synoptic conditions.

5.2 Comparative Temperature Trends

The possibility that the climate of northeastern Colorado has been affected by changes in landcover due to human activity is suggested by regional temperature trends. Decreasing northeastern Colorado summer temperatures have been reported in the past (Greenland et al. 1995; Stohlgren et al. 1998). Also reported was decreased solar radiation at some high elevation sites (Williams et al. 1996). Recent studies of plant successional trends and watershed discharge in the northeastern Colorado mountains also indicated a mid- to high elevation cooling over the last 50-100 years (Stohlgren et al. 1998). Low-level, depth-averaged (1000-850mb) temperature data taken from the NCEP reanalysis shows a regional cooling over the period 1979-1997 in the summer (June, July, August) averages to the east of the Rocky Mountains (Chase et al. 1999a). The summer trend averaged over the region of northeastern Colorado (40-41N,102-105W) was –0.51C during this period.

As a comparison, we present the July average temperature regression slopes for area averages over the globe, the northern hemisphere, the continental United States, and the southwestern United States region in Table 5.1 along with unweighted area-averaged trends for 10 northeastern Colorado stations, 5 southeastern Colorado stations and 14 western Colorado stations for a 62-year time series as well as two shorter periods. The global and hemispheric data are from Vinnikov et al. (1994) with more recent data filled in with Goddard Institute for Space Studies (GISS) surface temperature data (Hansen and Lebedeff 1987; Reynolds and Smith 1994). The non-Colorado United States data were taken from the National Climatic Data Center (NCDC) website (Karl et al. 1986). Regions within the United States are defined by the NCDC and areally weighted and averaged. Regions within Colorado were defined for the purposes of this paper and represent straight averages. Western Colorado consists of all portions of the state west of the eastern plains. (Refer to topography in Fig. 5.1.) Northeastern Colorado and southeastern Colorado were divided at roughly half the states north-south extent. Specific stations in each region are listed in Appendix A.

	1934-1995		1966-1995		1981-1995	
	slope	p	slope	p	slope	p
GLOBAL	0.0039	<0.01	0.0136	<0.01	-0.0125	-
NORTH HEM.	0.0028	0.04	0.0146	<0.01	0.0074	-
U.S.	-0.0093	0.02	-0.0025	-	-0.0331	-
S.W. U.S.	-0.0034	-	-0.0121	-	-0.0266	-
COLORADO	-0.0137	0.02	-0.0215	-	-0.1033	<0.01
N.E.COLO *	-0.0092	-	-0.0324	0.10	-0.1274	<0.01
S.E.COLO *	-0.0179	0.03	-0.0360	0.09	-0.1234	<0.01
W. COLO *	-0.0089	0.08	-0.0267	0.07	-0.0828	0.08

Table 5.1: Trend in average July temperature in °C/year (i.e., slope of the linear regression line) and significance p value for 62, 30, and 15-year time series. Regions with an asterisk are unweighted averages from individual station values. A dash indicates non-significant trends (p values greater than 0.1.)

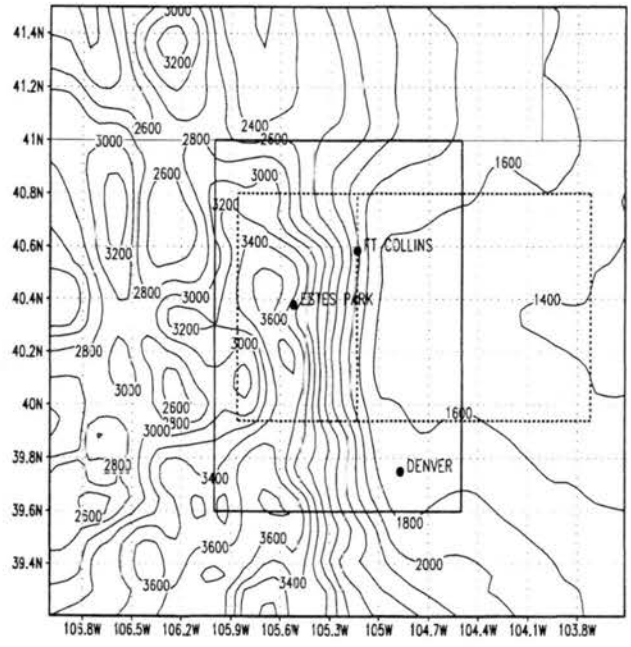

Figure 5.1: Topography on the fine (6.5 km) grid. Contours are by 200 m. The solid boxed region is a sub-domain used in Fig. 5.7c, d, e, and f. The dotted boxed region represents the subdomain used for meridional averages (discussed in text). The dotted line through Ft. Collins represents the approximate division between mountains and plains regions.

The 62-year time series has global and northern hemisphere temperatures rising significantly while the United States and Colorado temperatures declined significantly. Southwestern U.S. temperatures showed no trends. Colorado as a whole had a statistically significant cooling over this period driven by cooling in western and southeastern Colorado.

In the 30-year time series, global and northern hemispheric warming remained significant. Regional time series showed no significant trends though the three Colorado sub-regions all had weakly significant ($p = 0.1 - 0.05$) cooling. The magnitude of the Colorado cooling trend increased from the 62-year trend and was much larger in the eastern half of the state.

Over the 15-year time series, all scales larger than the state of Colorado are trendless. However, Colorado as a whole exhibits a strong, significant cooling which is several times larger than the trend in the 30-year time series. This is also the case with the three Colorado sub-regions. While southeastern Colorado had the largest trend in the 62- and 30-year time series, northeastern Colorado now has the largest trend. The western Colorado trend is quite a bit weaker than in the two eastern regions which seem to have had similar responses over time.

The regression results give little evidence that northeastern Colorado July cooling trends are coupled with the broadest scale trends despite an indication of a broad regional, depth-averaged cooling trend to the east of the Rockies in the NCEP reanalysis data during summer. There is some indication however, that trends in northeastern Colorado and southeastern Colorado are coupled to some degree. In order to examine this further, 62-year, 30-year and 15-year time series for 10 northeastern Colorado station were correlated using Spearman's rank correlation coefficients with all larger-scale regional averages and with each of the other Colorado stations used in this study. The results of these correlations and significance estimates are presented in Table 5.2.

There is no significant correlation between northeastern Colorado stations and global and hemispheric trends on any timescale. For the two longest time scales (30 and 62 years), all other regions are significantly, if weakly, correlated with northeastern Colorado. Only

	1934-1995		1966-1995		1981-1995	
	r	p	r	p	r	p
GLOBAL	0.04	-	0.01	-	-0.06	-
NORTH HEM.	0.12	-	0.05	-	0.03	-
U.S.	0.65	<.01	0.63	<.01	0.45	-
S.W. U.S.	0.49	<.01	0.43	<.01	0.37	-
COLORADO	0.77	<.01	0.80	<.01	0.72	<.01
WEST COLORADO	0.61	<.01	0.51	<.01	0.49	-
S.E. COLORADO	0.77	<.01	0.78	<.01	0.56	0.03
N.E. COLORADO	0.85	<.01	0.87	<.01	0.82	<.01

Table 5.2: Average Spearman rank correlation coefficient (r) between 10 northeastern Colorado stations and the averaged time series for the region listed and average significance (p) value for 3 time periods. A dash represents an average p value of greater than 0.1. Region compositions are described in Appendix A.

Colorado as a whole and southeastern Colorado region have a substantial (defined here as more than 50% of the variance explained or r=0.7) impact on northeastern Colorado temperatures. Moreover, these correlations dramatically decrease during the last 15 years of the time series so that southeast Colorado temperatures explain 31% of the variance in northeastern Colorado temperatures during this period while the average Colorado time series explains 52%. The correlation between the northeastern Colorado average and the average time series of each of the northeastern Colorado stations is consistently strong and remains at or above 0.82 in all 3 time periods.

Thus, it appears that the highly significant decrease in temperatures over the last 15 years in northeastern Colorado are, to some degree, a localized phenomenon and have occurred subsequent to large increases in the area of irrigated agricultural land in northeastern Colorado. We next discuss the dominant summertime circulation pattern in this region which links the weather and climate of mountain and plains and how observed landcover change might affect it.

5.3 The Mountain-Plains Circulation

During intervals of weak synoptic-scale winds, such as generally occurs under summer high pressure systems, a regularly observed feature in northeastern Colorado (and other

mountain-plains/mountain-valley systems) is a regional circulation which flows from the plains upslope toward the highest topography during the day and reverses direction at night (Toth and Johnson 1984; Wolyn and McKee 1994). This mostly east-west circulation is driven by daytime heating on a topographical gradient which warms higher elevations to a greater degree than air at the same altitude over the plains. The opposite chain of events occurs at night. A horizontal pressure gradient is created which drives a circulation which regularly reaches 5 – 10 m s^{-1} in magnitude. This circulation dominates the summer climatology of northeastern Colorado and is related to summer rainfall because low-level convergence is initiated near the highest topography as the local, low-level easterlies converge with ambient westerlies (Toth and Johnson 1984). This provides forcing for the initiation of convective rainstorms given favorable environmental conditions. These storms often travel eastward onto the plains under the influence of large-scale westerlies as the day continues.

The generation of circulation (C) in time by the solenoidal term in the circulation theorem describes the spin up of the mountain-plains circulation. By Stoke's theorem, circulation can be expressed as a surface integral of vorticity, where the surface integral is taken over a $x - z$ plane circuit:

$$\frac{\partial C}{\partial t} = \int\int_s \frac{\partial \eta}{\partial t} ds = \int\int_s g\nabla \times \hat{\mathbf{k}} \left(\frac{\alpha'}{\alpha_0^2} \right) \approx \int\int_s g\nabla \times \hat{\mathbf{k}} \left(\frac{\theta'}{\alpha_0 \theta_0} \right), \tag{5.1}$$

where η represents the vertical component of the total vorticity vector, g is the gravitational acceleration, α_0 is the area-averaged specific volume, α' is the specific volume perturbation, θ_0 is the area-averaged potential temperature, θ' is perturbation potential temperature, and $\hat{\mathbf{k}}$ is a vertical coordinate unit vector.

The approximate integral on the righthand side of (1) is suitable for shallow systems (Pielke and Segal 1986) and indicates that the strength of this circulation is a direct result of the magnitude of the horizontal temperature gradient and the depth to which this gradient exists. Atkinson (1981) points out that temperature differences of only fractions of a degree are effective in spinning up circulations such as this and cites Wenger's (1923) rough calculation that near-slope horizontal velocity (U) is approximately $9\Delta T$ m s^{-1} where T

is the temperature in Celsius. Therefore, a quite small change in temperature, 0.1° for example, will change the magnitude of the circulation by nearly 1 m s^{-1}. This is approximately 10-20% of the average magnitude of observed northern Colorado circulations (Toth and Johnson 1984; Wolyn and McKee 1994).

The simplest order of magnitude calculation of the sensitivity of the initiation of convective activity to changes in surface conditions can be performed using conservation of mass arguments. We assume a 2-dimensional slice through the domain from east to west and assume a vertical barrier 10 km high occurs on the western boundary. This barrier represents the Continental Divide. Assuming an incompressible atmosphere, the 2-dimensional continuity equation is written

$$\frac{\partial U}{\partial X} + \frac{\partial W}{\partial Z} = 0 \,, \tag{5.2}$$

where U and W are the horizontal and vertical velocity components, respectively, and X and Z are the horizontal and vertical coordinates. We assume negligible large-scale winds in the lower atmosphere and integrate over the east-west extent of the mountain-plains circulation from the Continental Divide out to where the circulation is no longer felt (i.e., where $U = 0$; on the order of 100 km). Vertical velocities are defined to be 0 over the domain except within a 20-km region just east of the barrier (representing the leeside region of low-level convergence). By integrating vertically over the depth of the circulation (assumed to be the depth of the boundary layer) and assuming no vertical motion at the bottom boundary we arrive at an expression for the change in vertical velocity in the convergent zone due to changes in horizontal winds across the domain. Applying this equation to two cases, a control and a perturbed case (designated by subscripts 1 and 2), we find that the change in vertical velocity in the leeside convergent zone between the two cases can be expressed as

$$W_2 - W_1 = \frac{(\Delta U_1 - \Delta U_2)(\Delta Z)}{(\Delta X)}. \tag{5.3}$$

Therefore, a change in vertical velocity at the top of the boundary layer is driven by a difference in the gradient of easterlies across the domain. Applying the realistic numbers

$\Delta U_1 - \Delta U_2 = 0.2$ m s^{-1}; $\Delta X = 20{,}000$ m; and $\Delta Z = 1{,}000$ m, we obtain a change in vertical velocity at the top of the boundary layer in the convergent zone of 1 cm s^{-1}. We can relate the above calculation to the minimum vertical velocity at the top of the boundary layer necessary to initiate convection (W_{MIN}) by the formulation (e.g., Bluestein 1992):

$$W_{MIN} = \sqrt{2CIN}, \tag{5.4}$$

where CIN is the convective inhibition (in J kg^{-1}) which is defined as the vertically integrated negative buoyancy a parcel must overcome by heating or mechanical means in order to freely convect. Equation 4 indicates that the strength of CIN that the rising air must overcome increases as a function of the vertical velocity (W) squared. Therefore, small changes in vertical motion can have significant effects on the ability to initiate convection. For example, a 5% increase in W from 10.0 cm s^{-1} to 10.5 cm s^{-1} increases the amount of negative buoyancy that a parcel can overcome by 10% and thereby enhances the potential for convective activity. These highly simplified calculations suggest the generation of convective activity near the Continental Divide is quite sensitive to the magnitude of the mountain-plains circulation which, in turn, is very sensitive to changes in east-west temperature gradient created by changes in surface conditions.

The potential effects of changes in low-level atmospheric moisture and temperature on the strength of convection or on the atmosphere's ability to maintain convection once it is initiated must also be considered. These effects are measured by the convective available potential energy (CAPE) of the atmosphere which is defined as the vertically integrated positive buoyancy. CAPE is highly sensitive to changes both in low-level moisture and heat (e.g., Bluestein 1992) and changes its distribution are expected to strongly affect convective activity.

Based on the above analysis, we demonstrate that the mountain-plains circulation is a mechanism whereby the weather and climate of mountains and plains interact. We hypothesize that observed changes in landuse on the plains are extensive enough to have altered the mean summertime mountain-plains circulation thereby affecting climate at higher elevations some distance from the plains. These effects potentially exist in the

magnitude and westward penetration of the low-level easterlies generated during the day and in the strength of low-level convergence, cloud cover, and precipitation near the Continental Divide. It may also affect the amount of moisture and heat transported to higher elevations during the day by the low-level regional circulation and so affect CAPE values. This is one mechanism by which changes in plains surface properties might be communicated to remote regions and is a mechanism which can be investigated using a numerical model.

5.4 The Experiment and Model Description

We used the Colorado State University Regional Atmospheric Modeling System (RAMS) Version 3b (Pielke et al. 1992) to perform the integrations detailed below. RAMS is a comprehensive regional-scale numerical model of the atmosphere which includes land-surface and subsurface physical processes. The radiation parameterization includes the effects of the important atmospheric gases, but has no interaction with condensed water species (Mahrer and Pielke 1977). A turbulence closure parameterization following Smagorinsky's (1963) deformation K coefficients is used. Land-surface/atmosphere interaction is based on a bulk aerodynamic formulation of vertical fluxes of heat, momentum, and moisture from the surface (Louis 1979). An eight-level soil model stretched to a total depth of 1m has been used to explicitly calculate the moisture and heat content of each subsurface layer (Tremback and Kessler 1985). Vegetation covers a specified fraction of each grid cell and is described by a single level. Vegetation properties (e.g., albedo, vegetated fraction, and roughness length) are all functions of surface vegetation category, and values are those used in the Biosphere Atmosphere Transfer Scheme (BATS; Dickinson et al. 1993) (e.g., Table 5.1). A constant leaf area of 1.0 was used for all vegetation types. Surface types in this region are short grassland, evergreen forest, mixed woodland, alpine tundra, dry agriculture, and irrigated agriculture.

The atmospheric portion of the model has 24 vertical layers reaching approximately 20 km into the atmosphere. The first vertical level is at 48 m, with subsequent levels beginning at 110 m intervals and stretching to a maximum of 1500 m near the top of

the model volume. This configuration allows adequate resolution of near surface features while avoiding prohibitive computational expense simulating the upper atmosphere. In the horizontal, we used two interacting, nested grids with grid cell spacings of 24 km and 6.5 km, respectively (Fig. 5.2). The coarse grid covers much of the western United States and simulates large-scale conditions. The finer grid covers an area of both mountain and plains in northern Colorado. The fine grid spacing used in the smaller model grid results in a realistic representation of the region's topography which is of vital importance in forcing weather features of interest (Fig. 5.1). These topographic features include the Colorado Front Range including parts of the Continental Divide (the ridge of highest topography), inter-mountain valleys, and east-west topographic features such as the Cheyenne Ridge (north of Ft. Collins in Fig. 5.1) and the Palmer Divide (south of Denver in Fig. 5.1) which are also favored regions for convective activity (Toth and Johnson 1984). These topographic features are not resolved in General Circulation Models (GCMs) or in regional climate models applied to broad domains (Giorgi and Bates 1989; Copeland et al. 1996) because of their relatively coarse grid spacing (approximately 300 km and 60 km, respectively). Because of this, mountain-plains and other topographically-forced regional circulations which play a large role in summer precipitation patterns in this region (as well as winter snowpack) are not accounted for explicitly nor will the mass and moisture convergence generated by these circulations be recognized by convective parameterizations in those model simulations.

Because of the fine grid spacing used in these simulations we did not use a parameterization of convective rainfall but instead relied on resolving such disturbances through use of an explicit microphysics scheme which predicts mass mixing ratios of seven hydrometeor species including hail and graupel (Walko et al. 1995). This represents a compromise between resolved scales and length of integration; 6.5 km is too large a grid spacing to precisely resolve most convective storms or to accurately represent their intensity. Our objective, however, is to establish sensitivity and to capture a reasonable spatial pattern of convective activity as a first approximation. Simple parameterizations of convective rainfall are not in general applicable to such small scales, while more complex parameterizations detract significantly from computational efficiency.

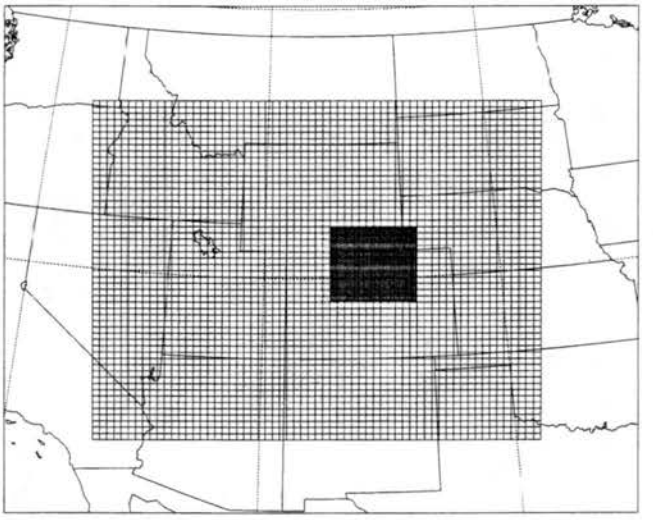

Figure 5.2: Domain covered by the Regional Atmospheric Modeling System (RAMS) two nested, interacting grids. The coarse grid interval is 24 km; the fine grid interval is 6.5 km. The fine grid is centered on Rocky Mountain National Park, Colorado.

This case study was performed using three different distributions of vegetation cover in the fine grid of the model domain which represent: (1) the potential natural vegetation distribution (NATURAL), (2) the state of landcover observed today (CURRENT), and (3) an hypothetical distribution which increases the area of irrigated vegetation in a realistic way to represent one potential future scenario (SUPER-IRRIGATED). The two cases CURRENT and SUPER-IRRIGATED are collectively referred to as ALTERED (Fig. 5.3).

The NATURAL state is derived from a map of potential natural vegetation by Küchler (1964). The observed state is based partially on satellite data of current landcover by the EROS Data Center (Loveland et al. 1991). In order to insure that regions not explicitly covered by an altered vegetation type (e.g., irrigated and non-irrigated farmland) were the same in all simulations, we set all cells with non-agricultural cover types in the EROS data set to the NATURAL state as estimated by Küchler. The EROS data were in many instances unrealistic in mountain and intermountain areas and so were ignored in favor of the Küchler estimate. The SUPER-IRRIGATED state (Fig. 5.3c) was generated by filling in much of the South Platte Valley region adjacent to the mountain

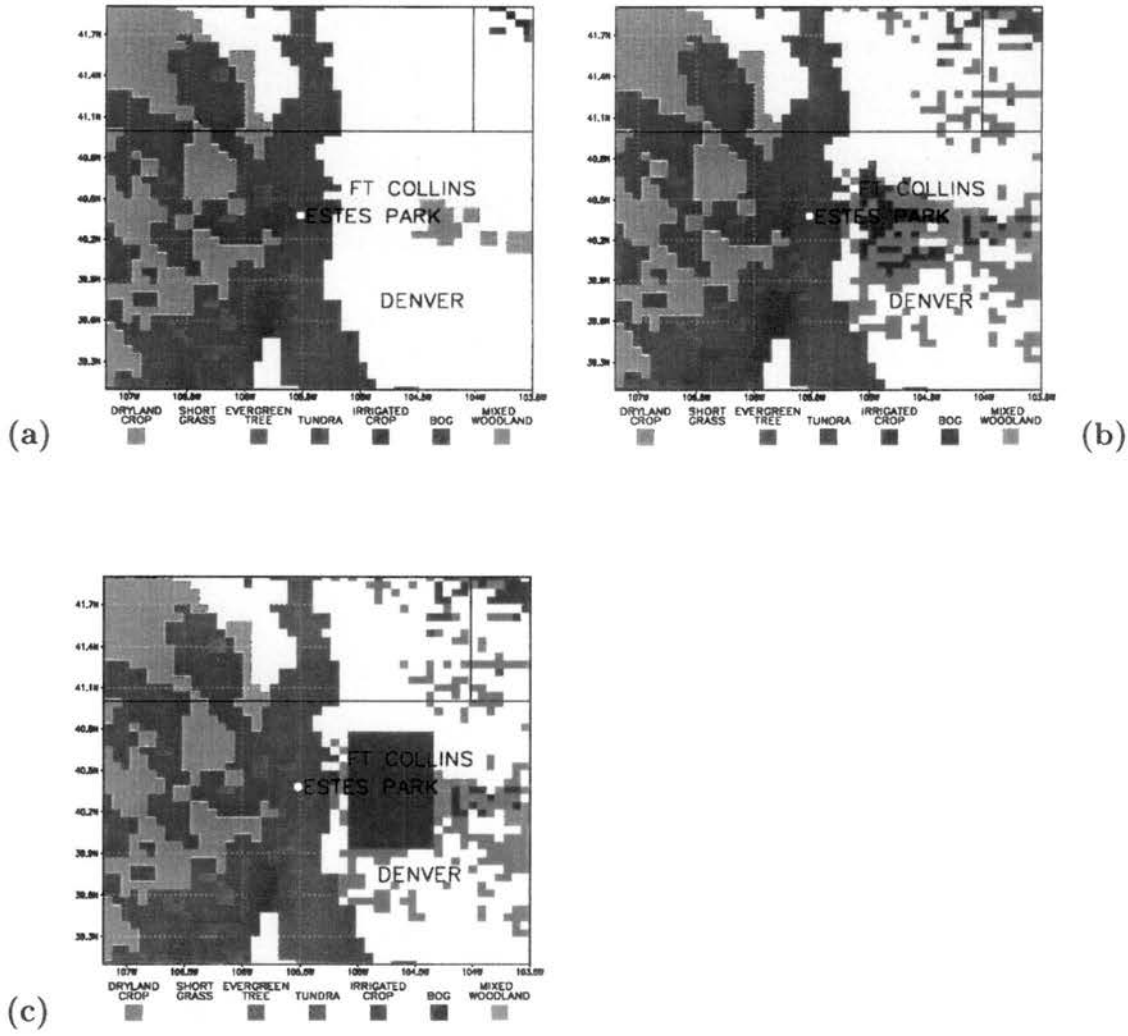

Figure 5.3: Landcover types on the finest grid for (a) NATURAL, (b) CURRENT, and (c) SUPER-IRRIGATED cases.

front with irrigated farmland so as to increase the soil moisture forcing in a potentially realistic way. This might represent an increase in irrigated cropland and urban watered landscapes associated with an increasing population and more importantly, provides a maximally forced comparison case for assessment of signal robustness. Irrigated regions in the SUPER-IRRIGATED case completely occupy a region of approximately 1000 km by 650 km. This is on the scale of the local Rossby radius thereby providing a maximum forcing for mesoscale circulations caused solely by discontinuities in soil moisture (Dalu et al. 1996). This type of mesoscale circulation would be expected to interact with the ambient mountain-plains circulation.

Both ALTERED scenarios have irrigated and non-irrigated farmland in large portions of the plains adjacent to the Rocky Mountains at the expense of shortgrass steppe. The change from short grass to agricultural land is described in the land-surface model by vegetation parameters including albedo, roughness length, fractional cover of vegetation, and initial soil moisture (Table 5.3). The change from grassland to irrigated cropland is reflected as a change in soil moisture which was initialized at 75% of saturation for irrigated regions, while all other regions were initialized at a 38% saturation meant to represent a dry soil. Soil moisture was allowed to evolve with time during the simulation with the potential effect of removing the higher soil moisture in irrigated regions. Despite this, irrigated regions retained high relative levels of soil moisture throughout the period of integration so that moisture forcing remained relatively constant. Irrigated croplands have lower vegetation albedo and increased roughness length relative to short grassland in the vegetated fraction of the grid. Increased soil moisture also decreases the albedo of the soil fraction in irrigated regions. Finally, in areas where croplands replace short grass, roughness length is tripled. This could allow a greater transfer of heat and moisture from surface to atmosphere over the croplands due to an increase in mechanically generated turbulence. A sandy-loam soil type with soil properties obtained from Clapp and Hornberger (1978) was assumed constant throughout the domain. Differences in soil properties in the simulation result only from differences in soil moisture.

The RAMS model was initialized with, and lateral and upper boundary conditions were provided by, National Meteorological Center (NMC) upper air analyses supplemented

	ALBEDO (FRACTION)	ROUGHNESS LENGTH (m)	INITIAL SOIL MOISTURE (% CAPACITY)
SHORT GRASS	0.1/0.3	0.02	38
DRYLAND CROP	0.1/0.3	0.06	38
IRRIGATED CROP	0.08/0.23	0.06	75

Table 5.3: Comparison of selected surface parameter values for landuse types which change in these experiments. Albedos are visible/near infra-red. From Biosphere Atmosphere Transfer Scheme (BATS) values (Dickinson et al. 1993)

by observational data from surface stations and rawinsonde. The simulations covered a three-day period (72 hours) from July 31 – August 2, 1992. This period was characterized by a 500 mb ridge centered over the central United States with weak upper-level flow over Colorado and weak inflow of low- and mid-level moisture from the Gulf of Mexico into the region as a result of the southwest monsoon. This is a common late-summer pattern and is representative of climatological average conditions (Toth and Johnson 1984). These conditions are ideal for the development of local upslope winds in the afternoon and convergence near the Continental Divide because of the weakness of large-scale forcing. This case was characterized by weak, scattered convective activity chosen so that the soil moisture distributions imposed in the ALTERED cases were not disturbed to a marked degree (i.e. no large, organized systems over the region for long periods of time). Station data show occasional, light, scattered convective activity during this period. Between 7 and 19% of stations throughout the domain recorded light precipitation on each of the three days. Modeled values of daily averaged precipitation are of similar magnitude to those observed. The large-scale modeled winds, water vapor distribution, and thermal structure compare well with observed conditions for each of the three days.

Observed afternoon averaged surface air temperatures (Colorado mesonet data obtained through the Cooperative Institute for Research in the Atmosphere) are compared with the model solution in Fig. 5.4 and show substantial agreement. Table 5.4 compares the observed diurnal cycle in temperatures with those simulated in the CURRENT case at three sites in the domain. Denver lies on the plains, Fort Collins abuts the foothills

in a transitional area, and Estes Park lies in a mountain valley on the eastern side of the Continental Divide near Rocky Mountain National Park. Differences between observed and modeled temperatures on the plains are generally within 3 degrees. Simulated temperatures in Estes Park are consistently cooler than observed. Model points are chosen by geographical proximity rather than terrain similarity, and model values represent an average over a 6.5 × 6.5 km (42 km^2) region. Discrepancies in observed versus simulated temperatures partially reflect the fact that in complex terrain, temperature values will differ greatly over short horizontal distances so modeled temperatures do not represent a single site in that grid.

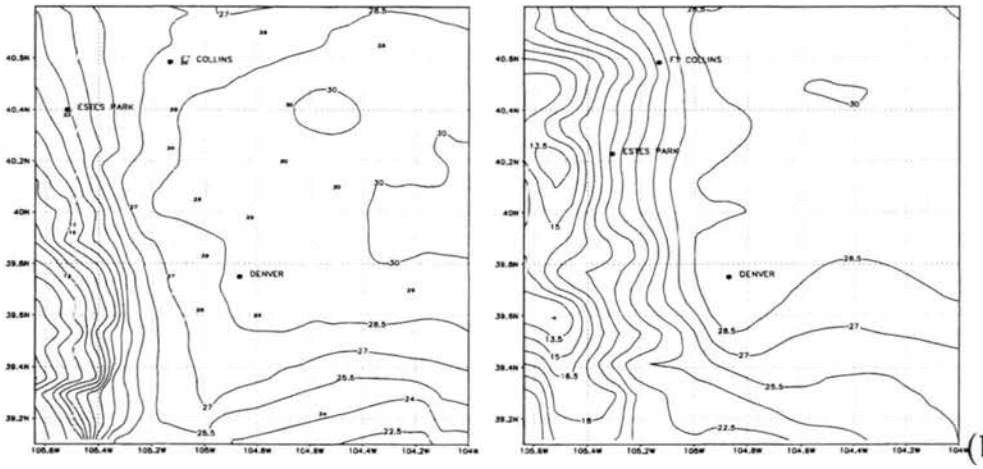

Figure 5.4: Comparison of modeled average temperatures (contour by 1.5 °C) with observed (Colorado mesonet) averages for (a) afternoon (12–18 hrs LST) observed temperature, and (b) afternoon (12–18 hrs LST) modeled temperature. Mesonet data provided by the Forecast Systems Laboratory (FSL) through the Cooperative Institute for Research in the Atmosphere (CIRA). Zero contour lines are omitted here, and in subsequent figures, for clarity.

Average dewpoints (not pictured) show reasonable spatial structure though they tend to be 1–2 degrees drier over the plains with a steeper than observed decrease in dewpoint as topography increases. For example, daily 12 UTC dewpoint temperatures at the Denver station for the time period tend to be slightly dry in the simulations and are (observed/modeled, in °C): 10/11, 11/10, 8/5. On all three afternoons an easterly/southeasterly (upslope) flow developed in the simulations during the daylight hours at low levels to a maximum depth of somewhat less than 800 m and reversed itself at night

		DENVER		FORT COLLINS		ESTES PARK	
		obs	sim	obs	sim	obs	sim
MAXIMUM TEMP (°C)	Day 1	28	27	23	23	20	16
	Day 2	34	34	29	31	24	22
	Day 3	31	32	31	31	26	20
MINIMUM TEMP (°C)	Day 1	14	13	10	13	10	5
	Day 2	18	15	19	9	18	9
	Day 3	13	18	13	20	na	12
AVERAGE TEMP (°C)	Day 1	21	20	17	18	15	10
	Day 2	25	24	24	21	21	15
	Day 3	22	25	22	25	na	16

Table 5.4: Comparison of observed (obs) versus simulated (sim) temperatures in °C at selected sites. Average temperatures are averaged maxima and minima. na = not available.

in accordance with observed flow. Three-day average modeled easterlies ranged from 4–10 m s^{-1} and were slightly stronger than observed with maximum differences of 1–2 m s^{-1}.

Simulated mountain precipitation occurred mainly in association with the highest topography. In addition, on the third day of the simulation a large convective disturbance developed in southeastern Colorado which also occurred in the observations. Because most convective precipitation in this case is still a subgrid-scale phenomenon even at this relatively high model resolution, point comparisons with station data were not attempted.

Because of the high resolution necessary to accurately resolve the regional circulation, we were unable to integrate for a period long enough to evaluate a climatological response or perform statistical significance tests. However, daily consistency in a diurnally-forced system allows for greater confidence in the generality of the results while the dominance of regional forcing allows us to evaluate the potential effect of landcover change on the region's summer circulation patterns.

Previous studies of topographically-induced thermal circulations (Wolyn and McKee 1994; Ookouchi et al. 1984; Pielke et al. 1991; Poulos 1996) have generally used idealized topography, a horizontally homogeneous basic state, and a single day or less of simulation and so have not investigated with several realizations impacts both on the plains and at higher elevations under realistic initial and boundary conditions; this is the goal here.

5.5 Results

5.5.1 Spatial and Temporal Averages

In order to minimize daily variations in the signal which may not be representative of general behavior we present results as averages over the three-day period. All anomalies are presented relative to the NATURAL case. We compared the ALTERED and NATURAL simulations in terms of their averages over afternoon hours (12–18 hours LST) on all three days. These times represent the period when the mountain-plains circulation was most developed and mountain convection most active.

Soil moisture in the top, 2-cm deep, soil layer (Fig. 5.5a,b) was greater in the two ALTERED simulations consistent with initial conditions for the irrigated lands. Latent heat fluxes (Fig. 5.5e,f) also increased over large areas in the plains to maximum values of 160 – 180 W m^{-2} in the two ALTERED cases, while sensible heat fluxes (Figs. 5.5c,d) decreased over moist soils (maximum decreases were approximately 150 W m^{-2} in both ALTERED cases). The additional moisture supplied to the plains boundary layer at the expense of sensible heating represented the main driver for subsequent dynamical changes. Increased sensible heat fluxes just to the west of the irrigated regions as well as near the eastern grid boundary occur with similar magnitudes in both ALTERED cases. These increased sensible heat fluxes are a result of more efficient transport of heat to the atmosphere due to the large roughness length of the dryland cropping occupying those areas relative to the natural grasslands and emphasize the complicated and sometimes competing atmospheric forcings inherent in changing landcover.

The ALTERED cases had a maximum cooling of the lower atmosphere (0–640 m, though because this layer is well mixed these are indicative of surface air temperatures as well) over the regions of enhanced soil moisture of nearly 0.7° C in the CURRENT case and almost 1.0° C in the SUPER-IRRIGATED case relative to the NATURAL case (Fig. 5.6a,b). Due to the advection of colder air from the plains, this cooling is seen far up the eastern slope of the mountain front in both ALTERED cases especially in the SUPER-IRRIGATED case (refer to topography in Fig. 5.1).

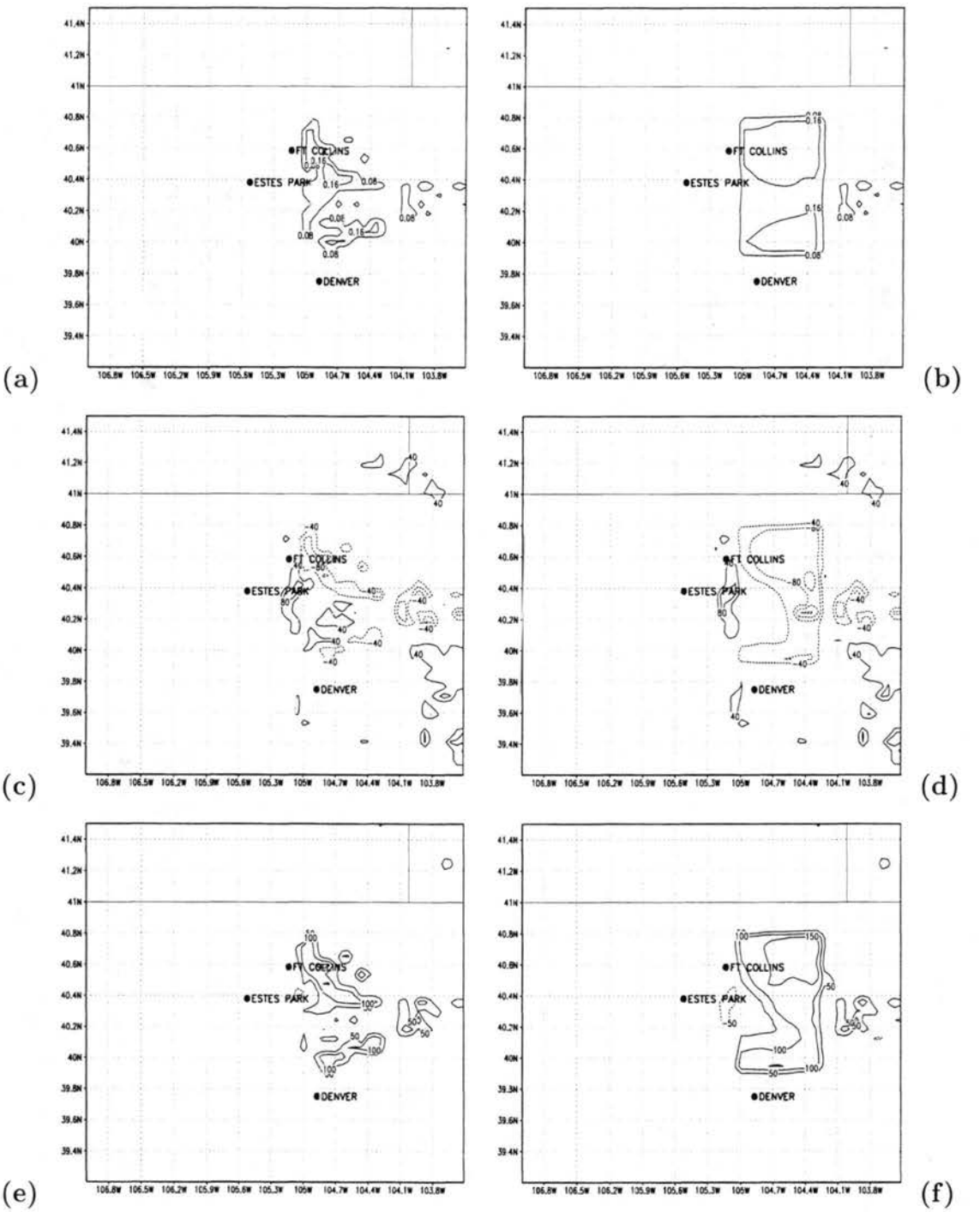

Figure 5.5: Difference fields of afternoon (12–18 hrs LST) averages across all three days. (a) Soil moisture (contour by 0.08 mm) CURRENT–NATURAL. (b) Soil moisture (contour by 0.08 mm) SUPER-IRRIGATED - NATURAL. (c) Sensible heat flux (contour by 40 W m^{-2}) CURRENT–NATURAL. (d) Sensible heat flux (contour by 40 W m^{-2}) SUPER-IRRIGATED - NATURAL. (e) Latent heat flux (contour by 50 W m^{-2}) CURRENT–NATURAL. (f) Latent heat flux (contour by 50 W m^{-2}) SUPER-IRRIGATED - NATURAL.

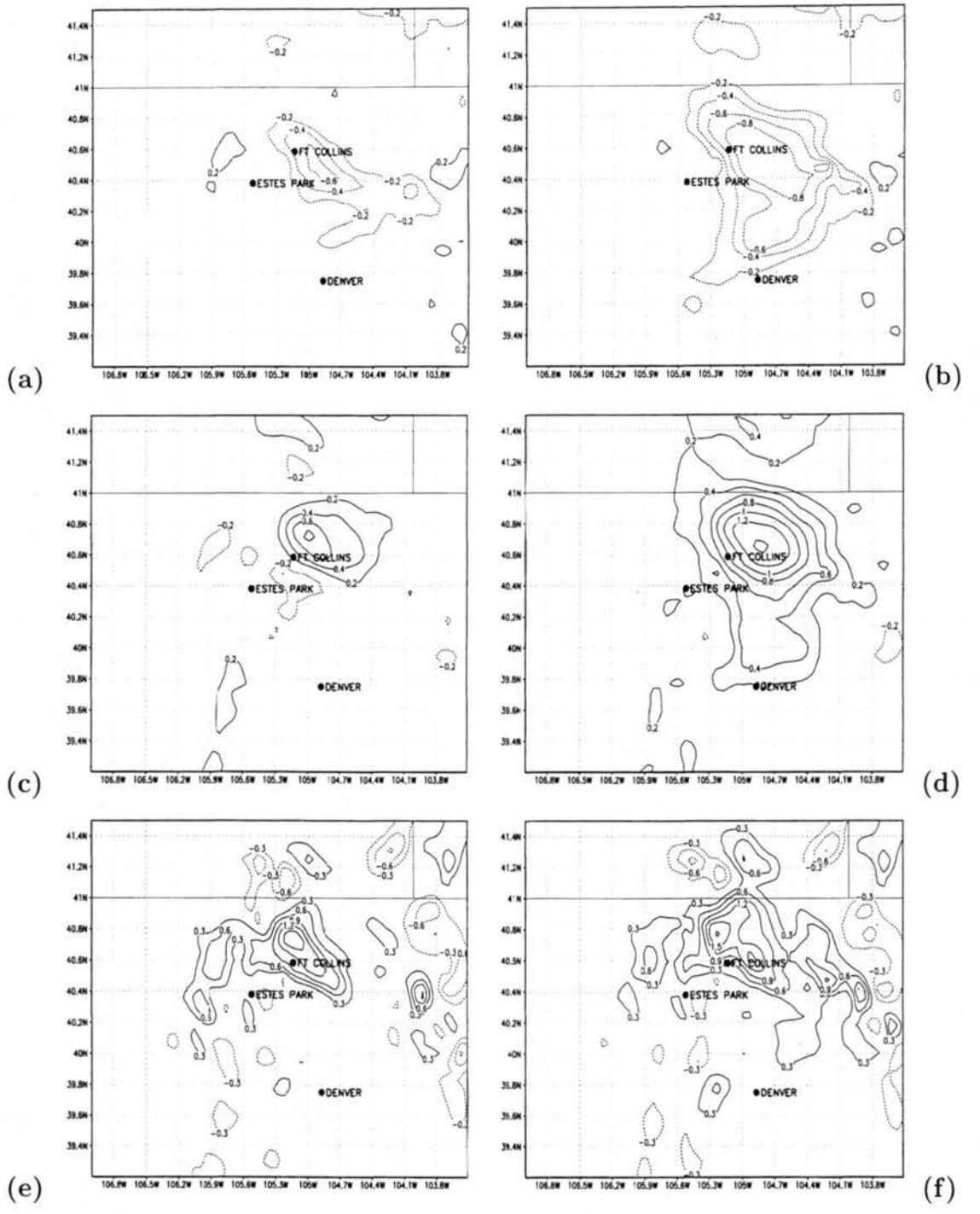

Figure 5.6: Fields averaged vertically from 0-640 m (first 5 model layers) and over afternoon hours (12–18 hrs LST). (a) Temperature difference (contour by 0.2 °C) CURRENT–NATURAL. (b) Temperature difference (contour by 0.2 °C) SUPER-IRRIGATED–NATURAL. (c) Dewpoint temperature difference (contour by 0.2 °C) CURRENT–NATURAL. (d) Dewpoint temperature difference (contour by 0.2 °C) SUPER-IRRIGATED–NATURAL. (e) East-west wind difference (contour by 0.3 m s^{-1}) CURRENT–NATURAL. (f) East-west wind difference (contour by 0.3 m s^{-1}) SUPER-IRRIGATED –NATURAL. and g) Undifferenced east-west winds in the NATURAL case provided for orientation of easterlies and westerlies (contour by 2.0 m s^{-1}). In (e) and (f), positive anomaly values represent decreases in easterly flows or increased westerlies relative to the NATURAL case.

(g)

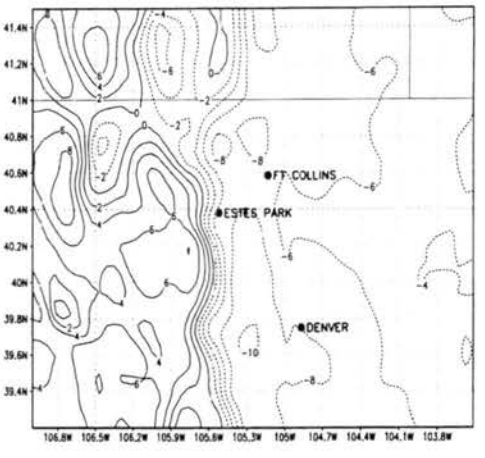

Figure 5.6: Continued.

The cooling of plains and mountains in the ALTERED cases caused decreased easterly upslope winds in the same regions due to the decreased sensible heating of the atmosphere and reduced pressure gradient (Fig. 5.6e,f). The plains are on a slope themselves and so the large cooling at the base of the Rockies substantially reduced upslope flow from points farther east. The maximum wind decrease, represented by positive anomalies in Fig. 5.6e and f, due to easterly (negative) ambient wind direction (average U winds in the NATURAL case are provided in Fig. 5.6g for locations of easterly and westerly flow), was more than 1.5 m s^{-1} in the CURRENT case and nearly 2 m s^{-1} in the SUPER-IRRIGATED case relative to the NATURAL case. The decreased easterlies extended to high elevations in both ALTERED cases.

The presence of irrigated land was also reflected in low-level atmospheric moisture differences where dewpoint temperatures increased in the northern part of the irrigated regions in the two ALTERED cases (Fig. 5.6c,d). This northward shift is a reflection of a southerly wind component which advected moisture slightly to the north. In the CURRENT case, dewpoint temperature decreased slightly to the west of the center of the irrigated region and at higher elevations as a result of flow patterns which moved dry air in from the south. This had impacts on mountain cloud cover and convection.

The increased low-level moisture in the ALTERED simulations relative to the NATURAL case caused increased Convective Available Potential Energy (CAPE) in the region

just north of Ft Collins by approximately 100–150 J kg^{-1} in both cases despite cooler temperatures (Fig. 5.7a,b). Decreased CAPE in the CURRENT case south of Ft. Collins resulted from decreases in both temperature and moisture in the area. In the SUPER-IRRIGATED case, a smaller decrease in CAPE occurs south of Ft Collins while a sizeable increase in CAPE occurs at higher elevations between Ft Collins and Estes Park due to enhanced upslope advection of moisture from the irrigated regions in spite of decreased easterly flow (Fig. 5.6f).

Figures 5.7c,d display the precipitation differences for a subset of the region focusing on higher elevations and the mountain-plains transition (solid boxed region in Fig. 5.1). Total accumulated rainfall was affected west of areas with altered landcover, including the transitional region between mountain and plains and at highest elevations. A precipitation increase occurred in the area of Ft. Collins in both ALTERED cases while two minima occurred at high elevations, one to the north and one to the south of Estes Park. These features are similar in both ALTERED cases though anomalies are of higher magnitude in the SUPER-IRRIGATED case.

The total condensate field differences, also presented for the solid boxed region in Fig. 5.1, reflecting changes in cloud cover, had a series of positive and negative anomalies in a north-south line along the Continental Divide reflecting an orderly arrangement of preferred areas of cloudiness (Fig. 5.7e,f). Anomalies were spatially similar in each ALTERED case but were of stronger magnitude in the SUPER-IRRIGATED case than in the CURRENT case.

As an indication of the daily extent of regions affected by landuse changes in the plains, standard deviations of afternoon averaged temperature and dewpoint temperature differences (CURRENT–NATURAL) are provided in Figs. 5.8a and b. These figures show that the effect of these landuse changes can penetrate into the mountains on individual days. The effect is similar but stronger in the SUPER-IRRIGATED case differences (not shown).

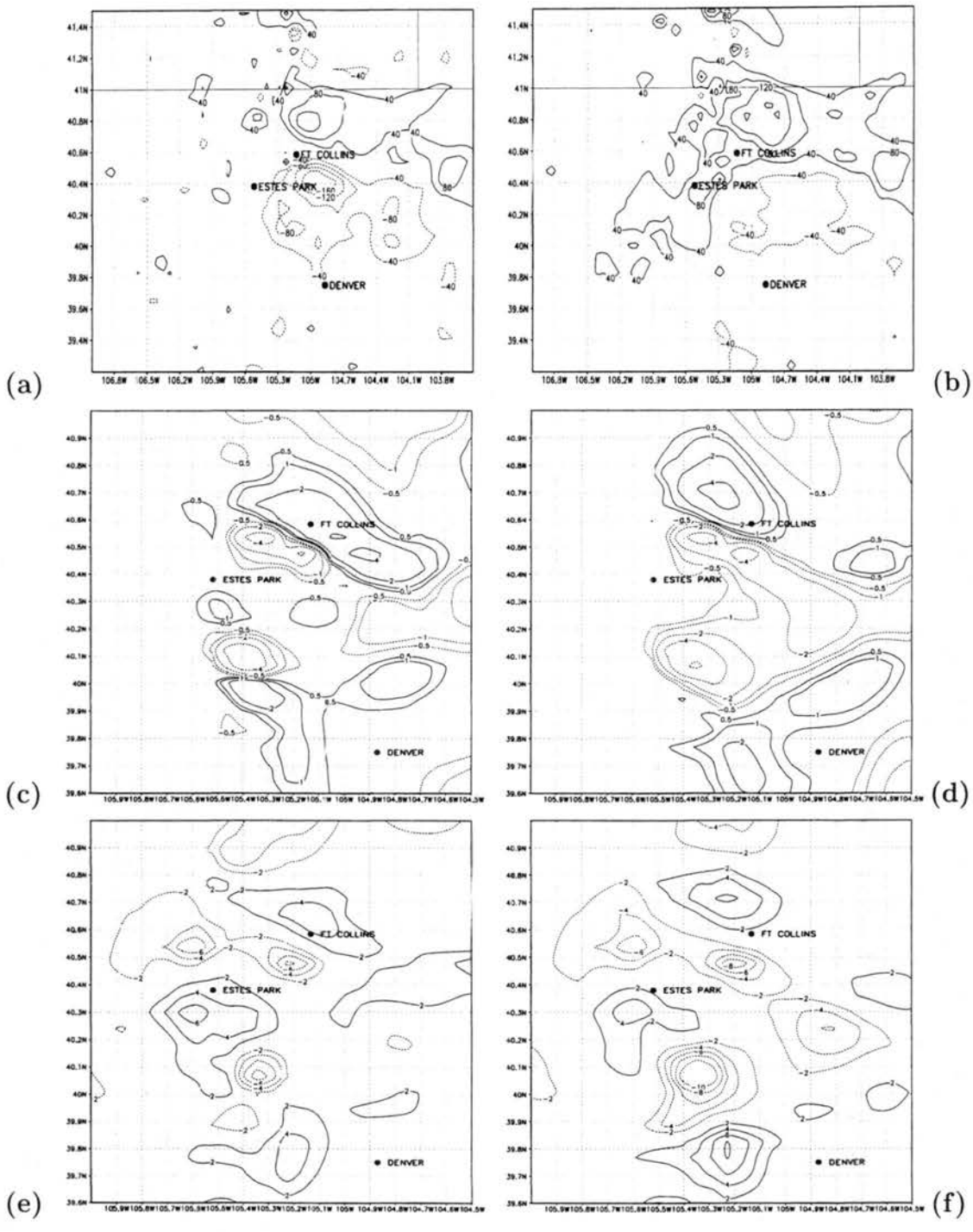

Figure 5.7: Difference fields averaged vertically from 0–640 m (first 5 model layers) and over afternoon hours (12–18 hrs LST). (a) CAPE (contour by 40 J kg^{-1}) CURRENT–NATURAL. (b) CAPE (contour by 40 J kg^{-1}) SUPER-IRRIGATED – NATURAL. (c) Mountain precipitation (contour by 0.5, 1.0, 2.0, 4.0, 8.0 mm d^{-1}) CURRENT – NATURAL. (d) Mountain precipitation (contour by 0.5, 1.0, 2.0, 4.0, 8.0 mm d^{-1}) SUPER-IRRIGATED – NATURAL. (e) Mountain vertically-integrated condensate (contour by 2 kg) CURRENT–NATURAL. (f) Mountain vertically-integrated condensate (contour by 2 kg), SUPER-IRRIGATED – NATURAL.

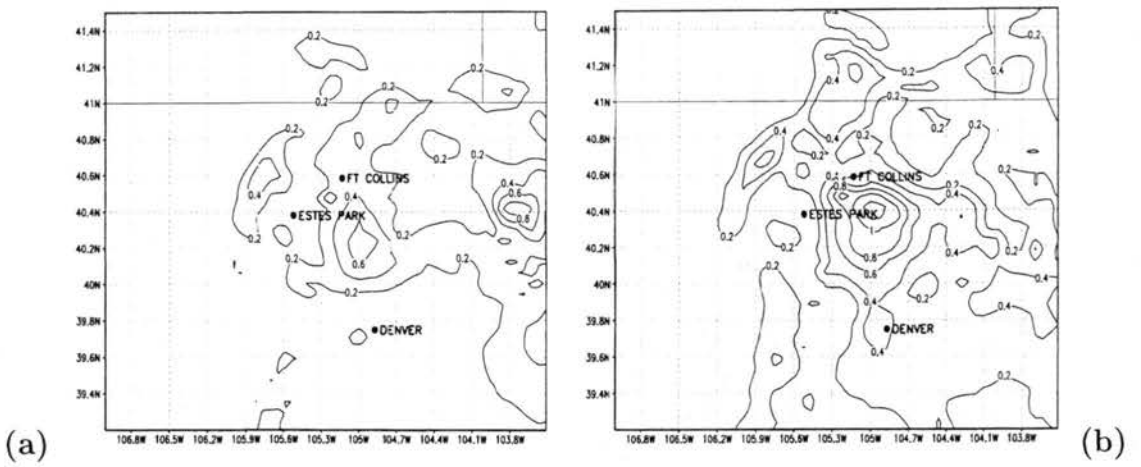

Figure 5.8: Standard deviation of differences in time. Differences were averaged vertically from 0-640 m (first 5 model layers) and over afternoon hours (12–18 hrs LST). a) Temperatures (contour by 0.2 °C) CURRENT–NATURAL, b) Dewpoint temperatures (contour by 0.2 °C). CURRENT–NATURAL.

5.5.2 Meridional Averages

To provide a picture of east-west structure, we took north-south averages over a subdomain where surface forcing mechanisms were strongest and were expected to have the greatest impact (see dotted box in Fig. 5.1). This region includes the largest irrigated regions on the plains and continues west past the highest topography.

The afternoon divergent maximum in the first 640 m of the atmosphere (Fig. 5.9a, at approximately gridpoints 27-29) and the weak divergence at most points farther east increased in each of the ALTERED cases while in the mountains, convergence decreased along the lower slope of the mountains (gridpoints 24 to 25) in the ALTERED cases as well as at the convergent maximum at gridpoint 21. Vertical velocity (not pictured) correspondingly decreased slightly in these regions in both ALTERED cases.

Meridionally-averaged daily precipitation (Fig. 5.9b) showed a spatially complicated response. Decreased precipitation on the eastern boundary of the domain was due to southern shifts of a precipitation center in both ALTERED cases which moved it outside the averaging area. A plains maximum occurred in the SUPER-IRRIGATED case centered at the boundary between wet and dry soils (gridpoint 39) which developed as

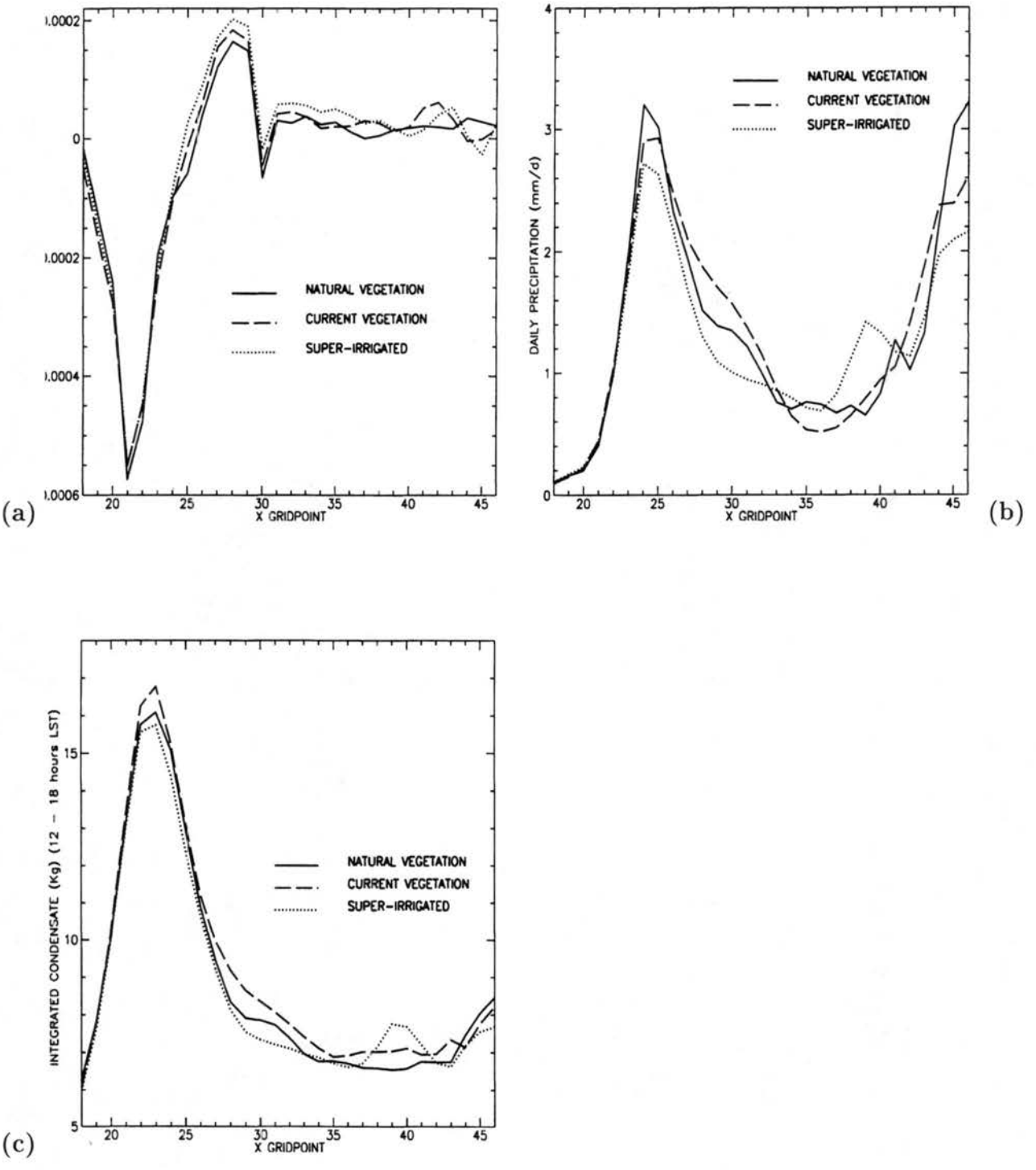

Figure 5.9: Comparison of north-south averages over dotted box in Fig. 5.1 for the three cases. (a) 12–18 LST divergence (s^{-1}) 0-640 m, (b) total daily precipitation (mm d^{-1}), and c) daily vertically-integrated condensate (kg) (solid and liquid). The mountain region approximately occupies gridpoints 18–28 while the plains region occupies gridpoints 29–46.

a result of a weak circulation generated at the discontinuity. The rainfall maximum in the mountains, somewhat east of the convergent maximum (Fig. 5.9a) due to advection of storms by ambient westerlies, decreased in both ALTERED cases consistent with the decreased convergence. The rainfall maximum in the CURRENT case had a broader areal distribution relative to the NATURAL case. The SUPER-IRRIGATED case had a narrower precipitation distribution and decreased precipitation both in the mountains and in lower elevations near the mountains relative to the NATURAL case.

Total condensate integrated throughout the atmosphere and averaged daily is a proxy for average cloud cover in the region (Fig. 5.9c). Meridionally-averaged condensate increased over most of the plains in the ALTERED cases with a secondary maximum in the SUPER-IRRIGATED case paralleling the precipitation field. The condensate maximum at high elevations increased in the CURRENT case but decreased in the SUPER-IRRIGATED case. Variables such as precipitation and condensate had highly variable spatial responses compared to the relatively consistent dynamic and thermodynamic forcings and their distribution were very sensitive to the chosen averaging domain.

5.6 Sensitivity to Added Model Complexity

The basic numerical model described above is unrealistic in several respects. Two obvious areas are in the use of a simple radiative parameterization and a constant leaf area index (LAI) between vegetation types. In an effort toward building a more comprehensive model of the effects of landuse change in this region, we explored the total response by adding each of these effects individually on top of landuse changes described earlier. We performed two sensitivity studies which covered the first 12 hours of the original three-day period. The first used a more accurate radiation parameterization which also allows for radiative interaction with clouds (Harrington 1997). In a second study we doubled green leaf area from 1.0 m^2/m^2 to 2.0 m^2/m^2 in agricultural areas to represent the increase in this parameter in observed systems. These results are shown in Fig. 5.10. We compare these figures simply to indicate sensitivity and to highlight the complexity of the issues involved. We do not examine the response in detail.

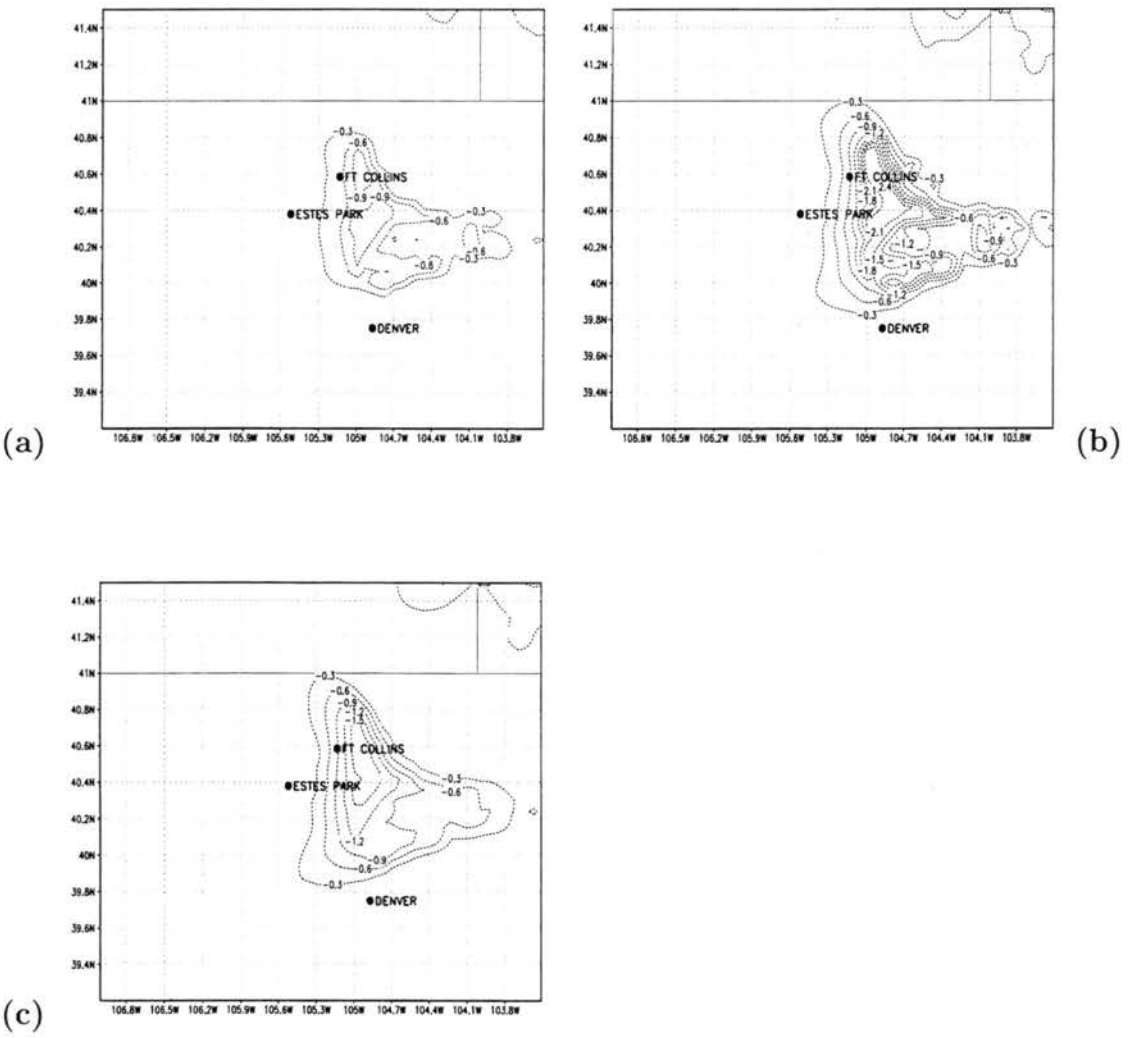

Figure 5.10: Comparison of 12–18 LST temperature differences (CURRENT–NATURAL) after the first simulated day averaged vertically from 0-640 m on the first day for, (a) the initial model configuration, (b) 2-stream radiation scheme included in both cases, and (c) increased green leaf area in agricultural areas in both cases.

Figure 5.10a shows the temperature difference between the CURRENT and NATURAL cases for the hours 12–18 LST on the first day of simulation. As a comparison, Fig. 5.10b shows the same field except with the alternate radiation scheme implemented. The temperature response with the alternate radiation covers a larger area than in the original simulation and has a maximum cooling which more than doubled. Similarly, a comparison in a case where agricultural LAI is doubled (Fig. 5.10c) also increases the initial response by more than 50% and broadens the area affected.

These changes in plains temperature affected the magnitude of the mountain-plains breeze where the afternoon easterly winds (not shown) decreased by up to 2.8 m s^{-1} in the CURRENT case with the alternate radiation scheme and up to 2.4 m s^{-1} in the CURRENT case with doubled LAI. The largest difference in the original model was 1.2 m s^{-1} on this day. Changes in the mountains-plains breeze of this magnitude would be expected to have further impacts on cloud cover and precipitation as in the results of Section 5.5.

5.7 Discussion and Conclusion

Experiments with a regional atmospheric model with explicit representation of natural, present day, and a hypothetical, future landcover distribution were performed in the region of Rocky Mountain National Park in northern Colorado. These experiments showed important effects on atmospheric dynamics, thermal structure, and hydrology in both the plains and adjacent mountains. Effects on the mountain-plains circulation induced by changes in landuse were of sufficient magnitude to affect cloud cover, precipitation, surface hydrology and temperature at higher elevations. The responses in the temperature and wind fields were proportionately stronger in the SUPER-IRRIGATED case than the CURRENT case indicating a monotonic response to surface forcing which was relatively linear. Behavior of the components of the hydrological cycle, especially when considering remote effects, was highly nonlinear however, so that perturbations varied widely between scenarios.

Some responses had, however, daily consistency over the course of the three-day simulation *and* between the two cases where altered vegetation was present (CURRENT

and SUPER-IRRIGATED cases). Compared to the NATURAL case, the effects of altered landcover in the plains included:

- Sensible heat fluxes decreased over moist regions.
- Latent heat fluxes increased over moist regions.
- Boundary layer was cooler during the day.
- Low-level moisture increased.

These changes altered the mesoscale flow dynamics leading to the following responses:

- Easterly low-level afternoon flow decreased over a wide area.
- Low-level afternoon convergence decreased in the mountains in the subdomain presented in Section 4.5.2.
- Eastern slope mountain regions cooled.
- Precipitation and cloud cover were non-linearly affected in magnitude and spatial pattern in both plains and mountain regions.

Though true significance testing cannot be run on such short simulations, confidence in the trends in the results was enhanced by daily consistency over the three days. These simulations also confirmed the predictions of a simple analytic model (Section 4.3) that temperature changes due to plains irrigation and other landcover changes can have large effects on the local dynamic response which in turn affects the hydrologic response which was communicated to higher elevations remote from actual landuse changes. These mountain regions have sharply defined vegetative zones in which species and ecological processes are strongly affected by temperature, soil moisture and insolation. Therefore, responses may be larger when feedbacks due to vegetation changes (which may already be occurring; Stohlgren et al. 1998) are included.

The sensitivity studies reported in Section 4.6 suggest that radiation characterization as well as the details of other processes such as vegetation physiology are likely to be

important to simulating climate change in Northeastern Colorado and that reasonable depictions of each must be included simultaneously in order to more thoroughly investigate the sensitivity of weather and climate to landscape structure. Because these effects are related in non-linear ways it would be a mistake to conclude that the temperature effects are additive. However, both sensitivity studies significantly enhanced the original signal both in magnitude and area which suggests our original model results may be underestimating the impact of observed landuse change during this simulated period in both magnitude and spatial extent.

Observed and inferred temperature trends in this region are also suggestive of the responses seen in these simulations. Analysis of observations shows a recent, regional, low-level averaged summer cooling trend and a surface station cooling trend in July which seems to be distinct from temperature changes at larger geographic scales. The simulations reported here show a cooling in afternoon temperatures and changes in cloudiness and precipitation in remote areas which could signal broader scale and longer-term responses. While we have chosen a time-period which is representative of climatological conditions, it is unclear how these hydrological effects might express themselves in a long-term climatology. This regional cooling and the fact that observed temperature responses at high elevation stations are highly variable in space suggest that there are local climate controls at work. We have demonstrated that one such control may be landuse change which may need to be accounted for in the climate record, (e.g., Pielke et al. 1998). However, it is unlikely that this is the only control. More complete models combined with climatological-length simulation periods and closer evaluation of climate records and surrogate measurements will be necessary to understand the effects of changing climate at all scales in the Colorado Rocky mountains, and other similar geographic areas. The regional effects of landcover change are in no way represented in large-scale model simulations such as the ones described in Chapter 2 and are another source of error which will need to be addressed in future investigations of the global effects of historical landcover changes.

Chapter 6

CONCLUSIONS

While the exact role of historical landcover changes on climate at the regional and global scale is still ambiguous, this research examined the role of landcover as a potentially important factor in anthropogenic climate change. Methods for determining the global extent of historical vegetation change from satellite data and balance models were discussed as were results from numerical modelling studies at the global scale and in a regional case study. An observational analysis of recent climatic trends in northeastern Colorado and in several global datasets was made. A comparison of the regional trends in the three global datasets was performed as was an assessment of the reliability and coherence of those data. Finally, the simulated climatic effects due to observed, global, landcover change were compared with the simulated effects of current levels of anthropogenic CO_2 loading and against the observational record.

Our results indicate that vegetation change, as it is observed to have already occurred, can have significant effects on both global and regional climate. These effects are generally not limited to the regions of direct landcover change forcing and, in fact, can be strongest where no direct forcing occurs. This shows that atmospheric feedback processes and adjustments, in some cases, are a more important climate signal than the original, direct forcing. Therefore, regional climate models which are forced by non-interactive, large-scale boundary conditions derived from GCMs from may miss a large, and perhaps, the largest portion of the climate change response. This result has implications for the northeastern Colorado case study presented here and suggests the possibility of a more widespread response to regional changes in land-use should the boundary conditions be responsive to the simulation details.

In the fine-scale case study in the Colorado Front Range, we showed that observed vegetation changes can have substantial effects on local temperatures and circulations which can act to transport climate change effects remotely. The simulated cooling has some substantiation in the observational data. These sorts of regional effects are not accounted for in any GCM and may have substantial impact both directly and due to complex atmospheric adjustment processes when summed over all regions of the globe.

In the global scale simulations we showed that, as a result of tropical landcover change, tropical atmospheric effects occurred which spread to global scales in a manner similar to the global effects due to El Niño Southern Oscillation. These include changes in the globally-averaged circulation as well as the generation of low frequency waves which appear to propagate to the extratropics in a well-defined teleconnection pattern. That tropical landcover change also reduced easterlies in the tropical Pacific in this experiment suggests the existence of a positive feedback loop between deforestation and warm ENSO events which may have played a role in the observed increase in the occurrence and strength of warm ENSO events at the expense of cold events in recent years.

The GCM simulations of global climate change due to observed landcover change compare favorably in spatial pattern and amplitude with recently observed regional temperature trends. Additionally, a comparison between simulations of climate changes due to land cover disturbance and those due to rising atmospheric CO_2 concentration show that in some instances, global landcover changes, as they have already occurred, are responsible for shifts in climate which are of the same magnitude as changes simulated as a result of current levels of CO_2 loading. Additionally, these climate effects occur in the same regions as those simulated by increased CO_2. This represent a confounding factor in the effort to detect anthropogenic climate change resulting from rising greenhouse gas concentration. A comparison of recent observational temperature in three independent, global datasets indicates that recent climate trends are not conforming to suggested greenhouse warming patterns and are more likely to be of a highly individualized, regional character.

REFERENCES

Arakawa, A., and W.H. Schubert, 1974: Interaction of cumulus cloud ensemble with the large-scale environment. Part I. *J. Atmos. Sci.*, **31**, 674-701.

Atkinson, B.W., 1981: *Meso-scale atmospheric circulations.* Academic Press. London.

Avissar, R., 1995: Recent advances in the representation of land-atmosphere interactions in general circulation models. *Rev. Geophys.*, Supplement, 1005-1010, U.S. National Report to International Union of Geodesy and Geophysics 1991-1994.

Balling, R.C., 1991: Impact of desertification on regional and global warming. *Bull. Amer. Meteor. Soc.*, **72**, 232-234.

Barlow, C., and T. Volk, 1990: Open systems living in a closed biosphere: A new paradox for the Gaia debate. *Biosystems*, **23**, 371-384.

Barnston, A.G., and P.T. Schickedanz, 1994: The effect of irrigation on warm season precipitation in the southern Great Plains. *J. Climate Appl. Meteor.*, **23**, 865-888.

Baron, J.S., M.D. Hartman, T.G.F. Kittel, L.E. Band, D.S. Ojima, and R.B. Lammers, 1998: Effects of land cover, water redistribution, and temperature on ecosystem processes in the South Platte Basin. *Ecol. Appl.*, 6, 1037 -1051.

Basist, A.N., and M. Chelliah, 1997: Comparison of tropospheric temperatures derived from the NCEP/NCAR reanalysis, NCEP operational analysis, and the Microwave Sounding Unit. *Bull. Amer. Meteor. Soc.*, **78**, 1431-1447.

Beebe, R.C., 1974: Large scale irrigation and severe storm enhancement. *Preprints: Symposium on Atmospheric Diffusion and Air Pollution.* Santa Barbara. AMS, Boston, 392-395.

Berbery, E.H., and J. Nogués-Paegle, 1993: Intraseasonal interactions between the tropics and extratropics in the southern hemisphere. *J. Atmos. Sci.*, **50**, 1950-1965.

Berendse, F., 1994: Litter decomposability - a neglected component of plant fitness. *J. Ecology*, **82**, 187-190.

Betts, A.K., J.H. Ball, A.C.M. Beljaars, M.J. Miller, and P.A. Viterbo, 1996: The land surface-atmospheric interaction: a review based on observational and global modeling perspectives. *J. Geophys. Res.*, **101**,7209-7225.

Bjerknes, J., 1969: Atmospheric teleconnections from the equatorial Pacific. *Mon. Wea. Rev.*, **97**, 163-172.

Bluestein, H., 1992: *Synoptic-dynamic meteorology in midlatitudes.* Oxford University Press, New York, 431 pp.

Boer, G.J. N.A. McFarlane, and M. Lazare, 1992: Greenhouse-gas induced climate change simulated with the CCC second-generation general circulation model. *J. Climate*, **5**, 1045-1077.

Bonan, G.B., 1996: A land surface model (LSM version 1.0) for ecological, hydrological and atmospheric studies: technical description and users guide. NCAR Technical Note NCAR/TN-417+STR.

Bonan, G.B., D. Pollard, and S.L. Thompson, 1992: Effects of boreal forest vegetation on global climate. *Nature*, **359**, 716-718.

Brown, R.G., and C.S. Bretherton, 1998: A test of the strict quasi-equilibrium theory on long time and space scales. *J. Atmos. Sci.*, **54**, 624-638.

Burde, G.I., and A. Zangvil, 1996: Estimating the role of local evaporation in precipitation in two dimensions. *J. Climate*, **9**, 1328-1338.

Campbell, G.C., T.G.F. Kittel, G.A. Meehl, and W.M. Washington, 1995: Low-frequency variability and CO_2 transient climate change. Part 2: EOF analysis of CO_2 and model-configuration sensitivity. *Global and Planetary Change*, **10**, 201-216.

Charney, J.G., 1975: Dynamics of desert and drought in the Sahel. *Quart. J. Roy. Meteor. Soc.*, **101**, 193-202.

Charney J.G., W.J. Quirk, S.H. Chow, and J. Komfield, 1977: A comparative study of the effects of albedo change on drought in semi-arid regions. *J. Atmos. Sci.*, **34**, 1366-1385.

Chase, T.N., R.A. Pielke, T.G.F. Kittel, R. Nemani, S.W. Running, 1996: The sensitivity of a general circulation model to large scale vegetation changes. *J. Geophys. Res.*, **101**, 7393-7408.

Chase, T.N., R.A. Pielke, Sr., T.G.F. Kittel, J.S. Baron, and T.J. Stohlgren, 1998a: Potential impacts on Colorado Rocky Mountain weather due to land use changes on the adjacent Great Plains. *J. Geophys. Res.*, In revision.

Chase, T.N., R.A. Pielke Sr., T.G.F. Kittel, J.A. Knaff, and J.L. Eastman, 1998b: A comparison of regional trends in 1979-1997 depth-averaged tropospheric temperatures. *Climatic Change*, submitted.

Chen, T.C., R.Y. Tzeng, and H. Van Loon, 1988: A study of the maintenance of the winter subtropical jet streams in the northern hemisphere. *Tellus*, **40A**, 392-397.

Chervin, R.M., and S.H. Schneider, 1976: On determining the statistical significance of climate experiments with general circulation models. *J. Atmos Sci.*, **33**, 405-412.

Christy, J.R., 1995: Temperature above the surface layer. *Climatic Change*, **31**, 455-474.

Clapp, R.B., and G.M. Hornberger, 1978: Empirical equations for some soil hydraulic properties. *Water Resources Res.*, **14**, 601-604.

Claussen, M., 1998: On multiple solutions of the atmosphere-vegetation system in present-day climate. *Global Change Biology*, in press.

Copeland, J.H., 1995: Impact of soil moisture and vegetation distribution on July 1989 climate using a regional climate model. Ph.D. Dissertation, Department of Atmospheric Science, Colorado State University, 124 pp.

Copeland, J.H., R.A. Pielke, and T.G.F. Kittel, 1996: Potential climatic impacts of vegetation change: A regional modeling study. *J. Geophys. Res.*, **101**, 7409-7418.

Cotton, W.R. and R.A. Pielke, 1995: *Human Impacts on Weather and Climate.* Cambridge University Press, New York, 288 pp.

Crowley, T.J., 1983: The geologic record of climate change. *Revs. Geophys. Space Phys.*, **21**, 828-877.

Dalu, G.A., R.A. Pielke, M. Baldi, and X. Zeng, 1996: Heat and momentum fluxes induced by thermal inhomogeneities. *J. Atmos. Sci.*, **53**, 3286-3302.

Davis, M.B., 1989: Lags in vegetation response to greenhouse warming. *Climatic Change*, **15**, 75-82.

Dickinson, R.E., 1995: Land-atmosphere interaction. *Rev. Geophys.*, Supplement, 917-922, U.S. National Report to International Union of Geodesy and Geophysics, 1991-1994.

Dickinson, R.E., and P.J. Kennedy, 1992: Impacts on regional climate of Amazonian deforestation. *J. Geophys. Res. Lett.*, **19**, 1947-1950.

Dickinson, R.E., A. Henderson-Sellers, and P.J. Kennedy, 1993: Biosphere-Atmosphere Transfer Scheme (BATS) Version 1e as coupled to the NCAR Community Climate Model. Technical Report NCAR/TN-387 + STR, NCAR, Boulder, CO, 72 pp.

Dirmeyer, P.A., and J. Shukla, 1996: The effect on regional and global climate of expansion of the world's deserts. *Quart. J Roy. Meteor. Soc.*, **122**, 451-482.

Dirmeyer, P.A., and J. Shukla, 1994: Albedo as a modulator of climate response due to tropical deforestation. *J. Geophys. Res.*,**99**, 20863-20877.

Eltahir, E.A.B., 1996: Role of vegetation in sustaining large-scale atmospheric circulation in the tropics. *J. Geophys. Res.*, **101**, 4255-4268.

Eltahir, E.A.B., 1998: A soil moisture-rainfall feedback mechanism 1. Theory and observations. *Water Resources Research*, **34**, 765-776.

Field, C.B., R.B. Jackson, and H.A. Mooney, 1995: Stomatal responses to increased CO_2: Implications from the plant to global scale. *Plant, Cell and Environment*, **18**, 1214-1225.

Fowler, W.B., and J.D. Helvey, 1974: Effect of large scale irrigation on climate in the Columbia Basin. *Science*, **184**, 121-127.

Gaffen, D.J., T.P. Barnett, and W.P. Elliot, 1991: Space and time scales of global tropospheric moisture. *J. Climate*, **10**, 989-1008.

Garratt, J.R., 1993: Sensitivity of climate simulations to land-surface and atmospheric boundary-layer treatments-a review. *J. Climate*, **6**, 419-449.

Geisler, J.E., M.L. Blackmon, G.T. Bates, and S. Munoz, 1985: Sensitivity of January climate response to the magnitude and position of equatorial Pacific sea surface temperature anomalies. *J. Atmos. Sci.*, **42**, 1037-1049.

Giorgi, F., and G.T. Bates, 1989: The climatological skill of a regional model over complex terrain. *Mon. Wea. Rev.*, **117**, 2325-2347.

Greenland, D., R. Ingersoll, M. Losleben, and T.R. Seastedt, 1995: A decrease in temperatures at high elevations in the Colorado Front Range USA. *Oregon Geog.*, **11**, 001-003.

Gutman, M.P., S. Gonzalez Baker, and S. Pullum, 1997: Ethnicity and land use in a changing environment: The Great Plains in the Twentieth Century. 1997 Annual Meeting of the Population Association of America, Washington, D.C., 26-29 March.

Hack, J.J., 1994: Parameterization of moist convection in the National Canter for Atmospheric Research Community Climate Model (CCM2). *J. Geophys. Res.*, **99**, 5551-5568.

Hack, J.J., J.T. Kiehl, and J.W. Hurrell, 1998: The hydrologic and thermodynamic characteristics of the NCAR CCM3. *J. Climate*, **11**, 1179-1206.

Hansen, J., and S. Lebedeff, 1987: Global trends of measured surface air temperature. *J. Geophys. Res.*, **92**, 13345-13372.

Harrington, J.Y., 1997: The effects of radiative and microphysical processes on simulated warm and transition season Arctic stratus. Ph.D. dissertation, Atmospheric Science Paper No. 637, Colorado State University, Dept. of Atmospheric Science, Fort Collins, CO 80523, 289 pp.

Henderson-Sellers, A. and K. McGuffie, 1995: Global climate models and 'dynamic' vegetation changes. *Global Change Biology*, **1**, 63-75.

Henderson-Sellers, A., K. McGuffie, and C. Gross, 1995: Sensitivity of a global climate model simulations to increased stomatal resistance and CO2 increases. *J. Climate*, **8**, 1738-1756.

Hoerling, M.P., and M. Ting, 1994: Organization of extratropical transients during El Niño. *J. Climate*, **7**, 745-766.

Holdridge, L.R., 1947: Determination of world plant formations from simple climatic data. *Science*, **105**, 367-368.

Hulme, M., 1996: Recent climatic change in the world's drylands. *Geophys. Res. Lett.*, **23**, 61-64.

Hurrell, J.W., 1996: Influence of variations in extratropical wintertime teleconnections on Northern Hemisphere temperature. *Geophys. Res. Lett.*, *23*, 665-668.

Hurrell, J.W., and K.E. Trenberth, 1997: Spurious trends in satellite MSU temperatures from merging different satellite records. *Nature*, **386**, 164-167.

IPCC, 1996: *Climate change 1995 - The science of climate change.* J.T. Houghton and others Eds. Cambridge University Press.

James, I.N., 1994: *Introduction to circulating atmospheres.* Cambridge University Press. Cambridge.

Jenne, R.L., and T.B. McKee 1985: Data, Chapter 42. *Handbook of Applied Meteorology*, D. Houghton, Ed., John Wiley and Sons, 1461 pp.

Jones, P.D., 1988: Hemispheric surface air temperature variations: recent trends and an update to 1987. *J. Climate*, **1**, 654-660.

Jones, P.D., 1995: Land surface temperatures - is the network good enough? *Climatic Change*, **31**, 545-558.

Jones, P.D., T.J. Osborn, T.M.L. Wigley, P.M. Kelley, and B.D. Santer 1997: Comparisons between the microwave sounding unit temperature record and the surface temperature record from 1979-1996: Real differences or potential discontinuities? *J. Geophys. Res.*, **102**, 30135-30145.

Kalnay, E., M. Kanamitsu, R. Kistler, W. Collins, D. Deaven, L. Gandin, M. Iredell, S. Saha, G. White, J. Woollen, Y. Zhu, M. Chelliah, W. Ebisuzaki, W. Higgins, J. Janowiak, K.C. Mo, C. Ropelewski, J. Wang, A. Leetmaa, R. Reynolds, R. Jenne, and D. Joseph, 1996: The NCEP/NCAR 40-year reanalysis project. *Bull. Amer. Meteor. Soc.*, **77**, 437-471.

Kang, I.-S., 1990: Influence of zonal mean flow change on stationary wave fluctuations. *J. Atmos. Sci.*, **47**, 141-147.

Karl, T.R., and P.D. Jones, 1989: Urban bias in area-averaged surface air temperature trends. *Bull. Amer. Meteor. Soc.*, **70**, 265-270.

Karl, T.R., C.N. Williams, Jr., P.J. Young, and W.M. Wendland, 1986: A model to estimate the time of observation bias associated with monthly mean maximum, minimum, and mean temperatures for the United States. *J. Climate Appl. Meteor.*, **25**, 145-160.

Karl, T.R., V.E. Derr, D.R. Easterling, C.K. Folland, D.J. Hofmann, S. Levitus, N. Nicholls, D.E. Parker, and G.W. Withee, 1995': Critical issues for long-term climate monitoring. *Climatic Change*, **31**, 165-221.

Kasting, J.F., 1989: Long-term stability of the earth's climate. *Paleogeography, Paleoclimatology, Paleoecology*, **75**, 83-95.

Kiehl, J.T., B. Boville, B. Briegleb, J. Hack, P. Rasch, and D. Williamson, 1996: Description of the NCAR Community Climate Model (CCM3). NCAR Technical Note NCAR/TN-420+STR, Boulder, Colorado.

King, G., and R.P. Nielson, 1992: The transient response of vegetation to climate change: A potential source of CO_2 to the atmosphere. *Water, Air and Soil Pollution*, **64**, 365-383.

Kirchner, J.W., 1989: The Gaia hypothesis: Can it be tested? *Revs. Geophys.*, **27**, 223-235.

Kleidon, A., and M. Heimann, 1998: Optimized rooting depth and its impacts on simulated climate of an atmospheric general circulation model. *Geophys. Res. Lett.*, **25**, 345-348.

Krishnamurti, T.N., 1961: The subtropical jet stream of winter. *J. Meteor.*, **18**, 172-191.

Krishnamurti, T.N., M.Kanamitsu, W.J. Koss, and J.D. Lee, 1973: Tropical east-west circulations furing the northern winter. *J. Atmos. Sci.*, **30**, 780-787.

Krueger, A.F., and J.S. Winston, 1973: A comparison of the flow over the tropics during two contrasting flow regimes. *J. Atmos. Sci.*, **31**, 358-369.

Kumar, A., A. Leetmaa, and M. Ji, 1994: Simulations of atmospheric variability induced by sea surface temperatures and implications for global warming. *Science*, **266**, 632-634.

Küchler, A.W., 1964: Potential natural vegetation of the conterminous United States. *Special Publication No. 36.* American Geophysical Society.

Lashof, D.J., 1989: The dynamic greenhouse: Feedback processes that may influence future concentrations of atmospheric trace gases and climatic change. *Climatic Change*, **14**, 213 242.

Lee, T.J., 1992: The impact of vegetation on the atmospheric boundary layer and convective storms. Ph.D. Dissertation, Atmospheric Science Paper No. 509, Colorado State University, 137 pp.

Legates, D.R., and C.J. Willmott, 1990: Mean seasonal and spatial variability in global surface air temperature, *Theor. Appl. Clim.*, *41*, 11-21.

Lettau, H., K. Lettau, and L.C.B. Molion, 1979: Amazonia's hydrologic cycle and the role of atmospheric recycling in assessing deforestation effects. *Mon. Wea. Rev.*, **107**, 227-237.

Livezey, R.E., and K.C. Mo, 1987: Tropical-extratropical teleconnections during Northern Hemisphere winter. Part II: Relationship between monthly mean northern hemisphere circulation patterns and proxies for tropical convection. *Mon. Wea. Rev.* **115**, 3115-3132.

Louis, J.F., 1979: A parametric model of vertical eddy fluxes in the atmosphere. *Bound.-Layer Meteor.*, **17**, 187-202.

Loveland, T.R., J.W. Merchant, D.O. Ohlen, and J.F. Brown, 1991: Development of a land-cover characteristics database for the coterminous U.S. *Photogrammetry, Engineering and Remote Sensing*, **57**, 1453-1463.

Lovelock, J.A., 1979: *Gaia: A new look at life on earth.* Oxford University Press. Oxford, 157 pp.

Lovelock, J.E., 1989: Geophysiology: The science of Gaia. *Revs. Geophys.*, **27**, 215-222.

Mahfouf, J-F., E. Richard, and P. Mascart, 1987: The influence of soil and vegetation on the development of mesoscale circulations. *J. Climate Appl. Meteor.*, **26**, 1483-1495.

Mahrer, Y., and R.A. Pielke, 1997: A numerical study of the airflow over irregular terrain. *Beitrage zur Physik der Atmosphare*, **50**, 98-113.

Manabe, S., R.J. Stouffer, M.J. Spelman, and K. Bryan, 1991: Transient response of a coupled ocean-atmospheric model to gradual changes of atmospheric CO_2 I: Annual mean response. *J. Climate*, **4**, 785-818.

Markos, A., 1995: The ontogeny of Gaia: the role of microorganisms in planetary information networks. *J. Theor. Biology*, **176**, 175-180.

Matthews, E., 1983: Global vegetation and land use: New high resolution data bases for climate studies. *J. Climate Appl. Meteor.*, **22**, 474-487.

McGuffie, K., A. Henderson-Sellers, H. Zhang, T.B. Durbridge, and A.J. Pitman, 1995: Global climate sensitivity to tropical deforestation. *Global and Planetary Change*, **10**, 97-128.

Mintz, Y., 1984: The sensitivity of numerically simulated climates to land-surface boundary conditions. *The Global Climate*, J. Houghton, Ed., 79-105.

Mitchell, D.L., J.M. Edwards, and P.N. Francis, 1997: GCM sensitivity of globally averged albedo and OLR to ice crystal shape. *Proceedings: 7th Atmospheric Radiation Measurment (ARM) Science Team Meeting*, March 3-7, 1997, San Antonio, Texas.

Neilson, R.P., and D. Marks, 1994: A global perspective of regional vegetation and hydrologic sensitivities from climatic change. *J. Vegetation Sci.*, **5**, 715-730.

Nemani, R.R., and S.W. Running, 1989: Testing a theoretical climate-soil-leaf area hydrologic equilibrium of forests using a satellite data and ecosystem simulation. *Agric. Forest Meteor.*, **44**, 245-260.

Nemani, R.R., S.W. Running, R.A. Pielke, and T.N. Chase, 1996: Global vegetation cover changes from coarse resolution satellite data. *J. Geophys. Res.*, **101**, 7157-7162.

Nobre, C.A., P.J. Sellers, and J. Shukla, 1991: Amazonian deforestation and regional climate change. *J. Climate*, **4**, 957-988.

North, G.R., and M.J. Stevens, 1998: Detecting climate signals in the surface temperature record. *J. Climate*, **11**, 563-577.

Olson, J.S., J.A. Watts, and L.J. Allison, 1983: Carbon in live vegetation of major world ecosystems. ORNL-5862. Oak Ridge National Laboratory, Oak Ridge, TN.

Ookouchi, Y., M. Segal, R.C. Kessler, and R.A. Pielke, 1984: Evaluation of soil moisture effects on the generation and modification of mesoscale circulations. *Mon. Wea. Rev.*, **112**, 2281-2291.

Oort, A.H., and J.J. Yienger, 1996: Observed interannual variability in the Hadley circulation and its connection to ENSO. *J. Climate*, **9**, 2751-2767.

Palecki, M.A., and D.J. Leathers, 1993: Northern Hemisphere extratropical circulation anomalies and recent January land surface temperature trends. *Geophys. Res. Lett.*, **20**, 819-822.

Parker, D.E., P.D. Jones, A. Bevin, and C.K. Folland 1994: Interdecadal changes in surface temperature since the late 19th century. *J. Geophys. Res.*, **99**, 14373-14399.

Parker, D.E., M. Gordon, D.P.N. Cullum, D.M.H. Sexton, C.K. Folland, and N. Raynes, 1997: A new global gridded radiosonde temperature database and recent temperature trends. *Geophys. Res. Lett.*, **24**, 1499-1502.

Philander, S.G., 1990: *El Niño, La Niña and the Southern Oscillation.* Academic Press. San Diego.

Pielke, R.A., and M. Segal, 1986: Mesoscale circulations forced by differential terrain heating. In: *Mesoscale Circulations.* Peter Ray, Ed. American Meteorological Society, Boston, 516-548.

Pielke, R.A., G. Dalu, J.S. Snook, T.J. Lee, and T.G.F. Kittel, 1991: Nonlinear influence of mesoscale land use on weather and climate. *J. Climate*, **4**, 1053-1069.

Pielke, R.A., W.R. Cotton, R.L. Walko, C.J. Tremback, W.A. Lyons, L.D. Grasso, M.E. Nicholls, M.D. Moran, D.A. Wesley, T.J. Lee, and J.H. Copeland, 1992: A comprehensive meteorological modeling system - RAMS. *Meteor. Atmos. Phys.*, **49**, 69-91.

Pielke, R.A., J.H. Rodriguez, J.L. Eastman, R.L. Walko, and R.A. Stocker, 1993: Influence of albedo variability in complex terrain on mesoscale systems. *J. Climate*, **6**, 1798-1806.

Pielke, R.A., T.J. Lee, J.H. Copeland, J.L. Eastman, C.L. Ziegler, and C.A. Finley, 1997: Use of USGS-provided data to improve weather and climate simulations. *Ecological Applications*, **7**, 3-21.

Pielke, R.A., J. Eastman, T.N. Chase, T.G.F. Kittel and J Knaff, 1998a: 1973-1996 trends in depth-averaged tropospheric temperature. *J. Geophys. Res.*, **103**, 16927-16933.

Pielke, R.A., J. Eastman, T.N. Chase, J. Knaff, and T.G.F. Kittel, 1998b: Errata to 1973-1996 trends in depth-averaged tropospheric temperature. *J. Geophys. Res.*, **103**, 28909-28911.

Plantico, M.S., T.R. Karl, G. Kukla, and J. Gavin, 1990: Is recent climate change across the United States related to rising levels of anthropogenic greenhouse gases? *J. Geophys. Res.*, **95**, 16617-16636.

Polcher, J., and K. Laval, 1994: A statistical study of regional impact of deforestation on climate of the LMD-GCM. *Climate Dyn.*, **10**, 205-219.

Ponte, R.M., and R.D. Rosen, 1994: Angular momentum and torques in a simulation of the atmosphere's response to the 1982-83 El Niño. *J. Climate*, **7**, 538-550.

Poulos, G.S., 1996: The interaction of katabatic winds and mountain waves. Ph.D. Dissertation, Department of Atmospheric Science, Colorado State University, 300 pp.

Prabhakara, C., J.-M. Yoo, S.P. Maloney, J.J. Nucciarone, M. Cadeddu, and G. Dalu, 1996: Examination of "Global atmospheric temperature monitoring with satellite microwave measurements": 2. Analysis of satellite data. *Climate Change*, **33**, 459-476.

Rabin, R.M., and D.W. Martin, 1996: Satellite observations of shallow cumulus coverage over the central United States: An exploration of land use impact on cloud cover. *J. Geophys. Res.*, **101**, 7149-7155.

Rasmussen, E.M., and J.M. Wallace, 1983: Meteorological aspects of the El Niño/Southern Oscillation. *Science*, **222**, 1195-1202.

Resnick, D.B., 1992: Gaia: from fanciful notion to research program. *Perspectives in Biology and Medicine*, **35**, 572-582.

Reynolds, R.W., and T.M. Smith, 1994: Improved global sea surface temperature analyses using optimal interpolation. *J. Climate*, **7**, 929-948.

Sagan, C., O.B. Toon, and J.B. Pollack, 1979: Anthropogenic climate changes and the earth's climate. *Science*, **206**, 1363-1368.

Santer, B.D., J.J. Hnilo, T.M.L. Wigley, J.S. Boyle, C. Doutriaux, M. Fiorino, D.E. Parker, and K.E. Taylor, 1998: Uncertainties in 'observational' estimates of temperature change in the free atmosphere. *J. Geophys. Res.*, submitted.

Sardeshmukh, P.D., and B.J. Hoskins, 1988: The generation of global rotational flow by steady idealized tropical divergence. *J. Atmos. Sci.*, **45**, 1228-1251.

Schimel, D.S., 1995: Terrestrial ecosystems and the carbon cycle. *Global Change Biology*, **1**, 77-91.

Schwartzman, D.W. and T. Volk, 1989: Biotic enhancement of weathering and the habitibility of earth. *Nature*, **340**, 467-460.

Segal, M., R. Avissar, M.C. McCumber, and R.A. Pielke, 1988: Evaluation of vegetation effects on the generation and modification of mesoscale circulations. *J. Atmos. Sci.*, **45**, 2268-2292.

Segal, M., W.E. Schreiber, G. Kallos, J.R. Garratt, A. Rodi, J. Weaver, and R.A. Pielke, 1989: The impact of crop areas in northeast Colorado on midsummer mesoscale thermal circulations. *Mon. Wea. Rev.*, **117**, 809-825.

Sellers, P.J., L. Bounana, G.J. Collatz, D.A. Randall, D.A. Dazlich, S.O. Los, J.A. Berry, I. Fung, C.J. Tucker, C.B. Filed, and T.G. Jensen, 1996: Comparison of radiative and physiological effects of doubled atmospheric CO2 on climate. *Science*, **271**, 1402-1406.

Seth, A., and F. Giorgi, 1996: Three-dimensional model study of organized mesoscale circulations induced by vegetation. *J. Geophys. Res.*, **101**, 7371-7391.

Slingo, T., 1983: Can plankton control climate? *Nature*, **336**, 421.

Smagorinsky, J., 1963: General circulation experiments with the primitive equations: 1. The basic experiment. *Mon. Wea. Rev.*, **91**, 99-164.

Spencer, R.W., J.R. Christy, and N.C. Grody, 1996: Analysis of 'Examination of "Global atmospheric temperature monitoring with satellite microwave measurements"'. *Climate Change*, **33**, 477-489.

Stendel, M., J.R. Christy, and L. Bengtsson, 1998: How representative are recent temperature trends? Report #264 Max-Planck-Institut Fur Meteorologie. and submitted to *J. Climate.*

Stohlgren, T.J., T.N. Chase, R.A. Pielke, T.G.F. Kittel, and J.S. Baron, 1998: Evidence that local land use practices influence regional climate and vegetation patterns in adjacent natural areas. *Global Change Biology*, **4**, 495-504.

Sud, Y.C., J. Shukla, and Y. Mintz, 1988: Influence of land surface roughness on atmospheric circulation and precipitation: A sensitivity study with a general circulation model *J. Appl. Meteor.* **27**, 1036-1054.

Sud, Y.C., G.K. Walker, J.H. Kim, G.E. Liston, P.J. Sellers, and W.K.M. Lau, 1996: Biogeophysical consequences of a tropical deforestation scenario: a GCM simulation. *J. Climate*, **9**, 3225-3247.

Tiedtke, M., 1984: The effect of penetrative cumulus convection on the large-scale flow in a general circulation model. *Beitr. Phys. Atmos.*, **57**, 216-224.

Ting, M., M.P. Hoerling, T. Xu, and A. Kumar, 1996: Northern hemisphere teleconnection patterns during extreme phases of the zonal mean circulation. *J. Climate*, **9**, 2614-2633.

Toth, J.J., and R.H. Johnson, 1984: Summer surface flow characteristics over northeast Colorado. *Mon. Wea. Rev.*, **113**, 1458-1468.

Tremback, C.J., and R. Kessler, 1985: A surface temperature and moisture parameterization for use in mesoscale numerical models. *Preprints: 7th conference on Numerical Weather Prediction.* June 17-20. Montreal, Canada, AMS, Boston.

Trenberth, K.E., and J.W. Hurrell, 1994: Decadal atmosphere-ocean variations in the Pacific. *Climate Dynamics*, **9**, 303-319.

Trenberth, K.E., and T.J. Hoar, 1996: El Niño Southern oscillation event: longest on record. *Geophys Res. Lett.*, **23**, 57-60.

Tribbia, J.J., 1991: The rudimentary theory of atmospheric teleconnections associated with ENSO. In: *Teleconnections Linking Worldwide Climate Anomalies.* M.H. Glantz, R.W. Katz, N. Nicholls Eds. Cambridge University Press, 285-307.

van Breeman, N., 1993: Soils as biotic constructs favoring net primary productivity. *Geoderma*, **57**, 183-211.

Vidale, P.L., 1998: Contributions of land surface forced mesoscale circulations to the total heat, moisture, and momentum budgets over BOREAS. Ph.D. Dissertation, Department of Atmospheric Science, Colorado State University, Fort Collins, CO.

Vincent, D.G., K.-C. Ko, and J.M. Schrage, 1997: Subtropical jet streaks over the South Pacific. *Mon. Wea. Rev.*, **125**, 438-447.

Vinnikov, K.Ya., P.Ya. Groisman, and K.M. Lugina, 1994: Global and hemispheric temperature anomalies from instrumental surface air temperature records. In *Trends '93: A Compendium of Data on Global Change ORNL/CDIAD-65. Carbon Dioxide Information Analysis Center,* Oakridge National Laboratory, Oakridge, Tennessee, 615-627.

Vitousek, P.M., H.A. Mooney, J. Lubchenco, J.M. Melillo, 1997: Human domination of earth's ecosystems. *Science*, **277**, 494-499.

Walko, R.L., W.R. Cotton, M.P. Meyers, and J.Y. Harrington, 1995: New RAMS cloud microphysics parameterization, Part I: the single moment scheme. *Atmos. Res.*, **38**, 29-62.

Wallace, J.J., and D.S. Gutzler, 1981: Teleconnections in the geopotential height field during Northern Hemisphere winter. *Mon. Wea. Rev.*, **109**, 785-812.

Wallace, J.R., Y. Zhang, and L. Bajuk, 1996: Interpretation of interdecadal trends in Northern Hemisphere surface air temperature. *J. Climate*, **9**, 249-259.

Wenger, R., 1923: Zur theorie der Berg-undtalwinde. *Met. Z.* **40**, 193-204.

Wentz, F.J., and M. Schabel, 1998: On the discrepancy between observed in situ surface warming and the cooling trend in MSU tropospheric temperatures. *Nature*, submitted.

Wiin-Nielson, A., and T.-C. Chen, 1993: *Fundamentals of atmospheric energetics.* Oxford University Press. New York.

Williams, G.C., 1992: Gaia: Nature worship and biocentric fallacies. *Quart. Rev. Biology,* **67**, 479-486.

Williams, M.W., M. Losleben, N. Caine, and D. Greenland, 1996: Changes in climate and hydrochemical responses in a high-elevation catchment in the Rocky Mountains, USA. *Limnology and Oceanography,* **41**, 939-946.

WMO, 1986: *Catalogue of radiosondes and upper-air wind systems in use by members.* World Meteorological Organization, Instruments and Observing Methods Report No. 27, WMO/TD No. 176.

Wolyn, P.G., and T.B. McKee, 1994: The mountain-plains circulation east of a 2-km-high north-south barrier. *Mon. Wea. Rev.*, **122**, 1490-1508.

Wu, Z.-X., and R.E. Newell, 1998: Influence of sea surface temperature on air temperature in the tropic. *Clim. Dyn.*, **14**, 275-290.

Xue, Y., 1997: Biosphere feedback on regional climate in tropical north Africa. *Quart. J. Roy. Meteor. Soc.*, **123**, 1483-1515.

Xue, Y., and J. Shukla, 1993: The influence of land surface properties on Sahel climate. Part I. Desertification. *J. Climate*, **6**, 2232-2245.

Yulaeva, E., and J.M. Wallace, 1994: The signature of ENSO in global temperature and precipitation fields derived from the Microwave Sounding Unit. *J. Climate*, **7**, 1719-1736.

Zhang, G.J., and N.A. McFarlane, 1995: Sensitivity of climate simulations to the parameterization of cumulus convection in the Canadian Climate Centre general circulation model. *Atmos. Ocean*, **33**, 407-446.

Zhang, D.L., and R.A. Anthes, 1982: A high resolution model of the planetary boundary layer-sensitivity tests and comparisons with SESAME-79 data. *J. Appl. Meteor.*, **21**, 1594-1609.

Zhang, H., A. Henderson-Sellers, and K. McGuffie, 1996: Impacts of tropical deforestation. Part I: Process analysis of local climate change. *J. Climate*, **9**, 1497-1517.

Zhang, H., A. Henderson-Sellers, and K. McGuffie, 1997: Impacts of tropical deforestation. Part II: The role of large scale dynamics. *J. Climate*, **10**, 2498-2521.

Zheng, X., and E.A.B. Eltahir, 1997: The response to deforestation and desertification in a model of West African monsoons. *Geophys. Res. Letts.* **24**, 155-158.